Rumpling phenomenon in platinum modified Ni-Al alloys

by

Benjamin Joseph Zimmerman

A thesis submitted to the graduate faculty

in partial fulfillment of the requirements for the degree of

MASTER OF SCIENCE

Major: Materials Science and Engineering

Program of Study Committee:
Brian Gleeson, Major Professor
Daniel Sordelet
Ashraf Bastawros

Iowa State University

Ames, Iowa

2005

Graduate College
Iowa State University

This is to certify that the master's thesis of

Benjamin Joseph Zimmerman

has met the thesis requirements of Iowa State University

Major Professor

For the Major Program

Table of Contents

Acknowledgements

I would like to thank my parents, Patrick and Patricia Zimmerman, for their support through these 19 years of school. I would like to thank my major professor, Brian Gleeson, for his guidance, insight and advice. I would like to thank Dan Sordelet, one of my committee members, for the time we spent going over results together and for helping make my research trips to both Argonne and Oak Ridge National Labs fruitful. I would like to thank Matt Besser for his assistance with the use of various laboratory equipment and for his work on the sample preparation, measurement, and analysis of the x-ray diffraction data. The high-temperature x-ray diffraction experiments were performed at the Midwest Universities Collaborative Access Team (MUCAT) sector at the Advanced Photon Source, which is supported by the U.S. Department of Energy, Office of Science, Basic Energy Sciences, through the Ames Laboratory. Use of the Advanced Photon Source was supported by the U.S. Department of Energy, Office of Science, Basic Energy Sciences, under Contract No. W-31-109-Eng-38. I would like to thank my officemates Shigenari Hayashi, Bingtao Li, Vinay Deodeshmukh, Nan Mu, and Takeshi Izumi for their assistance with experimental details and providing helpful advice on a variety of topics. I would like to thank Wallace Porter for his assistance with my research at Oak Ridge National Lab. I would like to thank Dan Whittenberger for performing all of the mechanical testing at NASA Glen Research Center. I would like to thank both David Cann and Seymen Aygun for performing resistivity measurements here at Iowa State University. I would also like to thank Eric Schulz for the time he spent proof-reading this thesis. Finally, I would like to extend a special thank you to Andrea Gerber for her patience, encouragement, and friendship over these last few years.

Abstract

Surface undulations known as rumpling have been shown to develop at the surface of bond coats used in advanced thermal barrier coating systems. Rumpling can result in cracking and eventual spallation of the top coat. Many mechanisms to explain rumpling have been proposed, and among them is a martensitic transformation. High-temperature x-ray diffraction, differential scanning calorimetry and potentiometry were used to investigate the nature of the martensitic transformation in bulk platinum-modified nickel aluminides. It was found that the martensitic transformation has strong time dependence and can form over a range of temperatures. Cyclic oxidation experiments were performed on the bulk alloys to investigate the effect of the martensitic transformation on surface rumpling. It was found that the occurrence of rumpling was associated with the martensitic transformation. The degree of rumpling was found to increase with an increasing number of cycles and was independent of the heating and cooling rates used. The thickness of the oxide layer at the surface of the samples had a significant impact on the amplitude of the resulting undulations, with amplitude increasing with increasing oxide-layer thickness. Rumpling was also observed in an alloy based on the γ-γ' region of the nickel-aluminum-platinum phase diagram. Rumpling in this alloy was found to occur during isothermal oxidation and is associated with a subsurface layer containing a platinum-rich phase known as α. Rumpling in both alloy systems may be explained by creep deformation of a weakened subsurface layer in response to the compressive stresses in the thermally grown oxide layer.

Chapter 1: Introduction

Gas turbine engines can benefit greatly from protective coatings on their internal parts. Protective coatings allow for increased working temperatures, which in turn lead to improved fuel efficiency and greater power output. The coatings can also significantly decrease the temperature of the substrate to which they are applied, resulting in longer component life. These advantages can significantly lower the operating costs of turbine engines.

The temperature of the combustion gasses within current gas turbine engines can exceed the melting point of nickel-based superalloys by over 250°C [1]. To overcome the high heat, various methods are used to decrease the temperature of the turbine blades. Blades are designed with internal channels and vents through which cooling gasses can flow. Unfortunately, this method of cooling is detrimental to the overall efficiency of the engine. The second method of decreasing the temperature of the blades is through the use of thermal barrier coatings (TBCs). A 150μm thick TBC can provide a 75°C reduction in the temperature of the superalloy blade substrate on its own [2], and up to a 150°C reduction when combined with internal cooling [1]. These values are very significant considering that a 10-15°C decrease in blade temperature doubles the creep life [3]. TBCs were first introduced in the 1980s and research is continuing in order to improve their effectiveness and to eliminate their various shortcomings.

The major mode of failure of TBC is due to delamination of the outermost coating layer from the bond coat to which it is applied. It has been determined that the oxidation behavior of the bond coat has a major impact on the life of the TBC. Current bond coats have oxidation behaviors that are not ideally suited for use in TBC systems.

This thesis proposal covers the oxidation testing of various representative bond coat alloys used in TBC systems. The transformations within the alloys and the resulting surface

morphologies and their potential impacts on TBC performance are investigated. The proposal is organized as follows:

-Chapter 2 is an in-depth review of current TBC systems and the reasons for their failures.

-Chapter 3 begins with an overview of the fundamentals of metal and alloy oxidation and will cover the oxidation behavior of current aluminide coatings.

-Chapter 4 is an overview of the various phase transformations that occur in bond coat alloys.

-Chapter 5 discusses the rumpling phenomenon in bond coats.

-Chapter 6 presents the aims of the current project.

-Chapter 7 is a discussion of the experimental procedures used.

-Chapter 8 contains the results and discussion of the experiments described in Chapter 7.

-Chapter 9 is a summary of this thesis.

-Chapter 10 contains suggestions for future work.

Chapter 2: Thermal Barrier Coating Systems

TBC systems generally consist of a series of layers on top of the superalloy substrate. The cross-section of a typical system is represented in Figure 1. The innermost layer is a metallic bond coat, followed by a thermally grown oxide (TGO), and the outermost layer is the TBC, which is also known as the top coat.

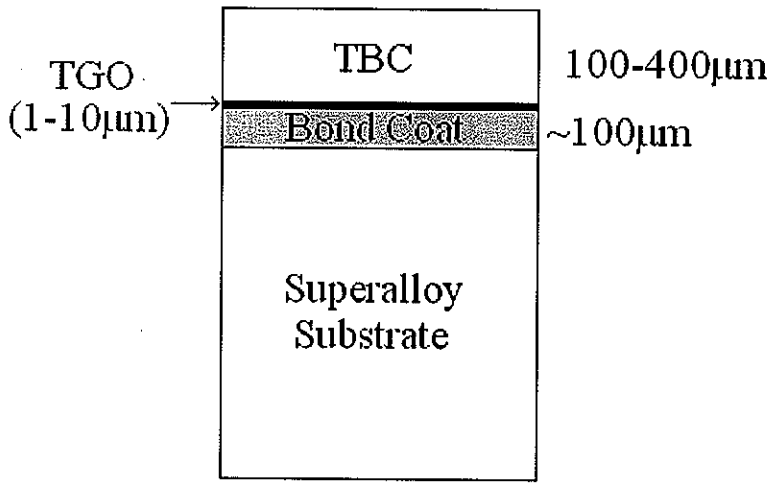

Figure 1. Structure of a typical TBC system

2.1 TBCs

The TBC is generally comprised of zirconia partially stabilized with 6-8% yttria (YPSZ). The yttria serves to stabilize the mechanically superior tetragonal crystal structure in the zirconia. The properties that make YPSZ a very good choice for TBCs are its low thermal conductivity (~1.8W/mK) [2], its chemical stability at high temperatures, relatively high toughness, and a high thermal expansion coefficient for a ceramic, thus allowing for less thermal stress when bonded to a metal. The TBC can be applied by either plasma spraying (PS) or by electron beam physical vapor deposition (EB-PVD). The PS method involves the spraying of liquid or semi-liquid YPSZ directly onto the surface of the bond coat where it then rapidly solidifies. The resulting structure is significantly porous and contains many microcracks perpendicular to the surface; this structure increases both the toughness and

thermal insulating properties of the TBC. The more recent EB-PVD method is the preferred method for use on components which face the highest thermal and mechanical stresses. EB-PVD is a process in which the YPSZ is evaporated and then grows on the bond coat in such a way that many columnar grains are formed. This structure provides improved strain tolerance, which leads to a much longer lifetime [1]. The differences between the two structures are illustrated in Figures 2 and 3.

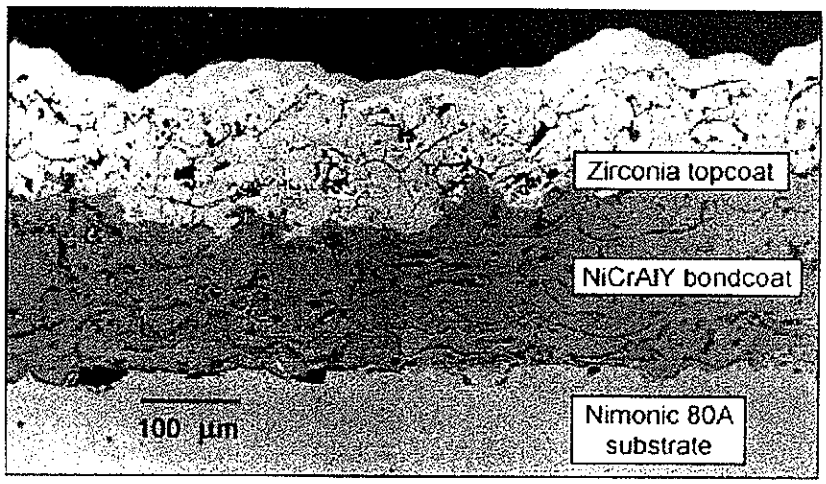

Figure 2. A system with a PS TBC [4]

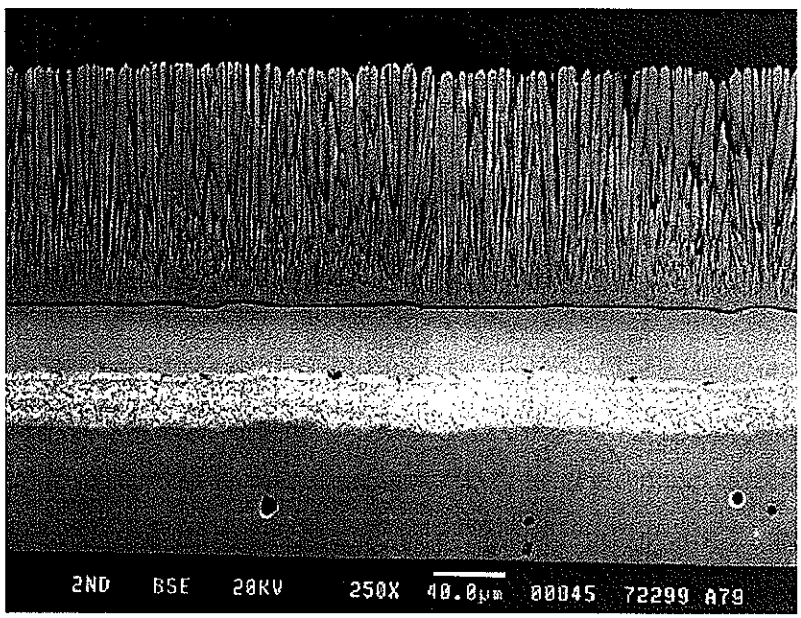

Figure 3. A system with an EB-PVD TBC [5]

2.2 Current Bond Coats

The primary purpose of the bond coat is to provide a surface for the TBC to bond to. It is also critical that the bond coat be oxidation resistant, as it also serves to prevent oxidation of the superalloy substrate. An ideal bond coat will have a slow growing, planar alumina scale and will also have a coefficient of thermal expansion which matches the substrate and the TBC as well as possible. The alumina scale that forms between the bond coat and the TBC must bond very well with both the bond coat and the TBC to avoid delamination.

There are currently two different bond coats used in TBC systems. The first type is the MCrAlY bond coats, where M is a metal such as Ni and/or Co. The second type is platinum-modified nickel aluminides. The MCrAlY coatings generally consist of a mixture of phases known as γ (Ni, FCC crystal structure) and β (NiAl, B2-type crystal structure) [6]. Figure 4 is a phase diagram for the Ni-Cr-Al system at 1100°C [7]. The Pt-modified aluminides typically consist entirely of the β-phase, although both a reversible martensitic transformation ($L1_0$-type crystal structure) and the formation of γ' (Ni_3Al, $L1_2$-type crystal structure) can occur under certain conditions. Figure 5, a phase diagram for the Ni-Al-Pt system at 1100 and 1150°C, illustrates the relative positions of these phases [8]. Both coating types are applied to the superalloy substrate using various methods such as plasma spraying, chemical vapor deposition (CVD), physical vapor deposition (PVD), and diffusion coatings to a thickness on the order of 50μm. It is important to note that neither type of coating was developed for use specifically as a bond coat; their original purpose was to provide oxidation and corrosion resistance as standalone metallic coatings [8]. When used as a bond coat, the surface morphology becomes important, and the ability to heal the protective alumina layer becomes less important since the TBC will likely fail after a single spallation of the TGO [8].

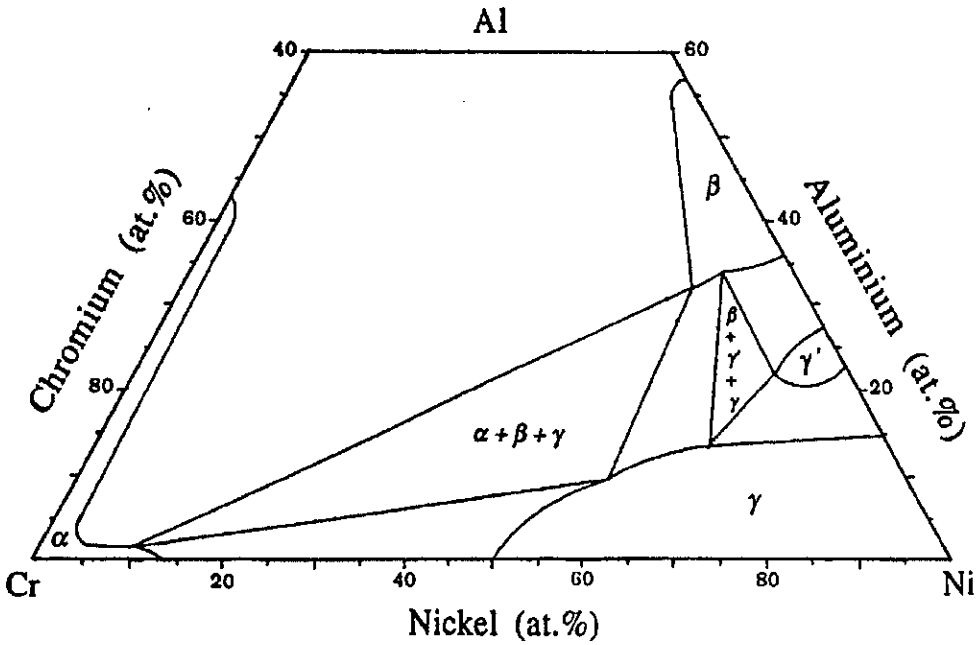

Figure 4. The Ni-Cr-Al phase diagram at 1100°C [7]

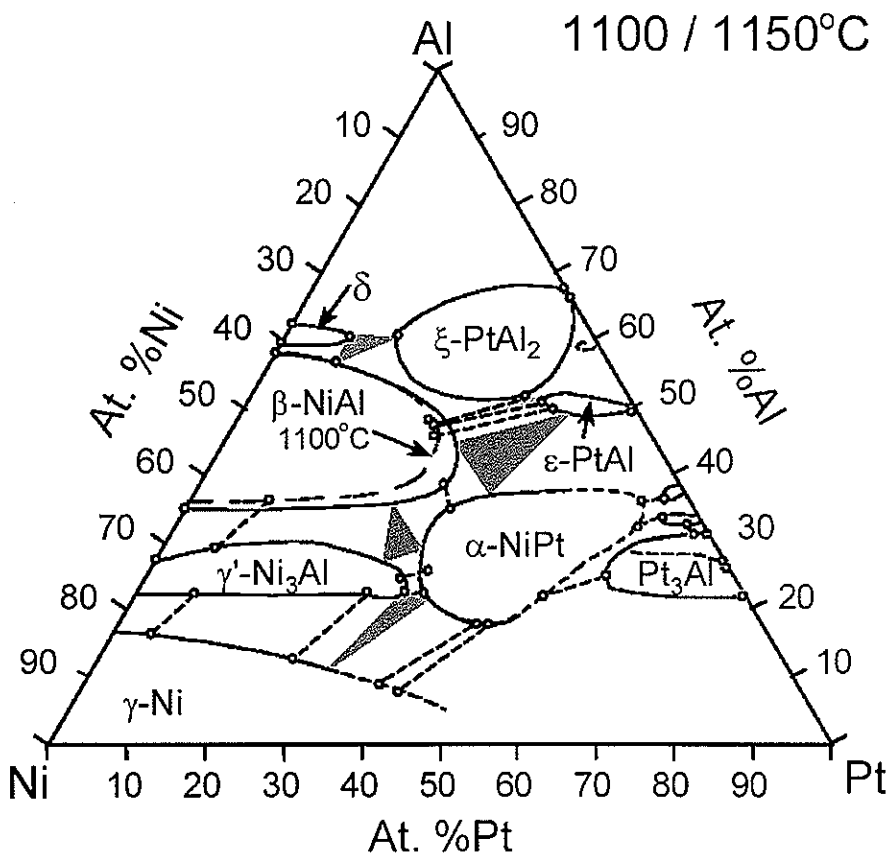

Figure 5. The Ni-Al-Pt phase diagram at 1100/1150°C [8]

2.2.1 MCrAlY Coatings

The MCrAlY coatings are most often applied by plasma spraying and are generally superior to the aluminide coatings with respect to hot corrosion resistance [9]. Hot corrosion is an accelerated mode of attack due to the presence of molten salt, either from the environment or from the fuel used, and results in the formation of metal sulphides. Hot corrosion is a major concern when temperatures are between approximately 650 and 1000°C [10]. Small amounts of yttrium are added to the bond coat in order to improve the adhesion of the TGO [11]. Above 1000°C oxidation becomes the dominant corrosion mechanism and the Pt-modified nickel aluminides are preferred because of their superior oxidation resistance [9].

2.2.2 Pt-Modified Aluminides

Binary NiAl alloys have relatively poor high-temperature oxidation resistance, but the addition of Pt promotes the exclusive formation of an adherent alumina scale and thereby inhibits the formation of Ni-rich oxides, which are very detrimental to oxidation performance [12]. Pt-modified aluminides are most typically applied using diffusion methods which result in an aluminum level of approximately 40at.% and a platinum level of up to approximately 10at.%. The most common method of creating Pt-modified aluminide coatings, which are also called beta coatings, involves first electroplating a Pt layer and then aluminizing via a CVD process such as pack cementation. Elements such as Cr and Hf are commonly codeposited with Al to improve the corrosion behavior [13].

2.3 Failure of TBCs

The spallation of the TBC top coat is a very destructive event, as it will generally result in failure of the substrate in a relatively short time due to a large increase in surface temperature of the metal. TBC spallation is initiated by cracking at either the TGO/bond coat interface or at or near the TGO/TBC interface [4]. It is widely accepted that once enough cracks form,

they eventually coalesce into a crack large enough for the TBC to buckle and spall. In the majority of cases the cracking is attributed to the mechanical forces that result from the interface becoming non-planar. Also, the presence of Ni or Cr-rich oxides instead of pure alumina will worsen the spallation behavior significantly [4].

Evans et al. [11] provided a more in-depth analysis of the various failure mechanisms of TBC systems. The mechanical failure mechanisms are the result of TGO thickness heterogeneities in an otherwise planar interface, the formation of interface undulations, or foreign object damage. The chemical failure mechanisms which result in the formation of Ni-rich oxides such as spinels are attributed to either Al-depletion, where the spinel forms below the alumina layer, or Ni diffusing through the alumina to form spinel on top of the alumina layer. In either case, the failure occurs within the spinel layer.

A 1987 paper by Deb et al. [14], and a large number of recent papers [6, 11, 15-23], have focused on surface undulations as a major cause of TBC failure. While these surface undulations, which are commonly referred to as rumpling, have been reported to occur in MCrAlY coatings [15], rumpling has not been found to contribute to TBC failure in these alloys. Thus, the majority of research on rumpling has focused on aluminide coatings. Rumpling is generally found to evolve during cyclic oxidation of coated samples. A rumpled bond coat will have a very negative effect on TBC adhesion as shown in figure 6. The mechanisms behind this rumpling phenomenon will be the focus of this thesis and will be presented in greater detail in later sections.

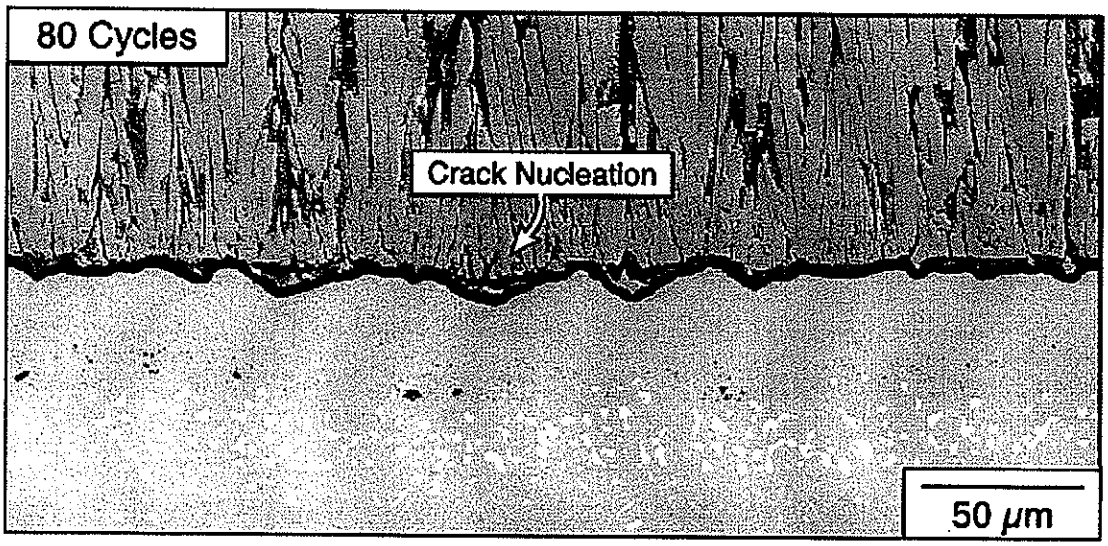

Figure 6. Rumpling on a NiAl bond coat after thermal cycling [6]

All mechanically-induced TBC separation, whether caused by rumpling or not, is ultimately due to the tensile forces that develop and allow cracks to nucleate and propagate. The relative locations of the tensile stresses that form around a perturbation are shown in figure 7. While the TBC is relatively strain tolerant for a ceramic, eventually the cracks form a separation large enough that the TBC layer buckles to relieve the stresses that develop [11]. A 2003 paper by H.E. Evans [4] explained how chemical failure can exacerbate the mechanical stresses present through the following process: Aluminum can not diffuse fast enough to the peaks of the perturbation to replace the atoms lost to alumina formation; once that occurs, fast growing Ni- and Cr-rich oxides form at the peaks. These fast growing oxides are detrimental due to both their mechanical strength and the increased tensile stresses that result in the TBC.

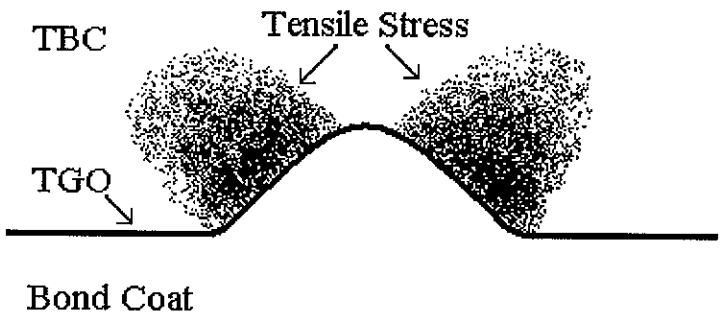

Figure 7. Tensile stresses in the TBC that form as a result of a surface imperfection

Chapter 3: Oxidation Behavior of Aluminide Coatings

As mentioned in Chapter 2, Pt-modified nickel aluminides are chosen for use as bond coats due to their excellent high-temperature oxidation behavior. In particular, the slow growing, adherent alumina scale is what makes these types of alloys so desirable. Before delving into the specifics of oxidation of the Pt-modified β-NiAl bond coat alloys, a brief overview of oxidation will be presented.

3.1 Metal and Alloy Oxidation

Growth of an oxide requires the diffusion of atoms through the existing oxide layer. Metal atoms can diffuse outwards from the metal and react with oxygen at the outer surface of the oxide, or oxygen can diffuse and react with metal atoms at the metal-oxide interface. Additionally, oxides can form subsurface precipitates instead of a discrete layer; this type of oxidation is especially common for high temperature alloys exposed to oxidation for extended time periods [25]. In some cases the diffusion of both the metal and oxygen are significant and new oxide can form within the oxide layer [26]. The desired behavior for oxide growth is the formation of a continuous, slow-growing scale. A scale of this type obeys diffusion controlled, parabolic kinetics [25]. Equations 1 and 2 [25] provide the means to calculate the weight change and thickness of the metal consumed, respectively.

$$W_S^2 = k_p t \tag{1}$$

$$x = \left(\frac{V_m}{\nu M_X} \right) * \Delta W_S \tag{2}$$

In the above equations, ΔW_S is the weight change due to oxidation, k_p is the parabolic rate constant, t is the time, x is the thickness of metal consumed, V_m is the molar volume of the alloy, ν is the stoichiometric factor for the scale product, and M_X is the atomic weight of oxygen [25].

In a binary alloy A-B, the more reactive element may be preferentially oxidized, either internally or externally, depending on content. It is desirable that the oxidized element will form a protective scale on the surface of the alloy and the other element will not oxidize. The growth of a protective scale requires a sufficient supply of the metal that is oxidizing. In order for the protective scale to continue growing, the rate of metal consumed due to oxide scale growth must be slower or equal to the rate at which the metal atoms can diffuse to the scale [25]. If the rate of consumption is greater than the rate of supply, then the protective scale can fail. The minimum necessary concentration of the metal that forms the protective scale, $N^0_{B(\min)}$, can be calculated using equation 3, derived by C. Wagner in 1952 [26]. D_B is the diffusion coefficient of the oxidizing metal B in the alloy.

$$N^0_{B(\min)} > \frac{V_m}{\nu M_0}\left(\frac{\pi k_p}{2 D_B}\right)^{1/2} \qquad (3)$$

3.1.2 Oxidation-Driven Stress

Stress can be generated in a metal/oxide system due to the oxide taking up a different volume than the metal that it replaces, differences in thermal expansion coefficients between the metal and the oxide, or because of more complicated mechanisms that take place, especially when alloys are considered.

A common value used to describe metal-oxide systems is the Pilling-Bedworth ratio, Φ, which is defined as the ratio of the volume of the metal oxide to that of the consumed metal. In general, if Φ is less than 1, the oxide that forms will be porous and non-protective. If Φ is very large, the oxide that forms will likely be under significant compressive stress which can lead to buckling and spallation of the oxide [27]. Interestingly, it has been shown mathematically and through experimentation that compressive stresses in the oxide can actually reduce the growth rate of the oxide [27]. For an oxide that grows at the oxide-metal interface the compressive stress slows down the flux of anion vacancies, thus slowing down

the diffusion of oxygen ions to that interface [27]. An additional oxidation mechanism that can cause stress to build up is due to oxygen going into solution in the substrate. Some metals have a very high solubility for oxygen, causing a large dilational strain that can lead to tensile failure of the oxide [27].

A numerical study of the stresses that can be induced in alloys where one element is preferentially oxidized is provided in a 2003 paper by Suo et al. [28]. While Suo's paper provides numerical examples for the Pt-modified NiAl system, the general ideas can be applied to a wide range of alloys. When an alloy contains two elements where one oxidizes at elevated temperature and the other does not, the element that oxidizes will diffuse to the surface and the other element will generally diffuse in the opposite direction, but not necessarily at the same rate. Differing rates of diffusion between the two species is known as the Kirkendall effect, and can generate a stress. If the stress is tensile, voids can be generated near the surface. An example of the voids that were observed is shown in figure 8 [28]. This oxidation-driven stress mechanism may exist simultaneously with the other mechanisms discussed previously.

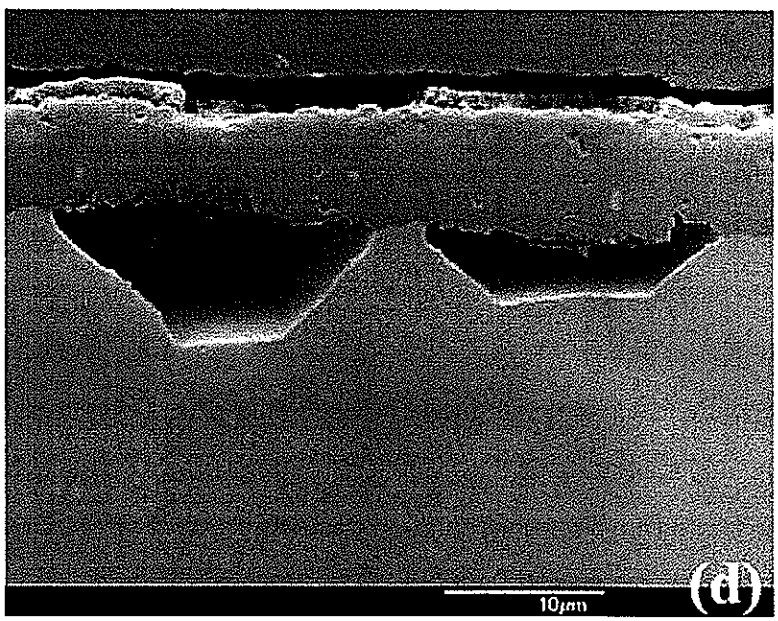

Figure 8. Voids beneath the oxide layer in Pt-modified NiAl after isothermal oxidation [28]

3.2 Oxidation of β-NiAl Alloys

The addition of precious metals, most commonly Pt and occasionally Pd or Ir [29], to NiAl allows for the formation of an adherent α-alumina scale. The alumina that grows on the surface requires a nucleation site, and thus, the grain size is largely dependent on surface finish. When Tolpygo and Clarke [16] observed the oxide that grew on an aluminide alloy, they found that both grain size and stress increased with finer surface finishes due to the lack of nucleation sites. The stress in the oxide layer plays an important role in the life of TBC systems.

The β-NiAl phase field covers a large composition range as shown in figure 4, and the oxidation behavior can depend greatly on the particular composition, i.e. whether the alloy is Ni or Al rich. It is known that sulfur is very detrimental to scale adherence, and that additions of small amounts of reactive elements such as Y, Hf, or Zr improve the adherence of the oxide scale in β alloys [29]. Oxidation behavior of aluminide bond coats can be influenced by the effects of the substrate; Al will diffuse from the bond coat into the substrate, effectively creating a bond coat lower in Al which is generally detrimental to the ability to maintain a purely alumina scale. Due to the complicating effect of bond coat/substrate interactions, the discussion of the oxidation behavior of coated substrates will not be covered in this chapter.

3.2.1 Isothermal Oxidation

The oxidation behavior of binary NiAl depends greatly on the Al content. Stoichiometric and near-stoichiometric NiAl forms an adherent alumina scale down to an Al content of ~43at.% Al [12]. Lower Al contents result in the formation of Ni-rich oxides and a much larger mass gain as shown in the experimental data for bulk alloys from Pint et al. [12] in figure 8. Figure 8 also illustrates the beneficial effects of Hf, one of the reactive elements

that have also been shown to improve cyclic oxidation behavior by promoting an adherent, slow-growing, alumina scale.

While Pt has been known to have a very beneficial impact on the oxidation behavior of NiAl, the exact mechanisms behind its role are still unclear. In 1977 Jackson et al. [30] reported that high concentrations of Pt were found at the surface of the alloy and surmised that Pt retarded the diffusion of refractory elements from the substrate, preventing them from oxidizing. A later paper by Schaeffer et al. [31] confirmed the diffusion retarding effect of Pt additions. Pt is apparently beneficial in preventing diffusion of detrimental elements, but this alone does not fully explain its role in promoting scale adherence. As figure 9 illustrates, Pt improves the oxidation behavior of aluminides even when no superalloy substrate elements are present; Pt prevents low aluminum β alloys from forming the fast growing Ni-rich oxides that they would form had they not included Pt. Gleeson et al. [8] also showed that Pt improved the scale adhesion in β alloys. The researchers also created ternary diffusion couples to better understand the role of Pt. It was found that although Pt decreases the chemical activity of Al (which would reduce the tendency to form alumina), "the interdiffusion coefficient for Al in its own concentration gradient, D_{AlAl}, increases with increasing Pt content". The latter observation serves to explain a possible mechanism behind the beneficial role of Pt; as the Al concentration near the surface decreases due to oxidation, Al will more readily diffuse to the surface, preventing the formation of detrimental Ni-rich oxides.

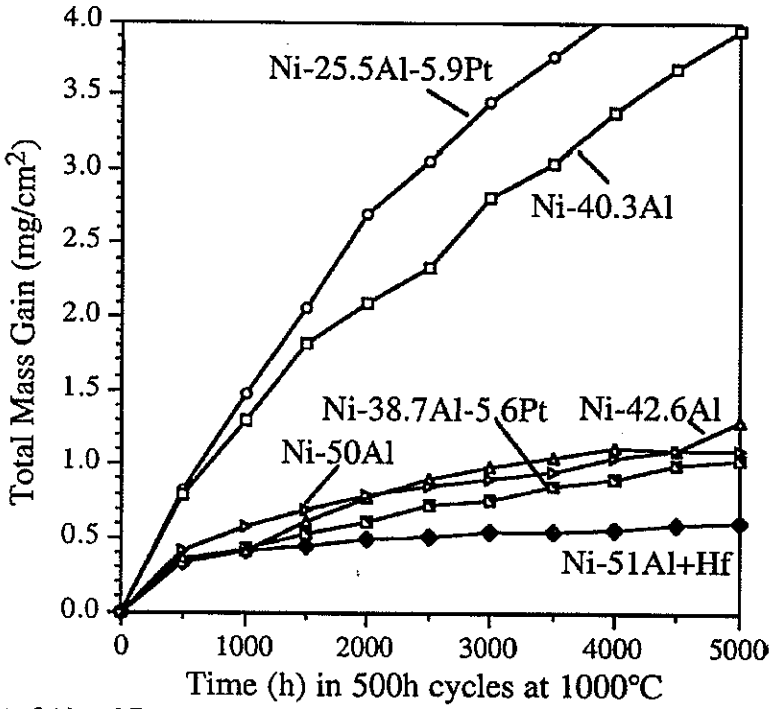

Figure 9. The effect of Al and Pt content on quasi-isothermal oxidation of β alloys [12]

3.2.2 Cyclic Oxidation

A β alloy which undergoes cyclic oxidation, i.e. where it is oxidized at a high temperature for a given length of time then cooled to a low temperature where it is held before repeating the heating and cooling cycle many more times, behaves much differently than the same alloy oxidized at the same temperature for the same amount of time under isothermal conditions. Because cyclic oxidation more closely resembles the conditions to which these alloys are exposed to while in service, it can be considered to provide more representative results than isothermal oxidation experiments. In general, cyclic oxidation is more severe than isothermal oxidation and can result in more undesirable oxidation behavior. The poorer performance of cyclically oxidized sample is attributed to the stresses that result from the differences in thermal expansion coefficients between the alloy and the oxide, and/or from phase changes that might occur upon heating or cooling.

As in isothermal oxidation, Pt has also been shown to have beneficial effects on alumina scale adhesion [8, 9, 12, 28] in cyclic testing. In one of the first papers to discuss the cyclic oxidation behavior of bulk nickel aluminides, Leyens et al. [9] explored the addition of small amounts (~0.05at.%) Hf and found that Hf improved the oxidation performance of binary NiAl to such an extent that Pt additions may be unnecessary. The researchers also reported that Cr, while known to promote alumina formation, results in accelerated scale growth and spallation of the alumina. Unfortunately, Cr additions are required to provide resistance to hot corrosion, thus leading the researchers to conclude that high temperature oxidation resistance and hot corrosion resistance may be mutually exclusive [9]. In a more recent paper [27] the same research group looked at the possible effect of Pt and Hf on thermal expansion of the alloy, but the results failed to provide sufficient explanation for the improvements in scale adhesion.

In a 2004 paper by Pint (also an author of the two papers discussed above) [12], various alloys were tested for up to 2000 1 hour cycles at 1100°C. Once again, the benefits of Pt and Hf additions were evident and oxidation behavior was excellent for alloys with Al contents as low as 37.2at.%. When the Al content was reduced to 34.7at.%, the sample experienced a much larger mass gain due to oxidation and exhibited macroscopic deformation. Due to its lower aluminum content, the alloy experienced a reversible transformation from single phase β to a two phase mixture of β and γ' upon cooling as would be expected from the binary Ni-Al phase diagram in figure 10. The formation of γ' and other transformations, such as a reversible martensitic transformation, can have detrimental effects on oxidation behavior and will be discussed in more depth in Chapter 4.

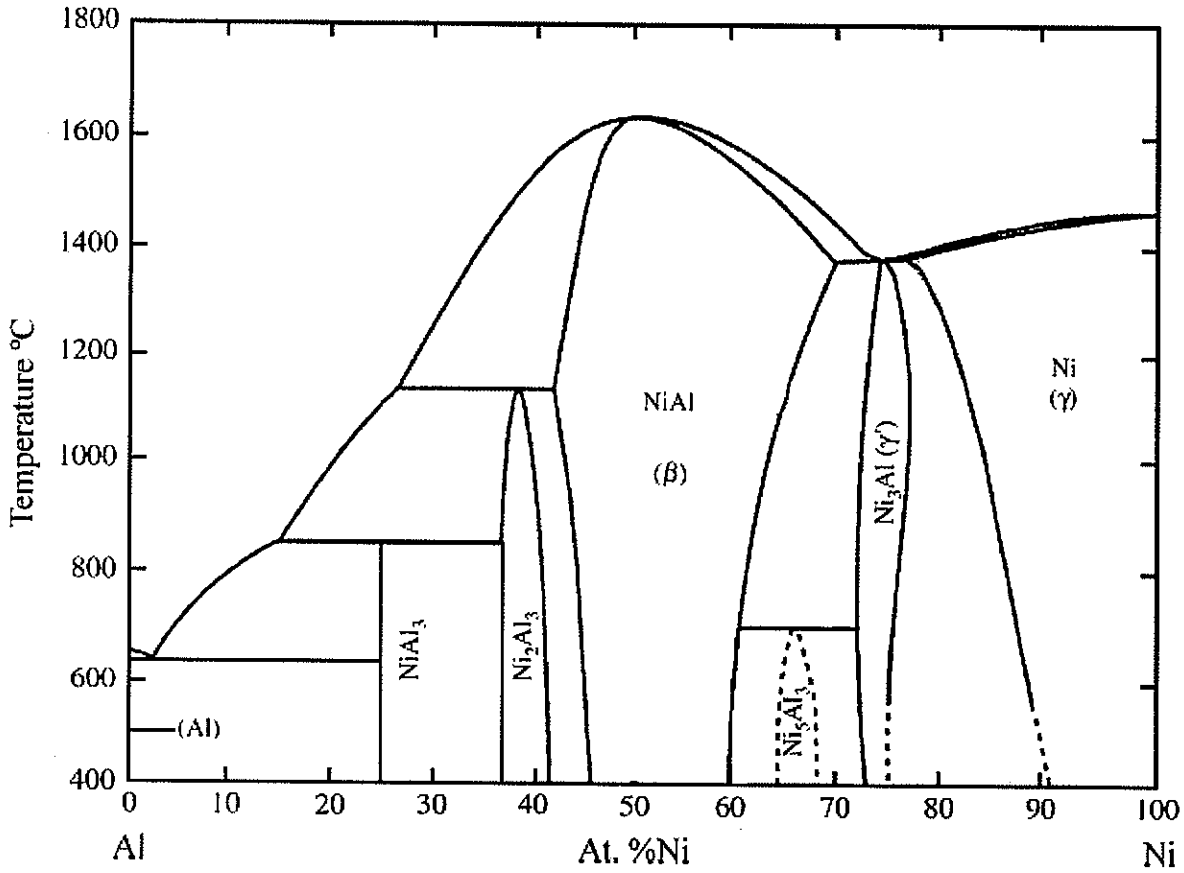

Figure 10. The nickel–aluminum phase diagram [32]

Chapter 4: Bond Coat Phase Transformations

All bond coat alloys are exposed to conditions such as high temperature oxidation where chemical change is inevitable. The changes can be due to elements diffusing to or from the TGO or superalloy substrate. If the composition of the bond coat changes enough, phase transformations can occur. While MCrAlY bond coats normally contain both β and γ phases, aluminide coatings are generally produced as single-phase β. Under cyclic oxidation it is found that β-NiAl can eventually form γ' or undergo a martensitic transformation. These two transformations in aluminide bond coats have been studied quite in-depth [16, 22, 33, 34] due to their implications on TBC failures. The differences in molar volumes and thermal expansion coefficients between the different phases cause stresses that result in oxide spallation or undulations at the surface of the bond coat.

Novel bond coats have been proposed by researchers at Iowa State [8] and are based on the Pt modified γ+γ' system. While these alloys have a microstructure that is generally stable, under certain circumstances the formation of a subsurface zone containing α (NiPt, $L1_0$-type crystal structure) is observed. The phase transformations in both β coatings and γ-γ' alloys will be discussed in this chapter.

4.1 Phase Transformations within the β System

Aluminide coatings have been applied to turbine components since the 1970s. The rumpling phenomenon led researchers to investigate phase changes within the bond coats. Phase transformations were not considered as a possible mechanism responsible for rumpling until the γ' precipitates were observed and determined to be a major cause of rumpling in the 2000 paper by Tolpygo and Clarke [16]. Interestingly, while a martensitic transformation had been known to occur in the NiAl system since 1954 [35] and was studied extensively by Smialek and Hehemann in 1973, it was not considered in aluminide bond coats until the 2003 paper by Chen et al. [34].

4.1.1 The β to γ' Transformation

The microstructure of the Pt-modified aluminide coating used by Tolpygo and Clarke [16] is shown in figure 11. The outermost layer is ~30μm thick and has a composition in at.% of 45% Ni, 44 %Al, 6% Pt, 3.5% Co and 1.5% Cr. This composition is well within the β phase field shown in figure 5; no γ' would be expected to form for this composition. The key to the formation of γ' is that the composition of the coating becomes Ni-enriched when exposed to high temperatures. After 100 1 hour cycles at 1150°C, the microstructure of the coating is completely different, as shown in figure 12 [16].

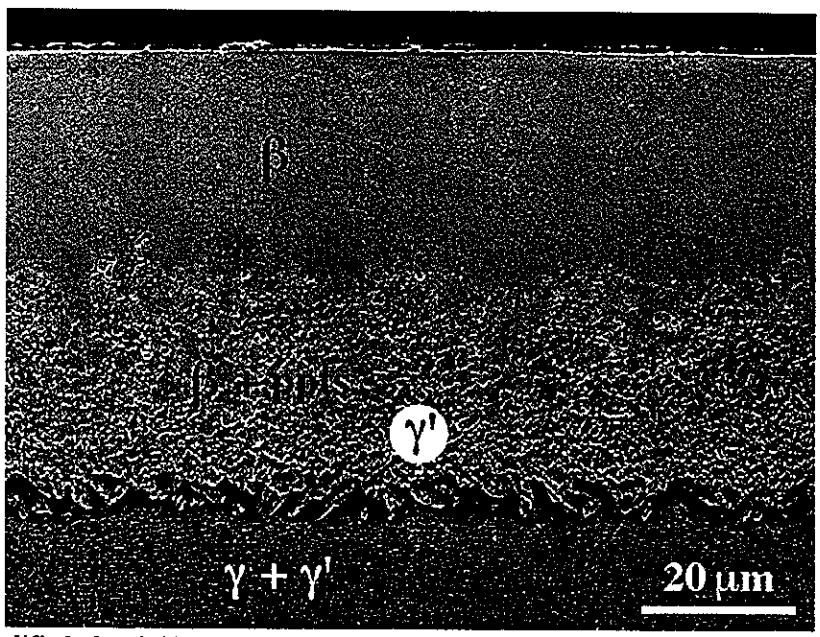

Figure 11. Pt-modified aluminide coating applied by electroplating and CVD on a superalloy substrate [16]

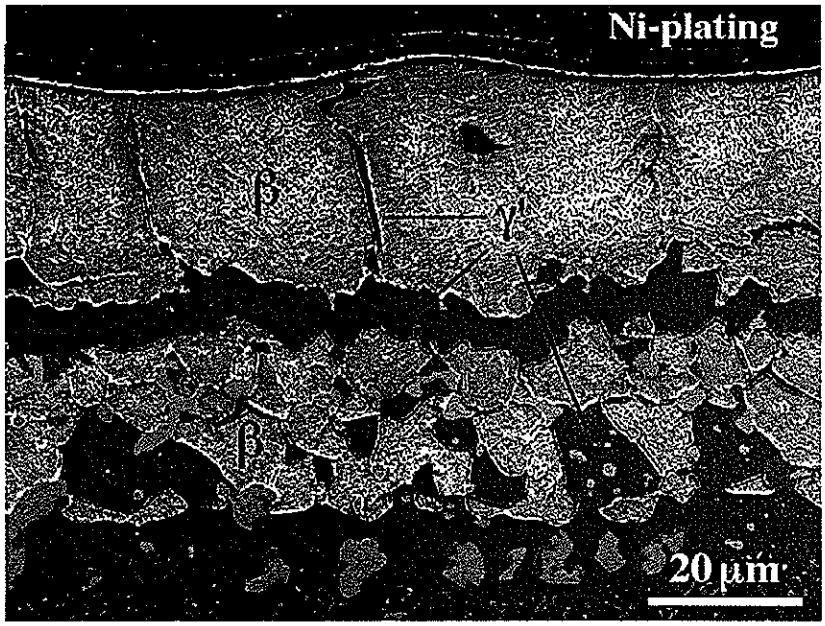

Figure 12. Microstructure of the coating in figure 9 after 100 1 hour cycles at 1150°C [16]

During oxidation aluminum was lost due to both oxidation and diffusion into the substrate. The concentration of Al in the β phase dropped to 32at.%, the lower limit of the β phase field. Further Al depletion caused the formation of γ'. If Pt-modified aluminide coatings are oxidized for longer times, more of the β phase will transform into γ'. Angenete et al. [36] tested coated alloys out to 20,000 hours and found that after 5,000 hours at 1050°C the coatings had nearly entirely transformed to γ'.

4.1.1 The Martensitic Transformation

A 1973 paper by Smialek and Hehemann [37] reported the martensitic transformation of binary NiAl and reported the martensite start temperature (M_s) as a function of Ni composition: M_s (K) = -7410 + 124* (at.% Ni). It is clear from this equation that martensite is only expected to form for Ni-rich compositions because the M_s decreases to well below ambient temperatures as the composition approaches stoichiometric NiAl. Further research on the reversible martensitic transformation was undertaken by Lašek and Chráska [38, 39] using electrical resistivity measurements. These researchers found that the martensitic transformation is more complicated than previously thought [37]. It was found that other

phases can influence the martensitic transformation of NiAl. The metastable phase Ni_2Al (hexagonal crystal structure) was observed for alloys between 62 and 63at.% Ni. For alloys with 63 to 66at.% Ni the Ni_5Al_3 (orthorhombic crystal structure) forms from martensite then decomposes into Ni_3Al and NiAl upon heating. Neither Ni_2Al nor Ni_5Al_3 have been reported in Pt-modified β bond coat alloys.

Another paper focusing on the martensitic transformation of binary NiAl [40] provided two very interesting observations. While this paper was primarily interested in the mechanical effects of martensite formation, two previously unreported mechanisms behind NiAl martensite formation were proposed. The first observation was that in addition to being thermally driven, martensite formation can also be stress-driven; the researchers found that martensite forms at crack tips within the β phase. The second observation was that β did not transform completely to martensite at the M_s temperature, but instead seemed to increase its volume fraction as it cooled. A graph showing the increase in martensite volume fraction is shown in figure 13.

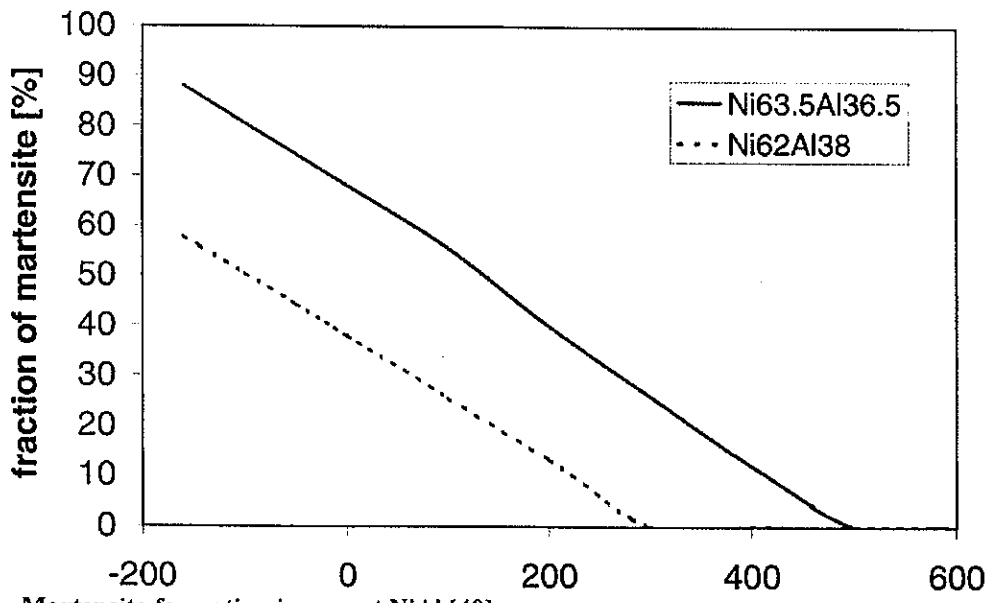

Figure 13. Martensite formation in as-cast NiAl [40]

In contrast to the binary NiAl system, the martensitic transformation in the Pt-modified aluminides has only very recently been reported. While martensite has been observed for both aluminide bond coats [23, 33, 41] and bulk alloys [12] which were cyclically oxidized, only one paper [42] studied the martensitic transformation in any detail. Chen et al. [42] used high temperature x-ray diffraction (HT-XRD) and differential thermal analysis (DTA) to examine the reversible β-to-martensite transformation that occurred within a commercial bond coat. The researchers concluded that the critical cooling rate for martensite formation was less than 25°C/min (faster cooling rates would form martensite, slower rates would not) and that the transformation temperature for the commercial bond coat was much higher than the binary alloy. Unfortunately, since a commercial coating was used, the composition dependence of the transformation was not investigated. Further study of the martensitic transformation in bulk Pt-modified aluminides will be a major focus of this thesis.

4.2 Phase Transformations Within the γ+γ' System

Only two papers [8, 12] have reported on the oxidation behavior of potential bond coat alloys based on the γ+γ' system. An alloy with the composition in at.% of 48Ni-22Al-30Pt was found to have good oxidation performance, but a cross-section revealed a rumpled surface as shown in figure 14 [8]. A subsurface γ layer formed due to selective oxidation of aluminum. Additionally, the rumpled alloy in figure 14 shows the formation of a layer containing α-NiPt(Al). The researchers attributed α formation to the back diffusion of Pt from the γ layer into the alloy. As of this date, there have been no papers published on the oxidation of superalloys coated with γ+γ' alloys. It is important to note that severe phase changes due to aluminum depletion (as have been observed in aluminide coatings) would not be expected for γ+γ' alloys due to uphill diffusion of aluminum from the substrate into the coating [8]. The transformations that occur in γ+γ' alloys will be researched for this thesis work.

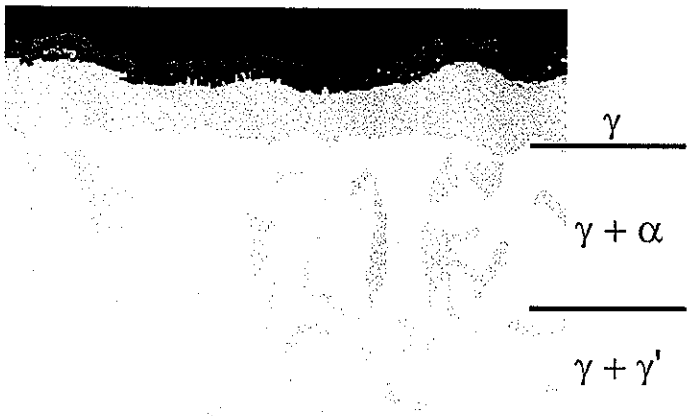

Figure 14. Microstructure of 48Ni-22Al-30Pt after 1000 1 hour cycles at 1150°C in air [8]

Chapter 5: The Rumpling Phenomenon

As mentioned in chapter 2, the rumpling of Pt-modified aluminide bond coats has emerged as a critical mechanism behind the failure of TBCs. While the negative consequences of these surface undulations are widely agreed upon, the mechanisms that lead to the formation of rumpling are very much disputed. A wide variety of mechanisms have been proposed, some papers have listed a combination of mechanisms while some have focused on only one mechanism. Nearly all studies have utilized cyclic oxidation of commercially prepared coatings on superalloy substrates.

In 1987 Deb et al. [14] published one of the earliest papers to focus on rumpling, and proposed three possible mechanisms that could be responsible for this phenomenon: the thermal expansion mismatch between the coating and substrate and possibly between the coating and oxide; thermal gradients within the coating system; and variations in coating mechanical properties. These researchers observed rumpling with a wavelength of approximately 100 μm and amplitude of 20 to 50 μm for samples cycled to 1100°C, but none for isothermally oxidized samples. All Pt-modified samples showed good bond coat/TGO adherence, as have nearly all similar coatings studies since. The researchers did not report any precipitates forming in the coating. It was found that thicker coatings, which had a higher concentration of Al, did not rumple as severely as the thinner coatings. The researchers attributed this to an increased strength in the thicker coatings that counteracted the effects of a larger coefficient of thermal expansion. Unfortunately, no measurements of mechanical strength or thermal expansion were reported by the researchers; instead, the changes in mechanical properties were only inferred from the results of the experiments.

There was very limited research on rumpling during the 1990's, with the noticeable exception of the 1995 paper by Pennefather and Boone [15], which reported rumpling in MCrAlY bond coats and stressed the importance of further research. In 2000 an extensive experimental investigation of rumpling in Pt-modified aluminide bond coats applied to single

crystal substrates was reported by Tolpygo and Clarke [16]. These researchers cyclically and isothermally oxidized the samples at both 1150°C and 1200°C. Rumpling was observed to have wavelengths between 30 and 50μm and amplitudes that increased during oxidation. These researchers investigated the effect of residual compressive stress in the oxide and found that even when compressive stresses differed by a factor of two after oxidation at 1200°C, no differences were observed in the extent of rumpling of the samples. The second possible mechanism behind rumpling that was investigated was the effect of differences in thermal expansion coefficients between the bond coat and the superalloy substrate. Samples exposed to the same number of cycles, but with different amounts of time at 1150°C showed major differences in rumpling. Since the samples experienced the same amount and severity of heating and cooling, differences in thermal expansion could not be the only mechanism behind rumpling. Upon examination of the bond coat after oxidation, γ′ precipitates were observed. As shown in figure 15, γ′ formed a continuous subsurface layer in the cyclically oxidized samples, while the isothermally oxidized sample had more randomly distributed γ′ precipitates along with large cavities in the bond coat layer. Mumm et al. [44] also observed a correlation between γ′ formation and rumpling.

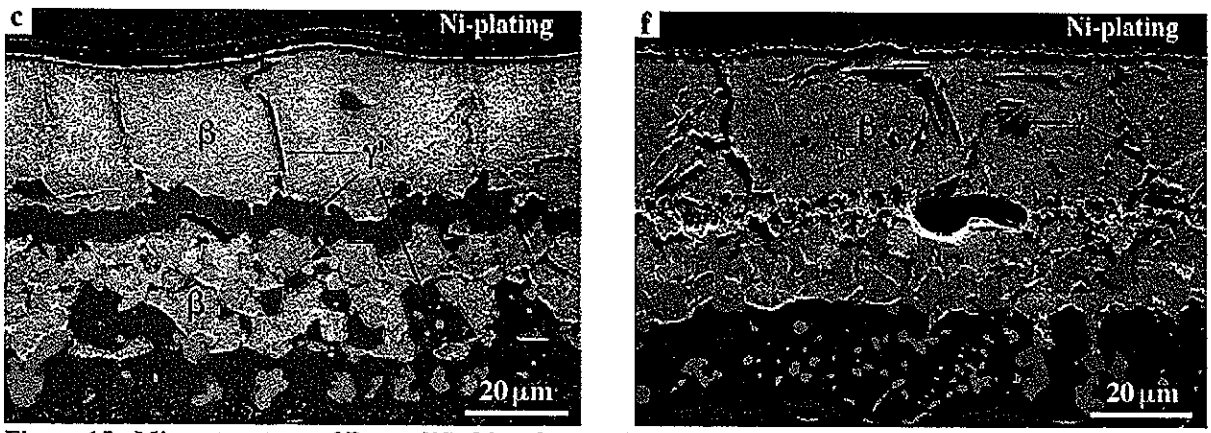

Figure 15. Microstructure of Pt-modified bond coat after cyclic (c), and isothermal (f) oxidation at 1150°C [15]

Tolpygo and Clarke [16] describe the work done in a previous paper by He et al. [43] in which a model to explain rumpling is presented. The mechanism described by He et al. [43]

relies on a phenomenon called "ratcheting". Ratcheting is said to be due to the differences in thermal expansion between the substrate and a surface film (the oxide in our case), and requires plastic yielding of the substrate once the stress becomes large enough. The model that was developed also required a critical sized undulation before the ratcheting could proceed. Tolpygo and Clarke [16] did not accept the mechanism proposed by Chen et al., [42] due to its implication that rumpling would be expected in all metal-oxide systems that develop compressive stresses in the oxide. The other issue that the researchers had with the model was that it would predict rumpling in bulk aluminides, which had not been observed.

The explanation for rumpling that is given by Tolpygo and Clarke [16] contains two mechanisms which both are related to a volume decrease of the bond coat during oxidation. As was previously mentioned, a transformation from β to γ′ was observed; according to these authors, this transformation has an associated volume reduction of 38%. In their calculations these authors appeared to neglect the stoichiometry of the phases, and the actual volume change would be lower. Since a non-zero volume change would still be expected for the β-to-γ′ transformation, the theory behind their model is still applicable. The model also requires a TGO that is relatively weak and plastically deforms to conform to any undulations that form in the bond coat. Since both the isothermal and cyclic samples showed γ′ formation, and yet, only the cyclic samples rumpled, these authors examined the voids that were only present in the isothermally oxidized samples. It was determined that the voids were most likely Kirkendall porosity resulting from the flux of vacancies which compensates for the diffusion of Ni and Al towards the surface of the alloy. Tolpygo and Clarke further theorized that under cyclic oxidation the pores collapsed due to thermal stresses, leading to a larger decrease in volume for the cyclic samples. This theory explains why rumpling is only seen in the cyclically oxidized samples.

In a 2003 paper by Panat et al. [20], the existing mechanisms that had been proposed to explain rumpling were considered, and a new mechanism based on studies from the

semiconductor industry was developed. The researchers propose that stress-driven diffusion is responsible for rumpling. The model focuses on diffusion in the bond coat near the TGO interface, and ignores any interaction between the bond coat and the substrate. The driving force behind the diffusion at the surface of the bond coat is the thermal mismatch stress that develops from thermal cycling. The thermodynamic quantity that then drives the shape change is the chemical potential. The chemical potential is affected by changes in the elastic strain energy, the surface energy of the bond coat, and curvature of the bond coat. Differences in chemical potential at the surface affect the diffusion of atoms there, leading to variations in the growth velocity. While the researchers developed a model which predicts rumpling wavelengths that are within the range that has been experimentally observed, their model requires the surface to have an initial waviness. The model does not include any other mechanisms besides stress-driven diffusion in its explanation of rumpling.

A model which considers the effects of the substrate, the bond coat and the TGO was developed by Balint and Hutchinson in 2003 [21]. This model first examines the oxide and bond coat individually, with an emphasis on the martensitic transformation as reported by Chen et al. [33]. The researchers then combined the substrate, the bond coat and the TGO which had an initial surface undulation, and executed a simulation which showed undulation growth with thermal cycling. The model did not take into account the formation of any precipitates in the bond coat. In a 2005 paper by Balint and Hutchinson [45], the researchers expanded on their previous model. The influence of the martensitic transformation on rumpling was expanded upon and it was discovered that decreasing the temperature at which the transformation occurs by 200°C could reduce the magnitude of rumpling by an order of magnitude. It was also found that the addition of a top coat could reduce the magnitude of rumpling by the same amount. Another observation was that undulations with longer wavelengths would grow faster than those with shorter wavelengths, thus leading to an increase in average wavelength as the simulation progressed. The model predicted that a

bond coat that was not connected to a substrate would not rumple and did not consider any compositional changes within the bond coat as the experiment progressed.

Three very recent papers by Tolpygo and Clarke [22-24] have expanded on their previous work on rumpling. The first paper [22] focused on the effect of coating thickness and found that rumpling was at a maximum with a coating thickness of between 100 and 150μm. The authors used this finding to show that neither the thermal expansion mismatch with the substrate nor the growth stress in the oxide could explain rumpling of the bond coat. The compositional differences in the coatings did not seem to be given enough consideration, and the authors' conclusion that bulk alloys or very thick coatings would not rumple, may be in error. In order for an accurate comparison to be made, the compositions of the bulk alloys or thick coatings would have to reflect the significant depletion of Al that takes place during oxidation of the thin coatings. Measurements of the tortuosity of the rumpled surface led the researchers to describe an "elongational strain" in the coating. As in their previous paper [16] a compositional change, i.e. the formation of γ', was considered a likely cause of rumpling due to its contribution to the elongational strain.

Tolpygo and Clarke also published a two-part paper covering the results various oxidation experiments [23] and the characterization of those results [24]. In addition to testing Pt-modified aluminide coatings, a bulk alloy was prepared with a similar composition to the bond coat; the composition created was: 45.5at.% Ni, 43.7at.% Al, 5.5at.% Pt, 3.6at.% Co, and 1.7at.% Ni. Between 50 and 200 ppmw Y was then added to improve scale adherence. The bulk alloy was never observed to rumple. One of the experiments involved thermally cycling a coated sample in a vacuum. This experiment minimized the possible role of oxidation on rumpling since the sample showed rumpling with only a very thin scale from pre-oxidation. The researchers also investigated the possible effect of a martensitic transformation on rumpling. Through cyclic oxidation experiments which were designed to avoid the martensitic transformation, but still resulted in rumpled samples, the martensitic

transformation was ruled out as a mechanism which causes rumpling. Additionally, it was found that attributing rumpling solely to the formation of γ' was incorrect, since rumpling was observed prior to any β transforming to γ'. The researchers again looked at the effect of thermal mismatch between the substrate and the coating, but the magnitudes of the calculated results using only differences in thermal expansion were much too low to account for the severity of the observed rumpling. None of the possible mechanisms sufficiently explained the formation of rumpling.

Part II of the two part paper by Tolpygo and Clarke [24] expanded on their observation of bond coat "swelling". During the first hours of oxidation, the bond coat increased in thickness by approximately 10%. The bond coats of samples which were cyclically oxidized continued to grow, eventually becoming 13 to 15% thicker. The isothermally oxidized samples had bond coats that did not get thicker after the initial period, and actually ended up being only 8 to 9% thicker than they were before oxidation. Since Al lost to the formation of the oxide would serve to reduce the thickness of the bond coat, interdiffusion between the coating and the substrate seems to be the cause of bond coat swelling. It was found that the rate of Ni diffusing into the bond coat was greater than the rate of Al diffusing from the bond coat into the substrate, thus the swelling of the coating. It is suggested that swelling, specifically of individual grains within the bond coat, may be responsible for rumpling. A detailed study of the mechanical effects of swelling has not yet been published.

Chapter 6: Aims of Current Project

The primary goal of this research is to gain a more detailed understanding of the rumpling phenomenon in current and potential nickel aluminum alloys. The specific goals can be summarized as follows:

-To determine the role of subsurface α-phase formation in the rumpling of γ-γ′ alloys

-To investigate the nature of the martensitic transformation in β alloys and the effects of Pt addition

-To determine the role the martensitic transformation in the rumpling of β alloys

Chapter 7: Experimental Procedures

The samples used in this study were prepared by the Materials Processing Center (MPC) at Ames Laboratory. The samples were prepared by arc melting high purity pieces of the constituents in an argon atmosphere. Next, the samples were then drop-cast into 10 or 12mm diameter rods while under argon. The rods were then annealed in argon for 24 hours at 1200°C, then 5 days at 1150°C to homogenize.

7.1 Isothermal Oxidation

1mm thick sections were cut from the annealed samples and the surface was polished using 1μm diamond polish or 240, 600, 1200 coarse, or 1200 fine grit SiC paper on one side only. The samples were placed polished side up in an alumina tray and then inserted into a preheated 1150°C horizontal tube furnace. Both ends of the furnace were left open to the atmosphere in the room. After the desired time for isothermal oxidation was reached, the samples were either cooled at 15°C/min in the furnace, pulled to the very end of the furnace tube to air cool, or were immediately quenched in water.

7.2 Cyclic Oxidation

Once again, 1mm thick sections were cut from the annealed samples and the surface was polished using a 1μm diamond polish or SiC paper to a 240, 600, 1200 coarse, or 1200 fine grit finish on one side only. Two different types of furnaces were used for cyclic oxidation experiments. The first type was a horizontal tube furnace open to the room atmosphere on both ends. The samples were placed polished side up on alumina trays and placed in the room temperature furnace. The furnace was programmed to ramp to 1150°C at 15°C/min, hold for one hour, then cool to a lower temperature at 15°C/min for an hour dwell. The cycles were repeated until the desired number of cycles was reached, upon which time the

furnace was programmed to cool to room temperature from the lower temperature at 15°C/min.

The second type of furnace used was a two zone vertical tube furnace which was open to the atmosphere in the room. The samples were placed in cylindrical alumina crucibles with the polished side facing upwards. Up to 5 crucibles, each containing one sample, were suspended from a rod which positioned the samples within the furnace. The upper and lower furnaces were set to the desired upper and lower dwell temperatures, respectively. The dwell time at each temperature, as well as the number of cycles, was programmed and the positioning rod transported the samples to the top zone of the furnace where the experiment would begin. If room temperature was desired for the low temperature dwell the sample positioning rod would lower the samples all the way to the bottom of the furnace tube.

7.3 Profilometry

After oxidation testing the surfaces of all samples were characterized using a Hommelwerke stylus profilometer. A 2mm wide by 3mm long area was scanned on all samples. The scanned area consisted of 600 2mm long scans. A TK300 stylus was used with a vertical measurement range of 80μm. A scan speed of 0.5mm/s and a cut-off length (λ_c) of 0.25mm were used. All measured surface parameters were recorded. After performing the scan a program entitled *HommelMap Basic* was used to generate images like the one shown in figure 16. A waviness filter with a cut-off of 0.4mm was applied to the surface profile in order to level the image.

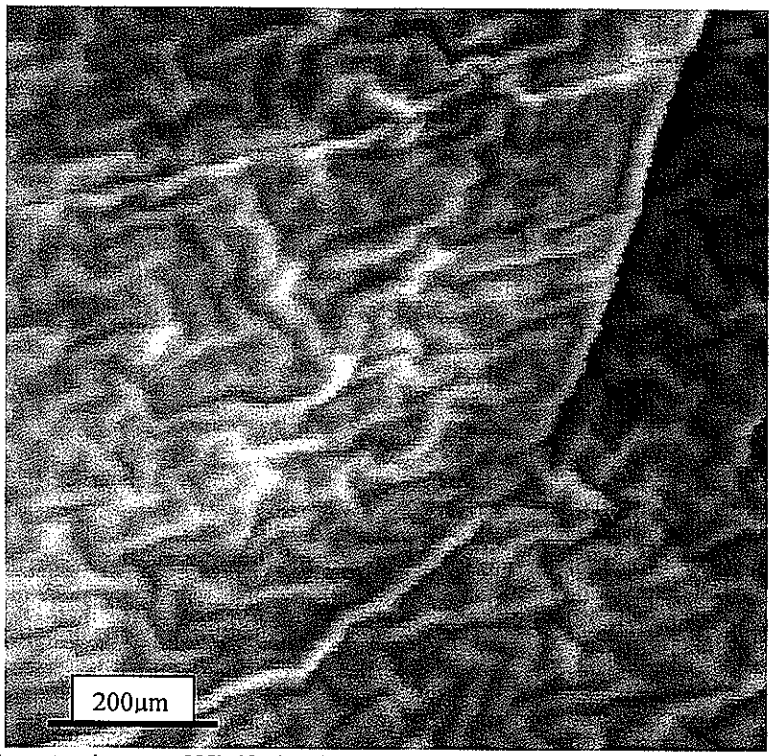

Figure 16. A profilometry image of Ni-40Al-15Pt cycled 100 times from 1150°C to 750°C after a 1μm polish

7.4 Microscopy

Both cross sections and surfaces of the oxidized specimens were observed using scanning electron microscopy (SEM). The specimens were first cut in half using a high speed cut off wheel. The specimens were then sputter coated with a thin layer of gold. One half was kept in the gold coated state for surface imaging. In order to preserve the TGO, the second half was electroplated with approximately 100μm of copper before mounting in epoxy. After curing, the epoxy mounted sample was ground using SiC paper, then polished using 1μm diamond polish to reveal the cross section. The polished surface was sputter coated with gold in preparation for SEM analysis. Both secondary and back-scattered electrons were used for analysis.

7.5 High-Temperature X-ray Diffraction (HT-XRD)

HT-XRD testing was performed at the 6-IDD MUCAT beam line at the Advanced Photon Source (APS) at Argonne National Lab. The energy of the photons from the APS was 97.844KeV. Samples were prepared by Matt Besser from homogenized ingots by pulverizing in a mortar and pestle, or in a freezer mill if the samples were too ductile at room temperature. The samples were pulverized until a particle size of less than 500μm was obtained. Next, the samples were then sealed in 2mm quartz capillaries under 1/3atm Ar. Then the samples were then placed in a resistively heated furnace directly in line with x-ray beam and continuously rotated during the experiments. A MAR 345 image plate collected the diffracted x-rays, with an exposure time of 30 seconds. Reitveld refinement of the data was performed by Matt Besser using GSAS software.

7.6 Differential Scanning Calorimetry (DSC)

Martensite forming Pt-modified nickel aluminides were tested at the High Temperature Materials Laboratory (HTML) at Oak Ridge National Lab. Specimens were created by machining discs 1.5mm thick and 6mm in diameter. The specimens were placed in Pt crucibles and tested under flowing Ar. A sapphire reference was used to obtain the measurements. The testing took place between room temperature and 1200°C. Heating and cooling rates of between 2 and 40°C/min were used, as were isothermal holds at various temperatures. Both phase transformation and heat capacity measurements were taken.

7.7 Mechanical Testing

In order to gain a better understanding of the mechanisms behind the rumpling that has been observed in the $\gamma+\gamma'$ alloy 48Ni-22Al-30Pt, mechanical testing was performed by Dr. J. Dan Whittenberger at the NASA-Glen Research Center. Compositions of the various phases present in this alloy and a lower Pt content alloy after oxidation (see figure 14) were

measured using an electron probe microanalyzer (EPMA), and alloys with the compositions of the various phases were cast by the MPC at Ames Laboratory. Additionally, 2 alloys were created to examine the effect of Pt on the strength of the γ phase. After homogenizing the alloys, electrical discharge machining (EDM) was used to create samples 4mm in diameter and 8mm in length from the original castings. In particular, the high temperature slow plastic flow properties of the alloys were tested using constant velocity compression tests which were performed in a universal test machine. The samples were tested at 1000, 1200, and 1400K with strain rates of approximately $2*10^{-3}$, $5*10^{-5}$, and $2*10^{-6}s^{-1}$.

7.8 Potentiometric Measurements

An additional method to observe the martensitic transformation in Ni-rich Pt-modified aluminides was through the use of potentiometric measurements. EDM was used to create 45mm long samples which were 3mm thick and 3mm wide. Four electrical connections were made on each sample by spot welding inch long pieces of 24 gauge Pt wire as shown in figure 17. The two electrodes welded near the ends of the sample were used to pass a current through the sample and the two inner electrodes, which were welded 1cm from the other electrodes, were connected to a voltmeter. The specimen was tested in Dr. David Cann's laboratory at Iowa State University. Testing took place inside of a sealed alumina tube under flowing argon. The tube was placed in a furnace and the voltage change as a function of temperature was recorded.

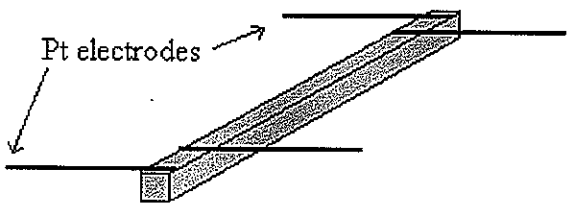

Figure 17. Resistivity specimen showing relative locations of Pt electrodes

Chapter 8: Results and Discussion

The experiments performed for this thesis can be separated into two groups by the type of alloy that was studied. The first group contains the isothermal oxidation experiments on γ-γ′ alloys and the mechanical testing results based on these alloys. The second group contains the experiments which were used to investigate the martensitic transformation and the cyclic oxidation experiments performed on β alloys.

8.1 Isothermal Oxidation of γ-γ′ Alloys

Two γ-γ′ alloys were chosen for study based on their previously observed oxidation behavior. The compositions of these alloys were Ni-22Al-30Pt (#7) and Ni-22Al-25Pt (#28) in atomic percentages, with Ni making up the remainder. (All alloy compositions in this work will be provided in atomic percent unless otherwise noted.) As illustrated in figure 18, it was discovered that after 100 hours at 1150°C, alloy #7 would rumple, while the alloy slightly lower in Pt, #28, would not.

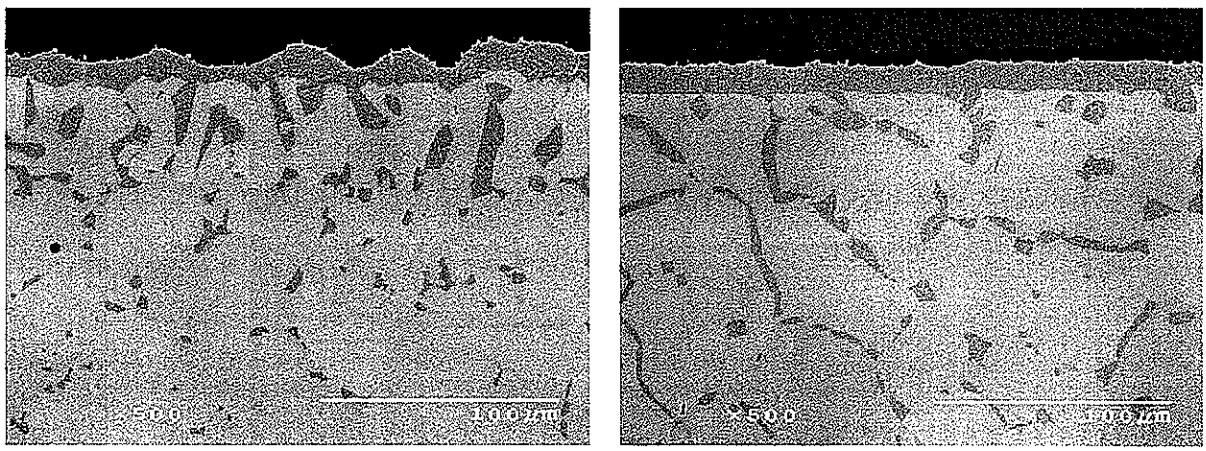

Figure 18. Alloys #7 (left) and #28 (right) after 100 hours at 1150°C, 1200 grit initial finish, cooled at 15°C/min

The following three variables affecting rumpling were examined: (i) the surface finish of the sample; (ii) the time of exposure; and (iii) the cooling rate from 1150°C. In order to quantitatively compare the samples, two statistical parameters from profilometry were

chosen to represent the amplitude and wavelength of the rumpled surface. The first parameter, $R_{z(DIN)}$, is the mean peak-to-valley height measurement and corresponds to the average amplitude of a given scan. The second parameter, λ_a, is the average wavelength within a given scan. $R_{z(DIN)}$ is calculated using a relatively simple method; the profile is divided into 5 equal sections (in this case, 400μm long) and the height difference between the lowest valley and the highest peak is measured for each section, then the 5 values are averaged to give a $R_{z(DIN)}$ value for that scan. λ_a is a slightly more involved calculation; it includes both wavelength and amplitude, differing it from the mean peak-to-peak parameter S_m. Since rumpling is at least somewhat periodic, λ_a is generally very close to the values calculated for S_m. λ_a is calculated by dividing the average roughness, R_a, by the slope, Δa, then multiplying by 2π. The average roughness was calculated using a sampling length of 1.67mm. The $R_{z(DIN)}$ and λ_a for each of the 600 scans which make up a 2 by 3mm area can then be averaged to obtain values for the entire scanned area.

To compensate for sample tilting or macroscopic deformations at the surface of the samples, a filtering algorithm was applied to the raw profilometry data. A cut-off of 0.8mm and a filter size of 0.8 by 0.8mm were used on all samples. The chosen cut-off size was sufficiently large enough for all features of interest to be unaffected. As a result of the filtering, 0.8mm in both the x and y-directions are lost in the final image. Profilometry images of the two samples shown in figure 18 are shown in figure 19. After filtering, individual profiles can be extracted from any location within the image. A horizontal extracted profile is essentially identical to the raw data for the scan at that location. An example of an extracted profile for the upper image in figure 19 is provided in figure 20. The $R_{z(DIN)}$ and λ_a values for that scan are included for reference.

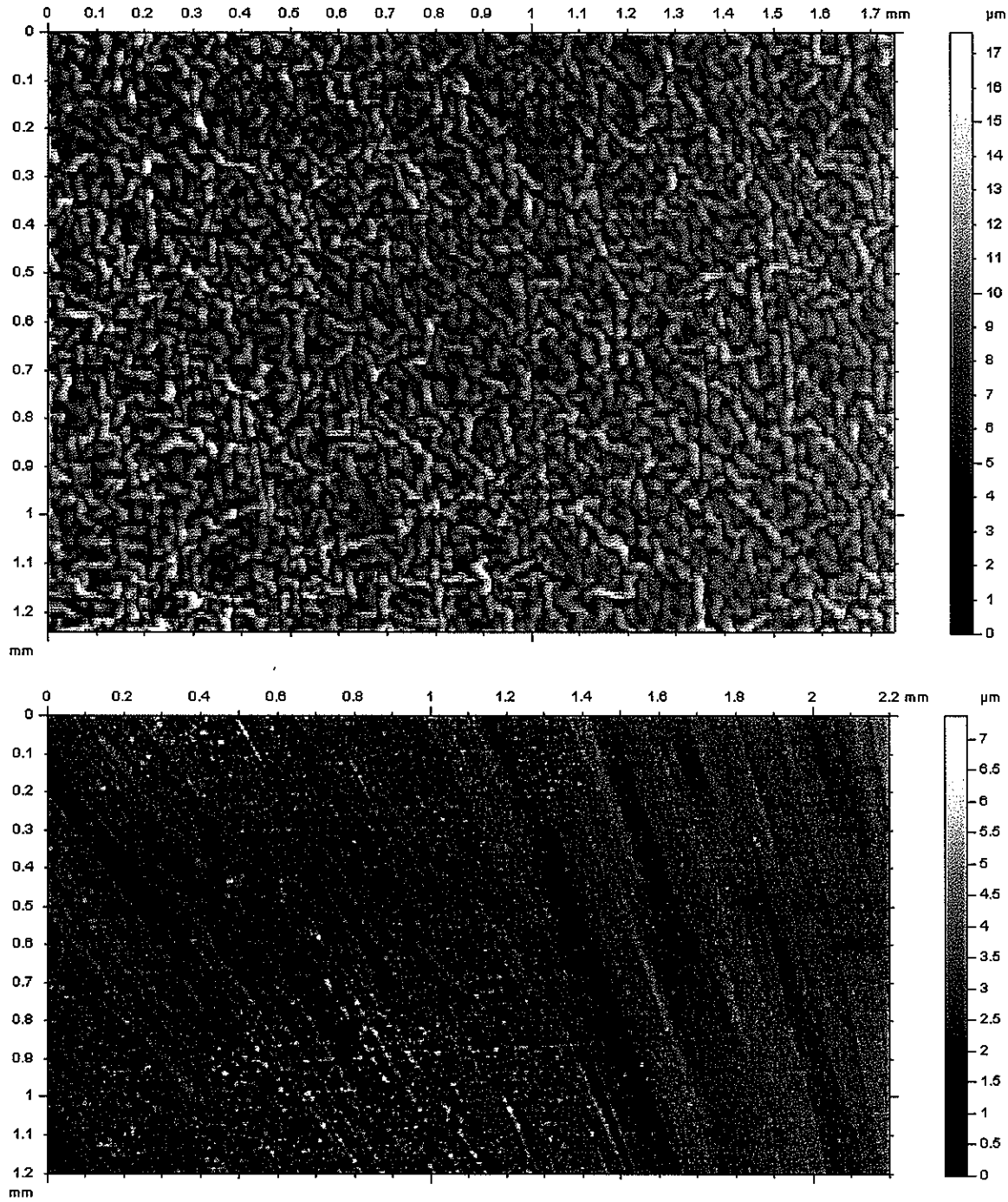

Figure 19. Alloys #7 (top) and #28 (bottom) after 100 hours at 1150°C, 1200 grit initial finish, cooled at 15°C/min

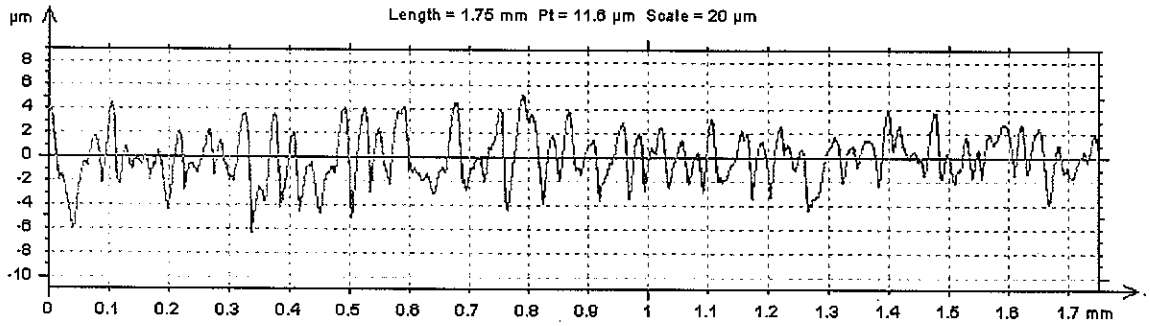

Figure 20. Extracted profile for alloy #7 after 100 hours at 1150°C, coarse 1200 grit initial finish, cooled at 15°C/min, $R_{z(DIN)}$ = 10.2 µm and λ_a = 32.2µm

Upon examination of the extracted profile in figure 20, it seems that the calculated $R_{z(DIN)}$ and λ_a values provide very reasonable values for both the peak-to-peak amplitude and the wavelength, respectively.

The results of the investigation on the effects of different initial surface finishes, oxidation times, and the cooling rate from 1150°C on the rumpling of alloy #7 are summaraized in table 1. These results are discussed in more detail in the following sections.

Table 1. Summary of results for isothermal oxidation of alloy #7

Surface Finish	Time at 1150°C	Cooling Rate	λ_a	R_{zDIN}
240-grit	no oxidation	n/a	21.8	4.6
1200-grit	no oxidation	n/a	6	0.6
240-grit	100hrs	15°C/min	34.6	12.4
1200-grit	100hrs	15°C/min	32.2	10.2
240-grit	100hrs	500°C/min	39	15.4
1200-grit	100hrs	500°C/min	33.8	11.7
1200-grit	286hrs	water quench	27.5	5.6
1200-grit	100hrs	water quench	29.3	10.3
1µm polish	100hrs	water quench	31.6	9.9
1µm polish	296hrs	water quench	38.9	13.3
1200-grit	110hrs	water quench	33.1	9.6
1µm polish	110hrs	15°C/min	32.9	10.1
1200-grit	110hrs	15°C/min	30.1	8.5

8.1.1 Effect of Initial Surface Finish

In order to illustrate the effect of initial surface finish on rumpling, the results for 2 samples which had identical oxidation exposure, but different surface finishes are presented in figure 21. It was found that samples which were prepared using 240-grit SiC paper had rumpling with both larger amplitude and wavelength than the sample which had been prepared using 1200-grit paper. Profilometry images for the two samples are shown in figure 22 using the same magnification. It is very clear from the images that the sample finished with 240-grit paper has rumpling with a much longer wavelength. When preparing the initial surface, the SiC paper was used in only one direction; top to bottom. It seems that in the case of the 240-grit sample that the rumpling follows the grooves left from the initial finish, while the rumpling in the 1200-grit sample appears independent of grinding direction.

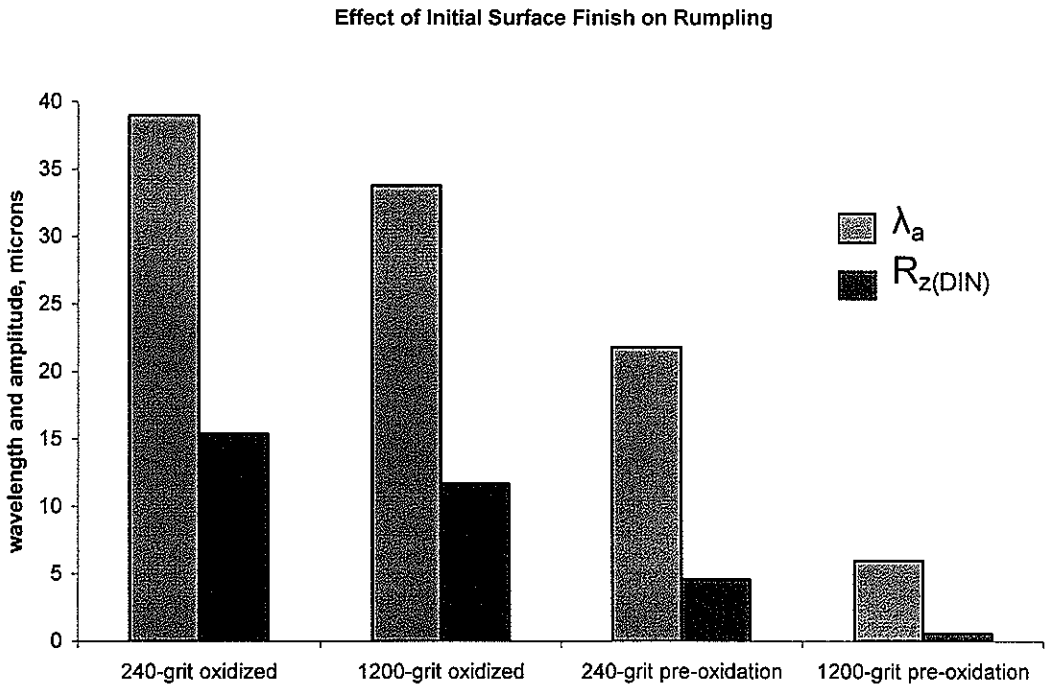

Figure 21. Comparison of the degree of rumpling in alloy #7 after 100 hours at 1150°C and cooled at 500°C/min for 2 different surface finishes, as well as the parameters for the samples prior to oxidation

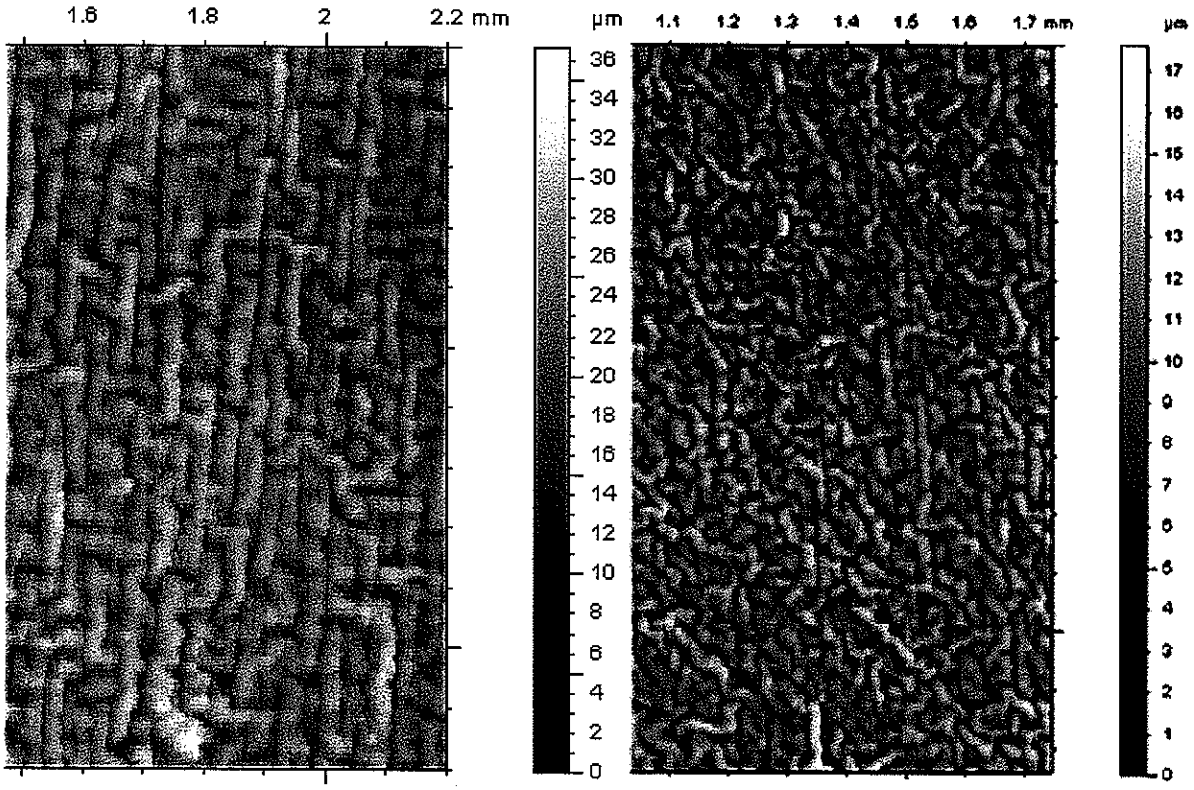

Figure 22. Alloy #7 after 100 hours at 1150°C, 240-(left) and 1200-(right) grit initial finish, cooled at 500°C/min

The results shown in figure 22 introduce an unfortunate limitation of the profilometer. The rumpling in the sample prepared with 240-grit paper is anisotropic and when the profilometer scanned from left to right, it was generally moving perpendicular to the rumpling. In contrast, the sample prepared with 1200-grit paper had nearly isotropic rumpling and the profilometer stylus generally did not perpendicularly cross the individual undulations. When scanning over an undulation at an angle less than 90°, the stylus will remain on the undulation for a greater distance. Because of this, the reported wavelength value, λ_a, will be greater for samples with isotropic rumpling. As illustrated in figure 21, the λ_a value for the 240-grit sample is only 15% greater than the λ_a value for the 1200-grit sample; while figure 22 shows that the true wavelength is closer to twice as great. While the amplitude parameter, $R_{z(DIN)}$, has a spatial component, it is not significantly affected by the direction of the rumpling. Cross-sectional analysis has the same disadvantage of not necessarily providing a perpendicular image of the individual undulations.

While λ_a does not provide the absolute magnitude of the wavelength for samples with isotropic rumpling, comparisons between samples is still possible. The rumpling in samples with 1200-grit and finer finishes does not seem to be influenced by the initial surface. The rumpling parameters of two samples of alloy #7 which were exposed to the same oxidation conditions, but had been polished using either 1200-grit paper or a 1μm polish, were very similar. As shown in figure 23, the rumpling of both samples appeared very isotropic. Because of the isotropic nature of the surfaces, it was determined that the initial surface defects generated by 1200-grit paper or a 1μm polish were small enough not to influence rumpling. In order to draw conclusions about the effects of the other experimental variables (length of exposure and cooling rate), 1200-grit or a 1μm finishes were used in order to eliminate any errors associated with anisotropic rumpling.

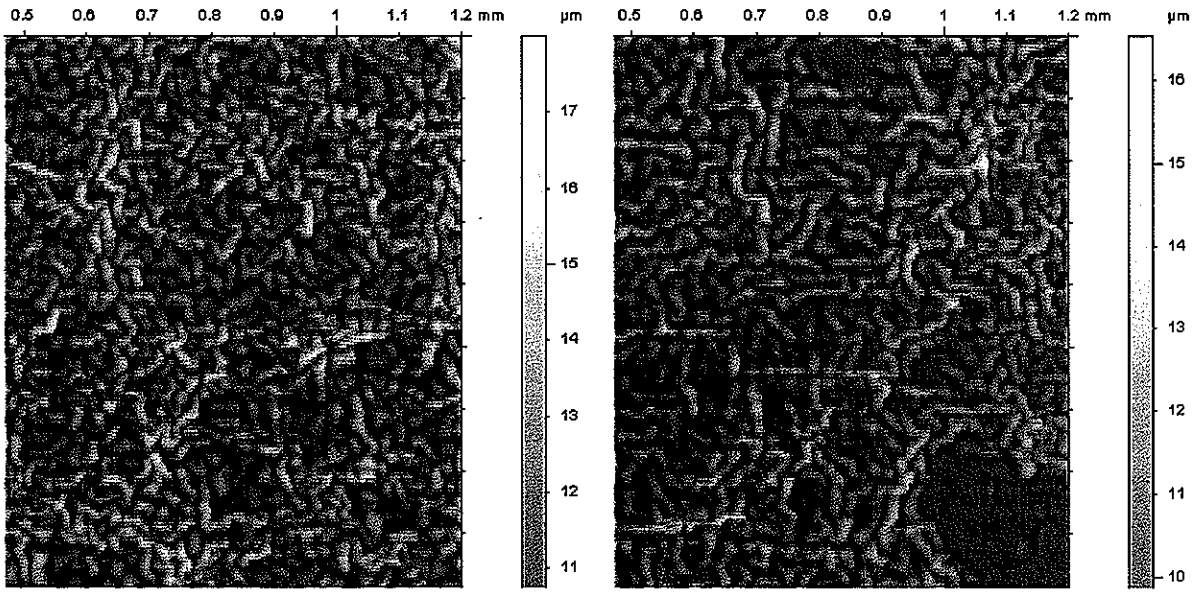

Figure 23. Alloy #7 after 110 hours at 1150°C, 1200-grit (left) and 1μm (right) initial finish, cooled at 15°C/min

8.1.2 Effect of Oxidation Time

In order to determine how the degree of rumpling changes with the length of isothermal oxidation, samples with a 1μm initial surface finish were oxidized at 1150°C for two different durations. Figures 24 and 25 show the resulting rumpling parameters and the

profilometry images, respectively. Error bars indicating plus or minus one standard deviation are included in figure 24. It is relatively clear that both the wavelength and amplitude of rumpling tend to increase with time. The increase in rumpling may be tied to an increase in thickness of a subsurface layer which is examined in the next section.

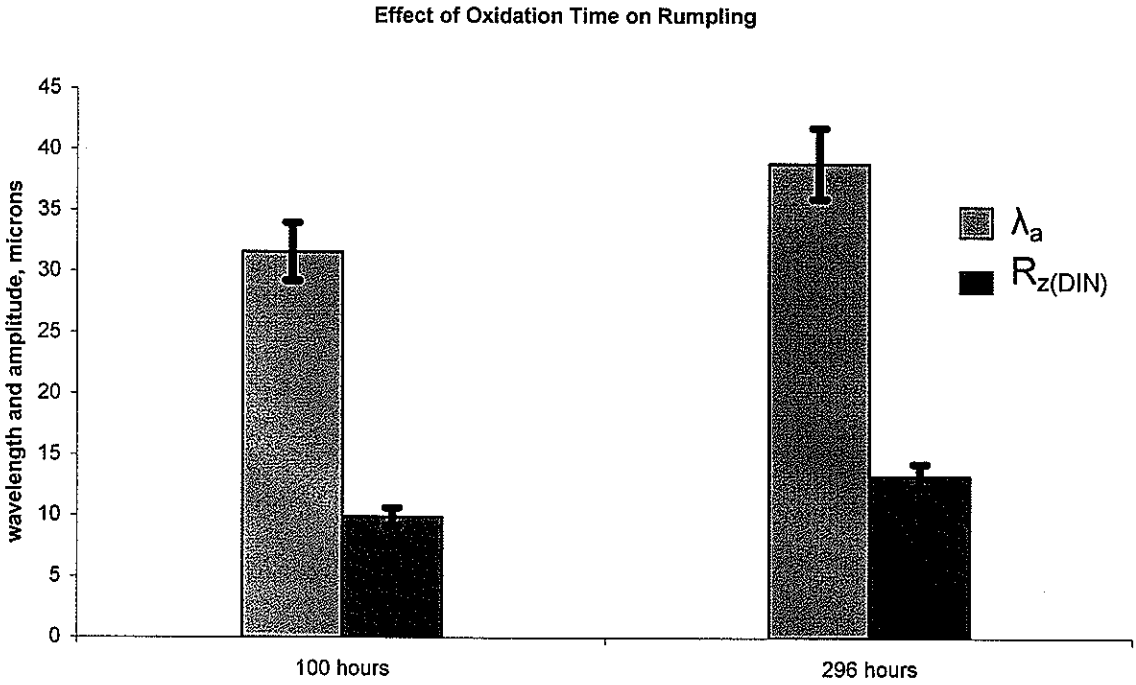

Figure 24. Comparison of the degree of rumpling in alloy #7 with a 1μm initial finish and different amounts of time at 1150°C followed by water quenching

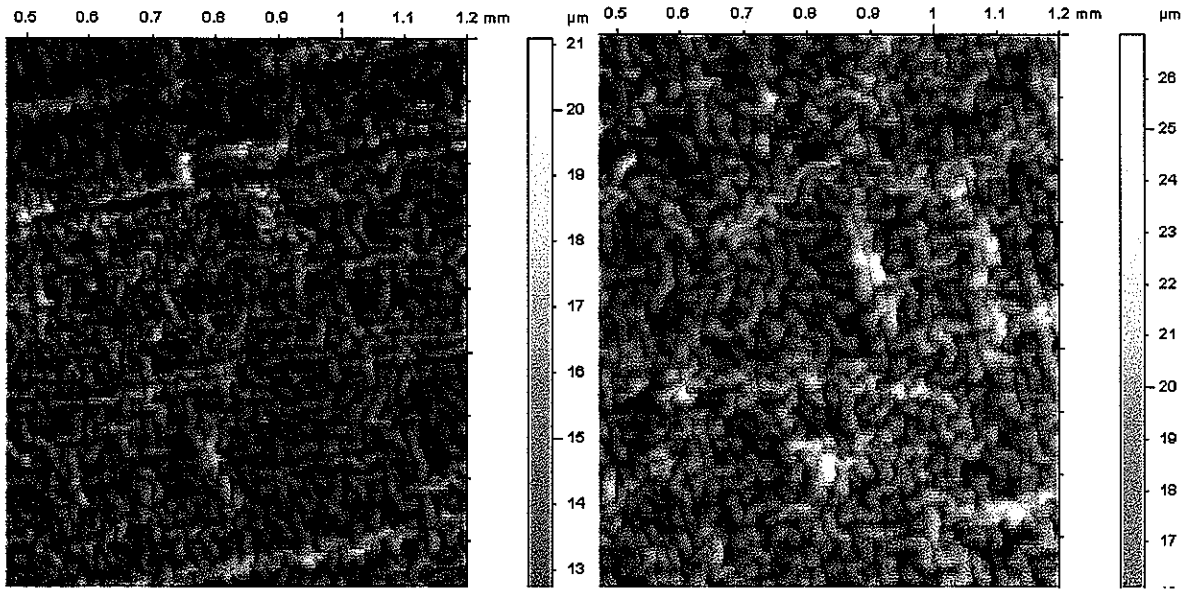

Figure 25. Alloy #7 with a 1µm initial finish after 100 hours (left) and 296 hours (right) at 1150°C followed by water quenching

8.1.3 Effect of Cooling Rate

While the effects of surface finish and oxidation time on rumpling on rumpling in Ni-22Al-30Pt (alloy #7) have been presented, these results offered little insight into the nature of its formation. It was unknown whether rumpling was caused by creep deformation during cooling or if it appeared at temperature during oxidation. If rumpling formed upon cooling then one would expect there to be a difference in the degree of rumpling for samples cooled at different rates, since samples cooled slowly would have longer for creep deformation to occur. A sample quenched in water from 1150°C cools to room temperature nearly instantaneously and would not have any time for creep deformation to occur. To test this, three identical samples were cooled from 1150°C at different rates upon the completion of 100 hours of oxidation at 1150°C. The results of this experiment are presented in figures 26 and 27, and show that rumpling is not significantly affected by the cooling rate. It is therefore reasonable to conclude that rumpling of alloy #7 occurs primarily during the course of oxidation rather than upon cooling. If rumpling occurs isothermally, then any differences in thermal expansion coefficients between the various phases present are irrelevant.

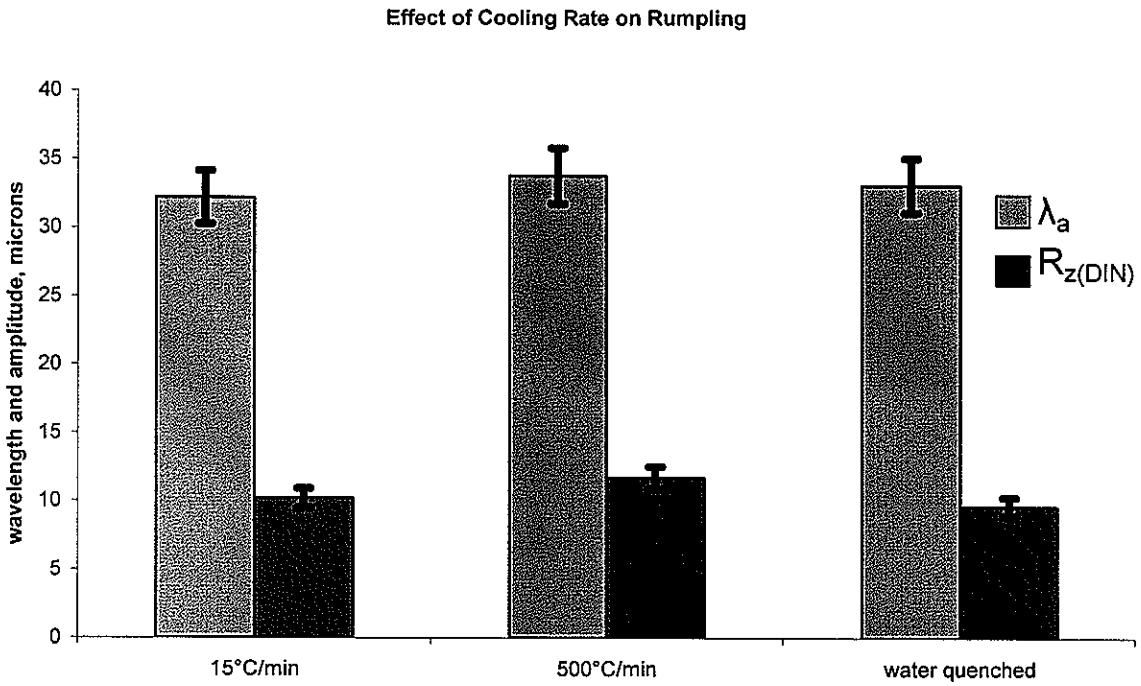

Figure 26. Comparison of the degree of rumpling in alloy #7 with a 1200-grit initial finish after 100 hours at 1150°C followed by cooling at different rates

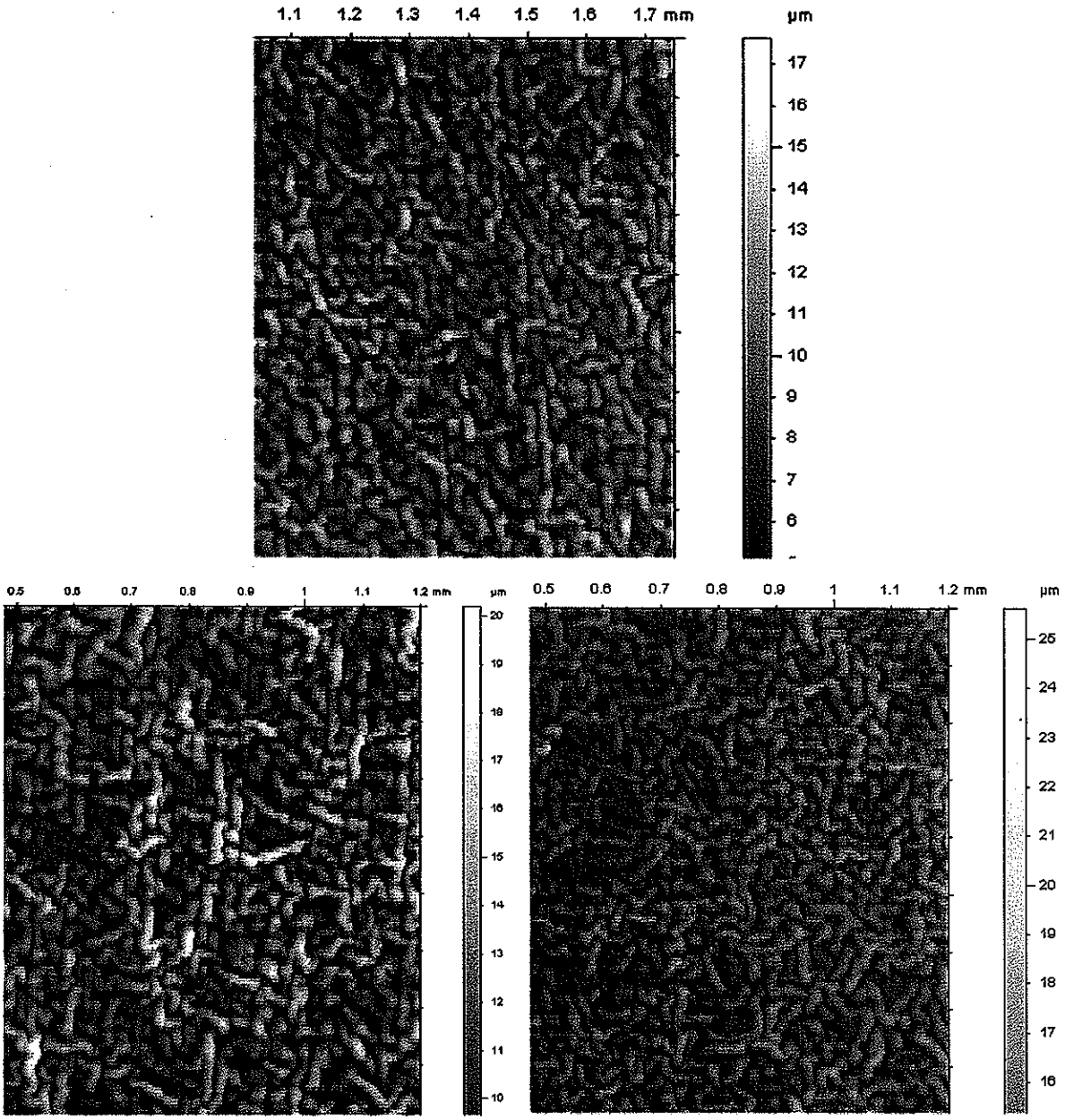

Figure 27. Alloy #7 with a 1200-grit initial finish after 100 hours at 1150°C followed by 15°C/min cooling (top), 500°C/min cooling (bottom left), and water quenching (bottom right)

As mentioned in Chapter 4, the γ- γ' system can undergo a phase transformation which has been shown to occur after isothermal oxidation. Cross sections of the sample cooled at 15°C/min and the sample quenched in water are given in figure 28. The layer closest to the surface consists of the γ phase due to Al depleting to form the alumina scale. While the scale is not visible in figure 28 because the contrast required adjustment to make the subsurface

phases clearly apparent, the thickness of the scale is approximately 4μm. The layer immediately below the γ layer consists of a mixture of γ and the high-Pt α phase. As the subsurface region depletes in Al, there is a simultaneous back diffusion of Pt from the near-surface layer as described in section 4.2. This back diffusion of Pt causes the steady-state diffusion path to enter the two-phase γ+α region as illustrated in figure 29. The microstructure of alloy #7 would be expected to resemble that of alloy #28 (figure 18), having just a γ region at the surface, until the subsurface layer had become sufficiently enriched in Pt to cause the formation of the α phase as shown in figure 28.

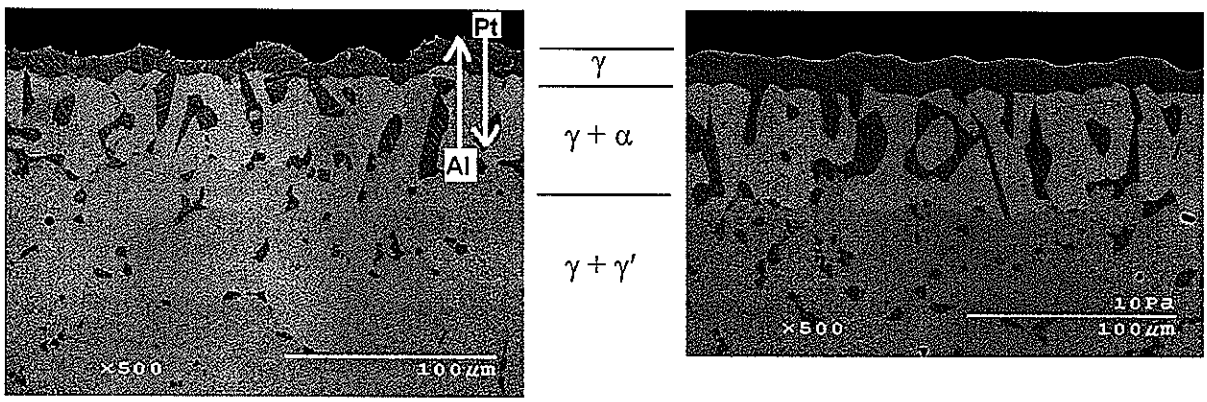

Figure 28. Alloy #7 with a 1200-grit initial finish after 100 hours at 1150°C followed by 15°C/min cooling (left) and water quenching (right) showing the direction of Al and Pt diffusion

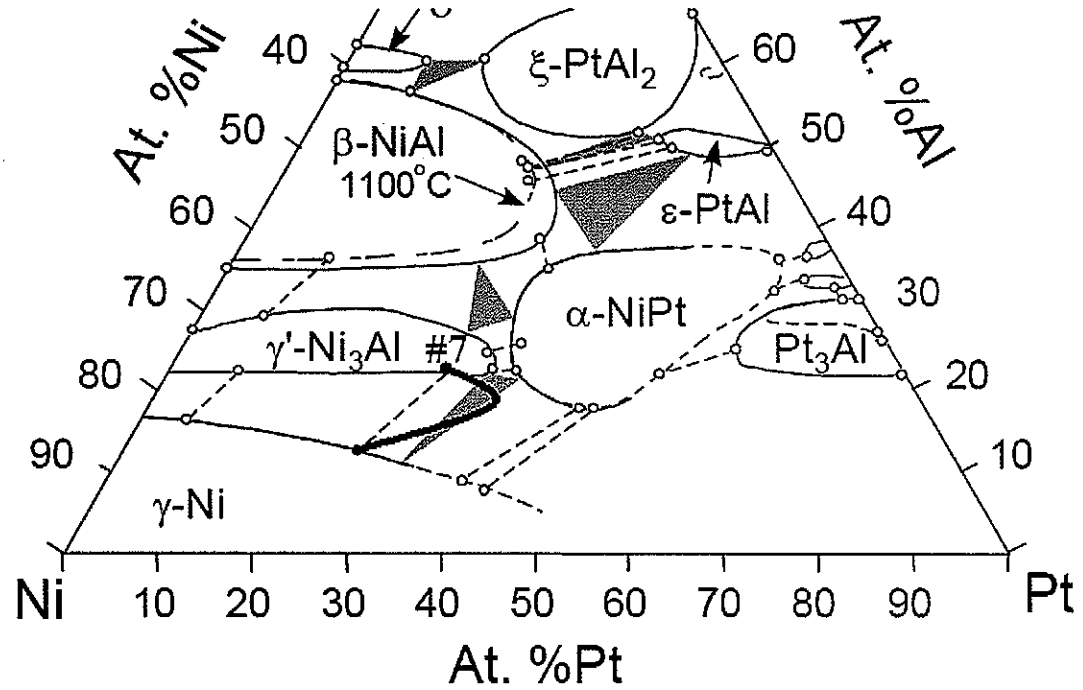

Figure 29. The Ni-Al-Pt phase diagram at 1150°C illustrating the steady-state diffusion path between the bulk composition of alloy #7 and its subsurface γ layer

The subsurface γ layer in the 15°C/min cooled sample from figure 28 contains some needle-like particles that are not present in the water-quenched sample. These particles have been shown to be γ′ that precipitate out of the γ upon cooling; the water-quenched sample does not have time for this precipitation to occur. Since the degree of rumpling in the 15°C/min cooled sample and the water quenched sample are nearly identical, the precipitation of γ′ from γ during cooling does not seem to be of much significance. It is further noted that the lower Pt sample #28 (Ni-22Al-25Pt) does not contain the α phase and does not rumple, as shown in figures 18 and 19. Thus, it appears that the formation of the α phase is associated with the rumpling of γ-γ′ alloys. It may be relevant to note that HT-XRD results (figure 30) have shown that there is a significant unit-cell volume increase associated with the formation of the α phase.

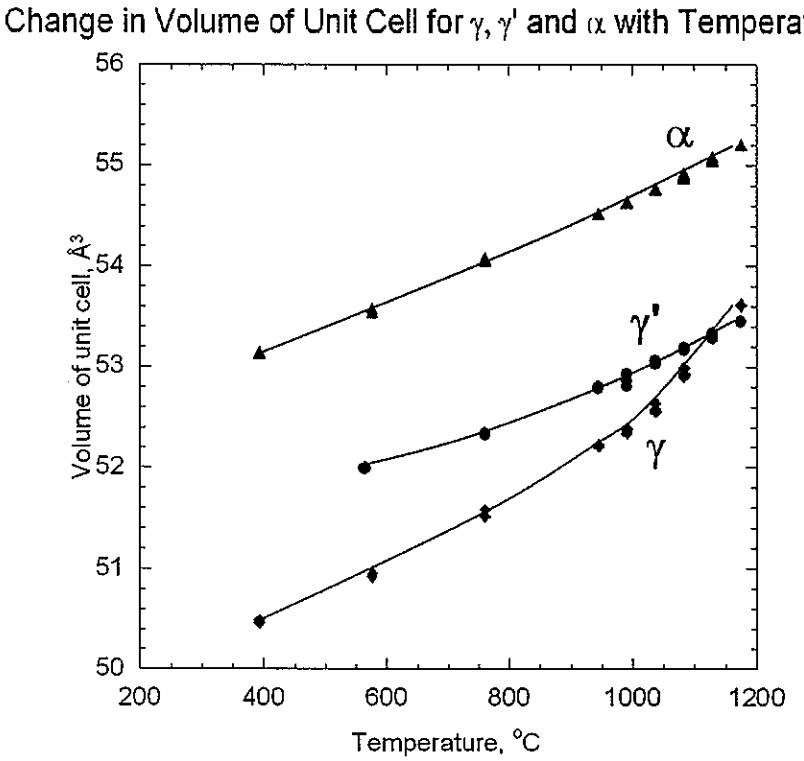

Figure 30. Unit cell volume for the α, γ, and γ' phases

8.2 Mechanical Properties of the γ-γ' System

One of the main objectives behind the testing of the high-temperature mechanical properties in the γ-γ' system was to investigate any effects that differing mechanical properties might have on rumpling. As mentioned in Chapter 7, high-temperature mechanical testing was performed on alloys that were created to have compositions that matched the compositions of the various layers present in γ-γ' alloys after oxidation. As mentioned in section 7.7, the compositions were measured using EPMA. Table 2 provides the origin of each of the 7 samples, as well as a summary of the completed tests. Although stress strain curves for all of the tests were recorded, Table 2 only provides the maximum stress reached in each test.

Table 2. Results for Mechanical Testing of Alloys Based on the γ-γ′ system, *=failed samples

		At fastest strain rate (~$2*10^{-3}s^{-1}$)	At medium strain rate (~$5*10^{-5}s^{-1}$)	At slow strain rate (~$2*10^{-6}s^{-1}$)
	temp (K)	max stress (MPa)	max stress (MPa)	max stress (MPa)
Ni-15Al-15Pt	1000	*876	*836	*567
lower Pt gamma (#28)	1200	*528	307	*161
	1400	129	42	
Ni-15Al-20Pt	1000	*816	*631	*632
subsurface gamma (#28)	1200	512	*307	*154
	1400	119	49	
Ni-15Al-25Pt	1000	*838	*703	
subsurface gamma (#7)	1200	539	*311	
	1400	135	62	
Ni-23Al-26Pt	1000	*845	*423	
gamma prime (#28)	1200	*521	*271	
	1400	312	*76	
Ni-22Al-30Pt	1000	*848	*673	
original #7	1200	*488	*404	*137
	1400	270	98	19
Ni-24Al-33Pt	1000	1200	869	662
alpha (#7)	1200	578	265	63
	1400	190	48	13
Ni-18Al-40Pt	1000	920	726	469
gamma + alpha (#7)	1200	485	214	77
	1400	161	62	

The asterisks in Table 2 indicate that the sample failed by either cracking or shear failure prior to the completion of the test at 8% strain. While the samples that were tested at 727°C had significantly higher strengths than those tested at 927°C or 1127°C, they were also much more likely to fail before reaching 8% strain. The α-containing samples had the highest strengths at 727°C and never failed during a test. At higher temperatures, however, the α phase lost its strength very quickly. At any given temperature, the maximum stress decreased due to increased creep of the sample as the strain rate decreased. Creep is minimized at higher strain rates, and a plot comparing the stress-strain curves for five of the alloys at the highest strain rate is shown in figure 31.

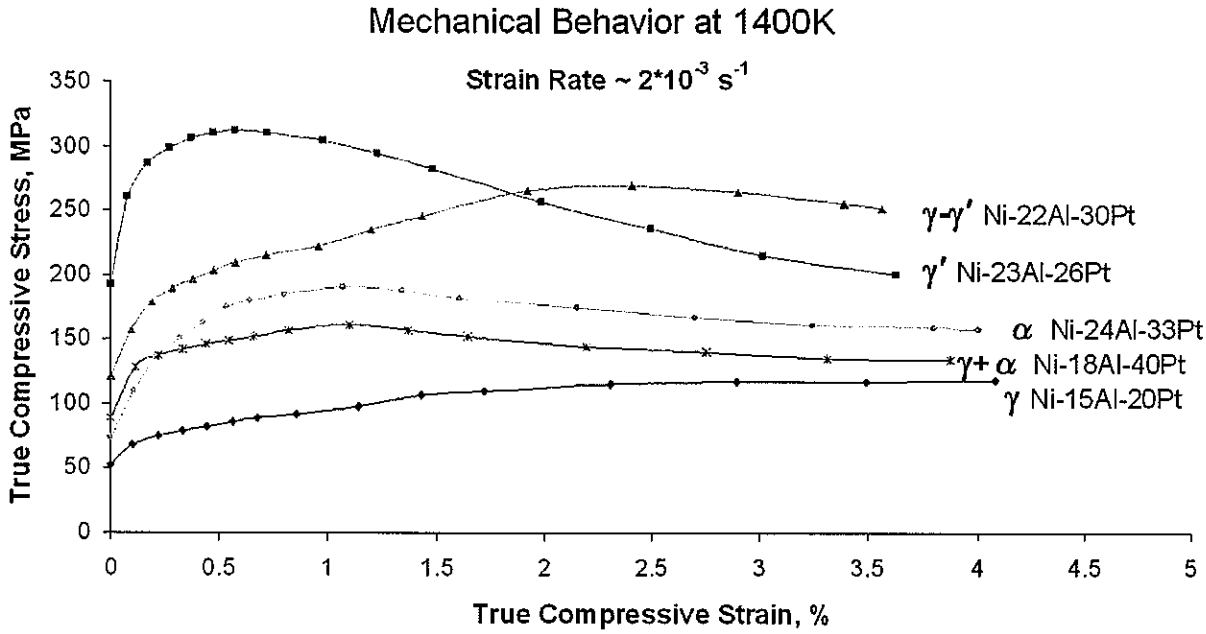

Figure 31. Stress-strain curves at 1127°C for the highest strain rate

Despite losing the majority of its strength at 1127°C, the α phase remains stronger than the subsurface γ phase but is significantly weaker than the γ-γ′ alloy. As shown in table 2, three γ samples with the same Al content, but with different Pt contents, were tested. Since the γ samples tended to fail at the lower temperatures, only the 1127°C results will be considered. The results for the highest and medium strain rate are shown in figures 32 and 33, respectively. While the sample containing 25at.% Pt had slightly higher maximum stress values in both cases, the data does not provide conclusive results as to the effect of Pt content on the strength of the γ.

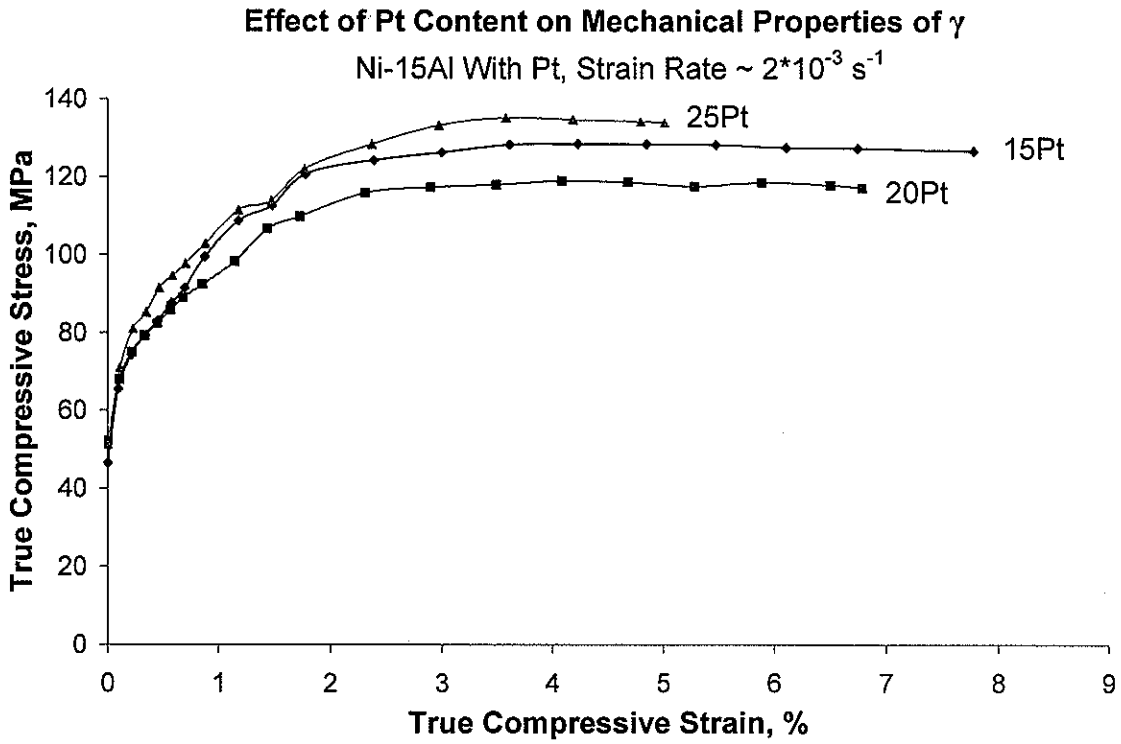

Figure 32. Stress-strain curves for γ alloys with different Pt contents at 1127°C for the highest strain rate

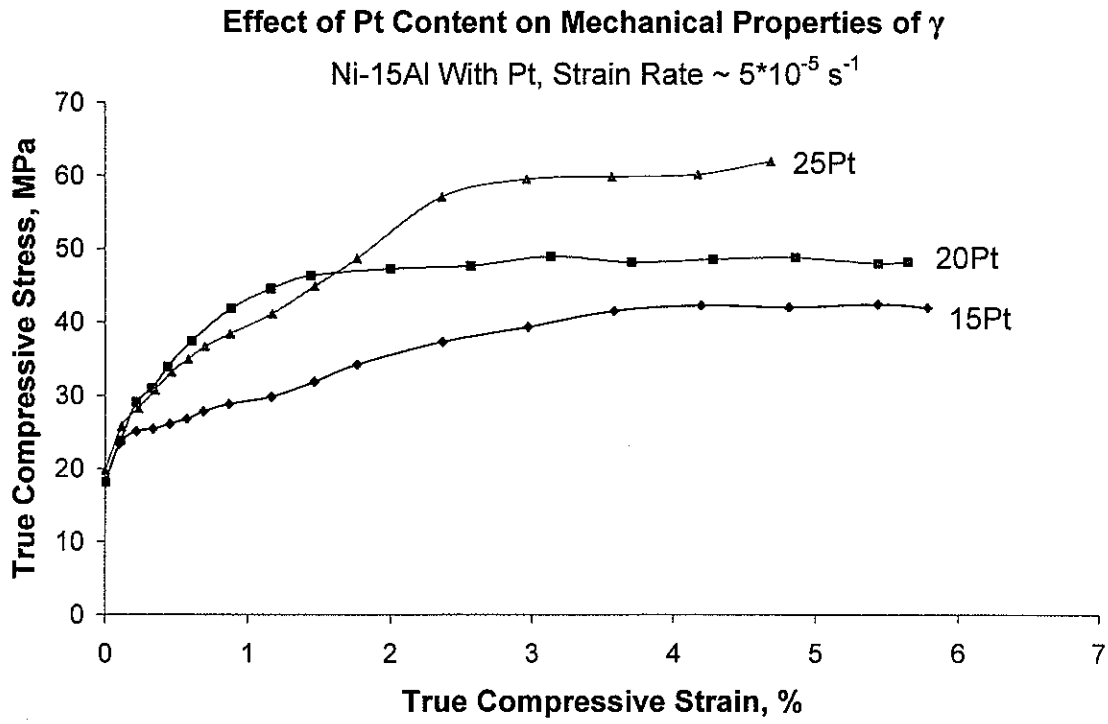

Figure 33. Stress-strain curves for γ alloys with different Pt contents at 1127°C for the highest strain rate

The isothermal oxidation experiments showed that rumpling of γ-γ′ alloys is closely associated with the formation of the α phase in the subsurface region. In order to examine the stresses present in Ni-22Al-30Pt during isothermal oxidation, four layers must be considered: (i) the alumina layer; (ii) the subsurface γ layer; (iii) the γ+α layer; and (iv) the γ+γ′ substrate. Alumina scales are commonly understood to form compressive stresses during their growth. The formation of the α phase, with its higher unit cell volume, would be expected to cause the γ+α layer to try to expand. Since the γ+α layer is constrained by the substrate, the layer would be under compressive stress. Therefore, both the upper and lower interfaces of the subsurface γ layer would be with other layers under compressive stresses. This is in contrast to the γ layer that forms in Ni-22Al-25Pt which only has the interface with the compressively stressed oxide to contend with. While an in-depth modeling of the stresses present in these alloys during isothermal oxidation is beyond the scope of this thesis, it appears that the γ layer would be expected to be under tension, which would seem to prevent rumpling.

Another possible explanation for rumpling could be made using the creep properties of the various layers in the alloys. If the composition of the γ layer in alloy #7 (5at.% greater Pt level) was such that it was less creep resistant than the γ layer in alloy #28, rumpling in the former could be attributed to high-temperature creep of the γ layer due to the growth of the oxide. The mechanical test results in figures 32 and 33 indicate that this is not the case. However, the γ+α layer has been shown to have inferior mechanical strength at 1127°C compared to the γ+γ′ substrate as shown in Table 2 and figure 31. In fact, the strength of the γ+α layer is relatively close to that of the subsurface γ layer. Thus, the γ and γ+α can be considered to make up a single, relatively thick, low-strength layer. If we examine the thicknesses of the low-strength layers in alloys #7 and #28 following isothermal oxidation we find a much thicker weakened zone in alloy #7, as shown in figure 34.

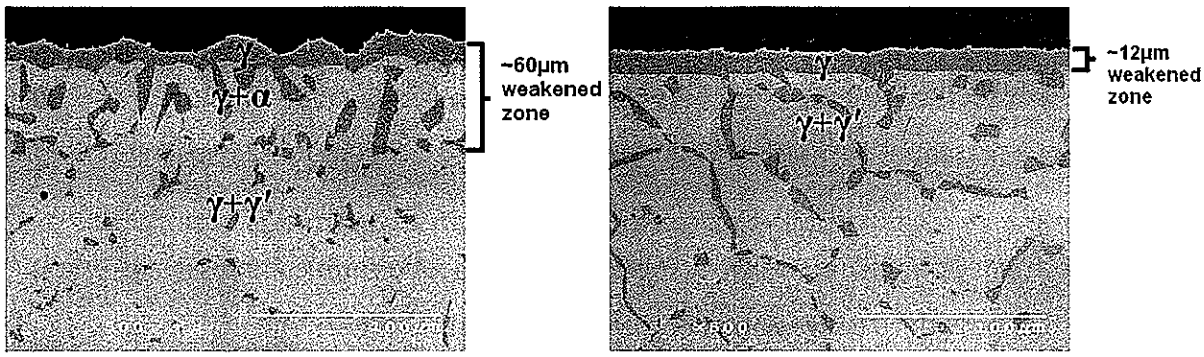

Figure 34. Schematic illustrating the thicknesses of the weakened zones in alloys #7 (left) and #28 (right) after 100 hours at 1150°C, 1200 grit initial finish, cooled at 15°C/min

The γ layer in alloy #28 (figure 34) is constrained to the relatively strong substrate and, because of this, may not be able to rumple. Conversely, the γ layer in alloy #7 borders the much weaker γ+α layer, and does not experience the strengthening affects of the substrate. The compressive stress in the oxide should be approximately the same for both alloys since the thickness is the same. It seems likely that rumpling forms in alloy #7 due to the increased thickness of the weakened of the subsurface region, allowing creep deformation of the γ layer by the compressive growth stress within the oxide.

8.3 Nature of the Martensitic Transformation in Pt-modified β-NiAl

Apart from some XRD and DTA measurements by Chen et al. [42] on the martensitic transformation temperature within an actual bond coat, no studies have reported actual measurements as to the effect of Pt or other elements on the transformation temperature. Chen et al. found that the addition of 20at.% of alloying elements including Pt, Cr and Co resulted in an increase of approximately 300°C over the binary alloy with the same Al concentration. Despite the very large effect of composition on the temperature change for the martensitic transformation, there are no publications which report the effect of Pt content on the martensite transformation temperature. Chen et al. [42] also reported that the difference between the β to martensite transformation temperature upon cooling and the martensite to β transformation temperature upon heating increased from approximately 20°C in the binary alloy to approximately 75°C in the bond coat. In order to gain a better

understanding of both the nature of the martensitic transformation in Pt-modified nickel aluminides and specifically the effect Pt concentration on the martensite transformation temperature, three different experimental methods were used to observe the transformation as it occurred.

8.3.1 DSC Investigation of the Martensitic Transformation

A study of bulk alloys containing 37at.% Al with varying amounts of Pt was performed using high-temperature DSC. The locations of the five 37at.% Al alloys are shown in figure 35 as red dots. Besides providing a means of determining the temperature of the martensitic transformation, the DSC provided some insight into the kinetics of the transformation.

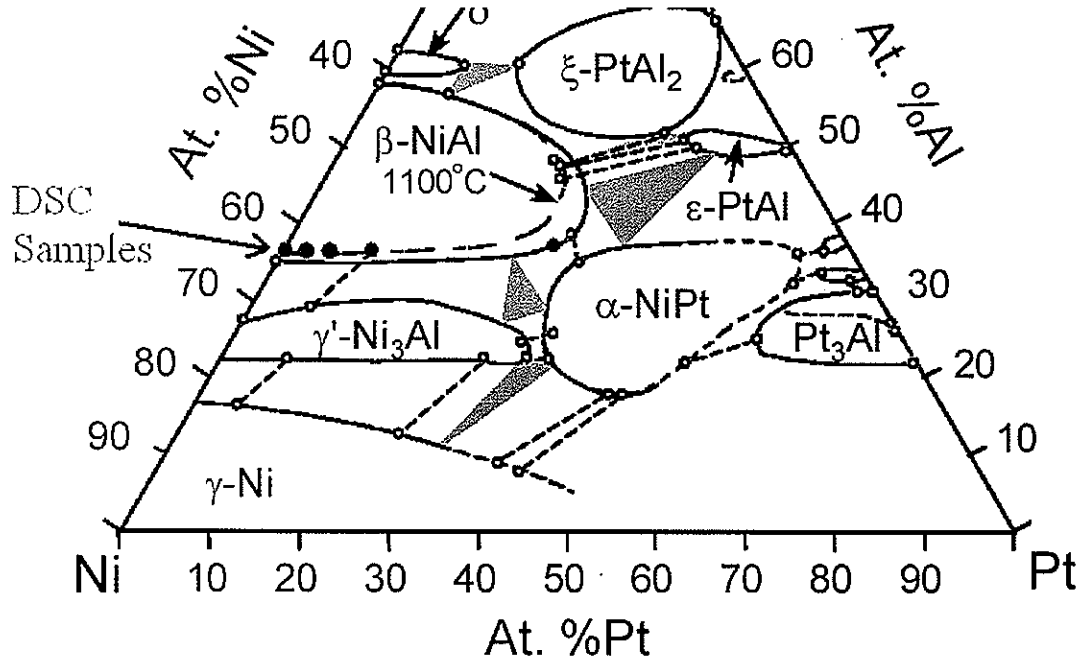

Figure 35. The Ni-Al-Pt phase diagram at 1100/1150°C [8] showing the locations of the DSC samples tested

The DSC results from the binary alloy Ni-37Al showed a transformation upon heating with an onset that varied from between 442°C for a heating rate of 20°C/min and 460°C for a heating rate of 40°C/min. According to Smialek and Hehemann [37], the temperature for the β-to-martensite transformation for this composition is 390°C. Taking into account the

approximate 20°C offset between the transformations upon heating and cooling for binary alloys [42] in addition to the fact that Smialek and Hehemann's [37] measurements utilized a cooling rate of only 0.1°C/min, the results from DSC appear very reasonable. The next alloy studied contained 2at.% Pt. The resulting DSC plots for this alloy with two different cooling rates are shown in figure 36. A positive DSC response indicates an exothermic event. The endothermic peak on the heating curve at approximately 525°C represents the martensite-to-β transformation. The exothermic peak on the cooling curve at approximately 475°C represents the formation of martensite. When compared to the 20°C/min curves, a rate of 40°C/min results in a decrease in the transformation temperature upon cooling and an increase in the transformation temperature upon heating. An onset temperature for the formation of martensite, which could be called the M_s temperature, is very difficult to determine from the DSC data due to a very gradual change in slope of the curve. In contrast, the onset of the formation of β is much more easily determined. The onset temperature for the martensite-to-β transformation for a 20°C/min heating rate was used as a basis for comparison between the different alloys.

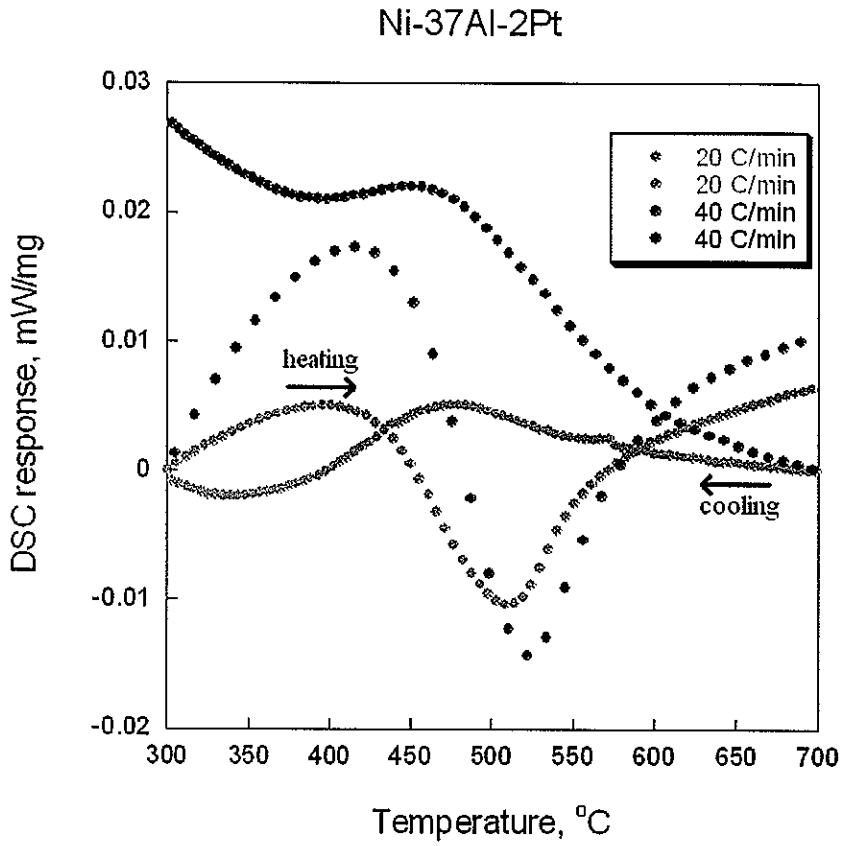

Figure 36. DSC plot for Ni-37Al-2Pt

An increase in the Pt level to 5at.% shifted all transformations to slightly higher temperatures as shown in figure 37. When the Pt level was increased to 10at.% a much greater shift was observed. Figure 38 shows that the onset of the martensite-to-β transformation has increased to approximately 750°C. A feature of note in figure 38 is the exothermic peak that forms upon heating only for the 40°C/min curve. Further examination of the data showed that this exothermic peak would form for any heating rate if the previous cooling rate had been 30°C/min or faster. It is hypothesized that this exothermic peak represented further transformation of β into martensite upon heating. This hypothesis implies that fast cooling rates resulted in an incomplete transformation upon cooling and resulted in retained β. An analysis of the areas of the peaks showed that the endothermic martensite-to-β transformation absorbed approximately 55 J/g in every case. Samples that were cooled slower than 30°C/min released approximately 55 J/g, but faster cooled samples released less energy per

gram. When the faster cooled sample was subsequently reheated, the area of the exothermic peak when added to the area of the peak from cooling would equal approximately 55 J/g. To clarify, in figure 38, the areas of both the red and green endothermic peaks are approximately 55 J/g. The green exothermic peak, representing a 20°C/min cooling rate, also has an area of 55 J/g. And finally, the sum of the areas of two exothermic red peaks is approximately 55 J/g. The indications that the transformation from β to martensite in a Pt-modified aluminide occurs more completely for slower cooling rates is in direct opposition to the conclusions reached by Chen et al. [42] in which only rates faster than some critical rate would cause the martensitic transformation.

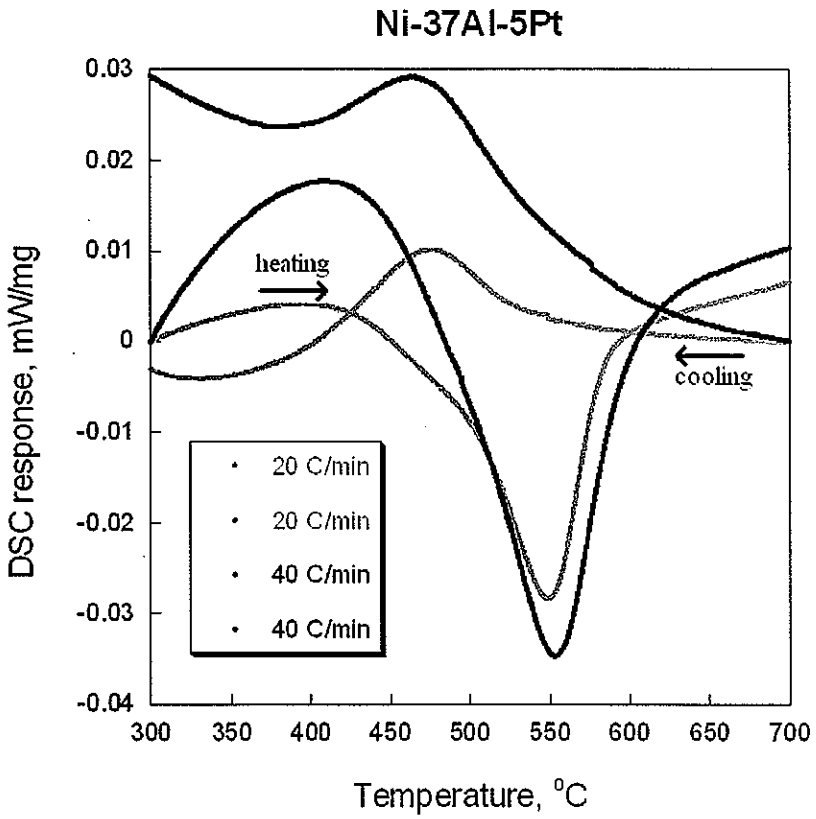

Figure 37. DSC plot for Ni-37Al-5Pt

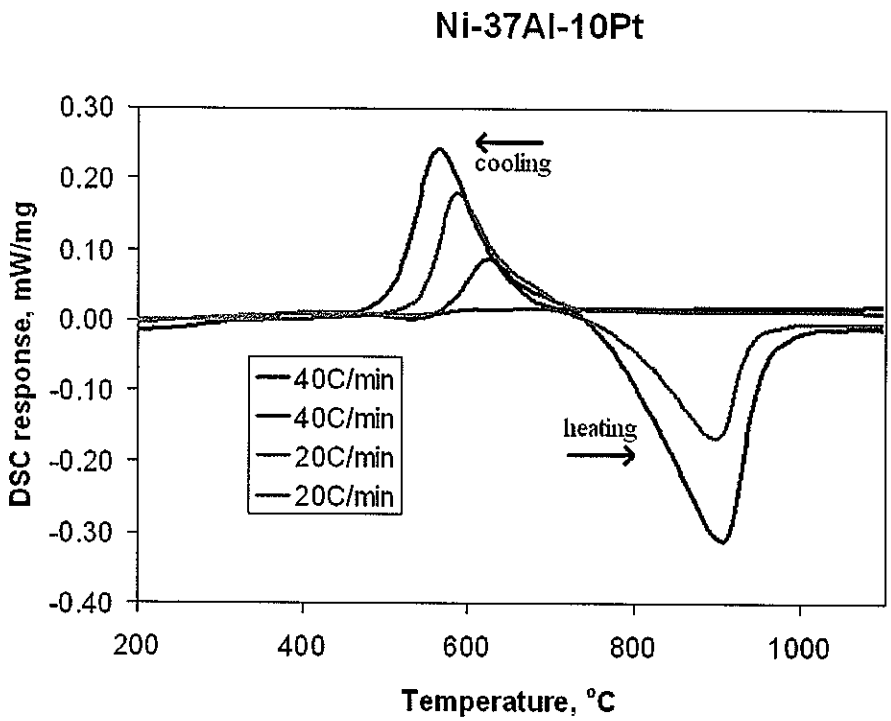

Figure 38. DSC plot for Ni-37Al-10Pt

The final alloy in the Ni-37Al series examined by DSC contained 30at.% Pt. The transformations within this alloy occurred at temperatures greater than 1100°C. The peaks in figure 39 indicate that more than one transformation is occurring in Ni-37Al-30Pt. The high Pt content of this alloy places it very close to the β+α two-phase region at 1150°C as shown in figure 35, and clearly within the 2-phase region at 1000°C. The precipitation of α would be expected to show up in a DSC plot as a very wide peak since it would continuously occur over a temperature range. The sharper peak was therefore assumed to represent the martensitic transformation. An SEM image (figure 40) of this alloy after cooling at 15°C/min shows that there are indeed two phases present. Based on EDS analysis, the darker phase is β (Ni-42Al-30Pt) and the lighter, majority phase is α (Ni-33Al-34Pt). The image does not show any martensite in the β phase, but this may be due to the phase becoming too Al-rich to be martensitic.

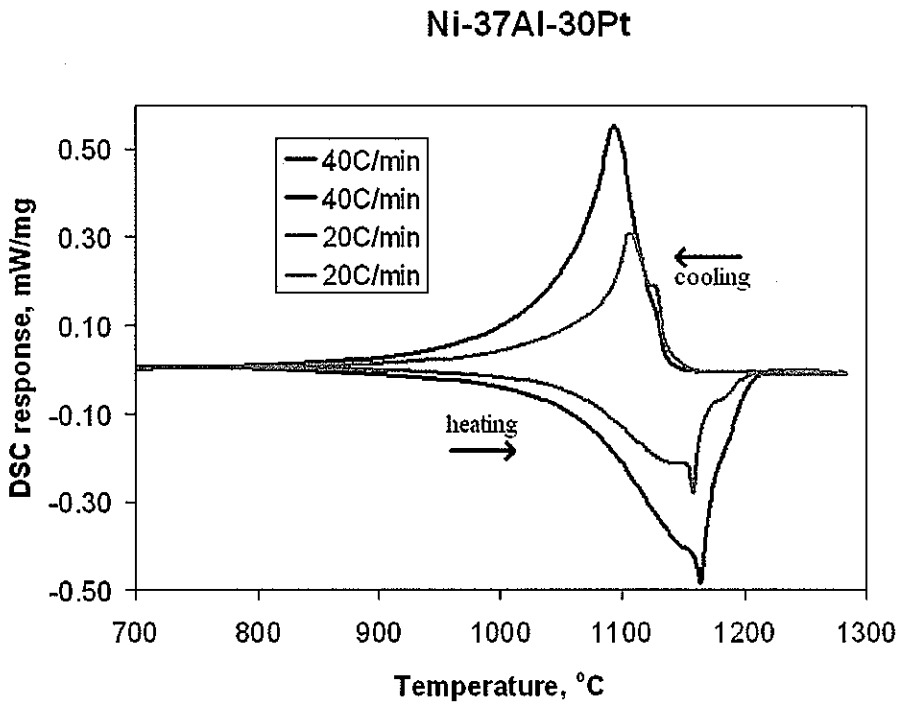

Figure 39. DSC plot for Ni-37Al-30Pt

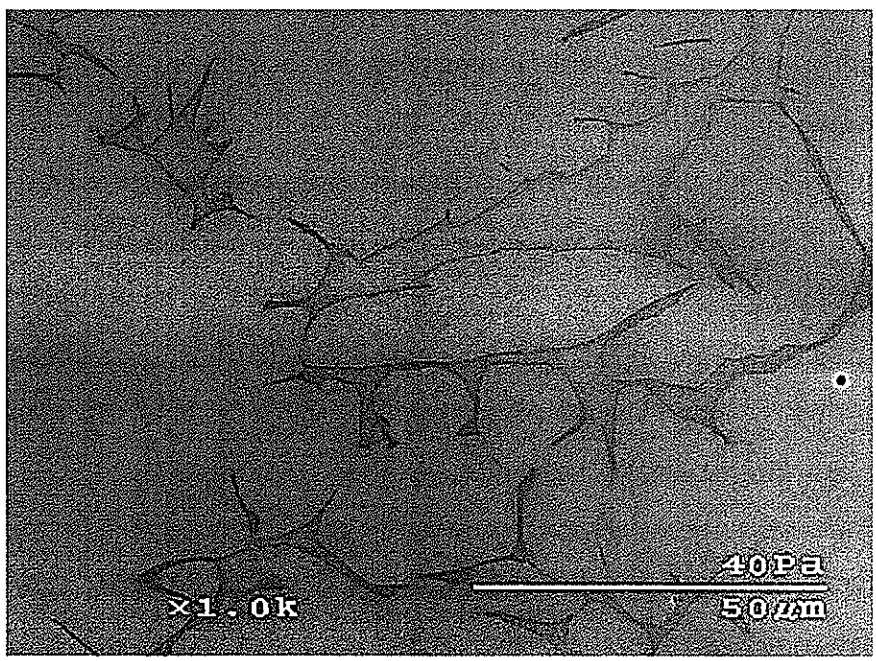

Figure 40. Backscattered SEM image of Ni-37Al-30Pt following 15°C/min cooling showing β (darker phase) and α (lighter phase)

As previously mentioned, the onset of the martensite to β transformation was used to illustrate the effect of Pt content on the martensitic transformation. The increase in the transformation temperature as Pt content increases is shown graphically in figure 41.

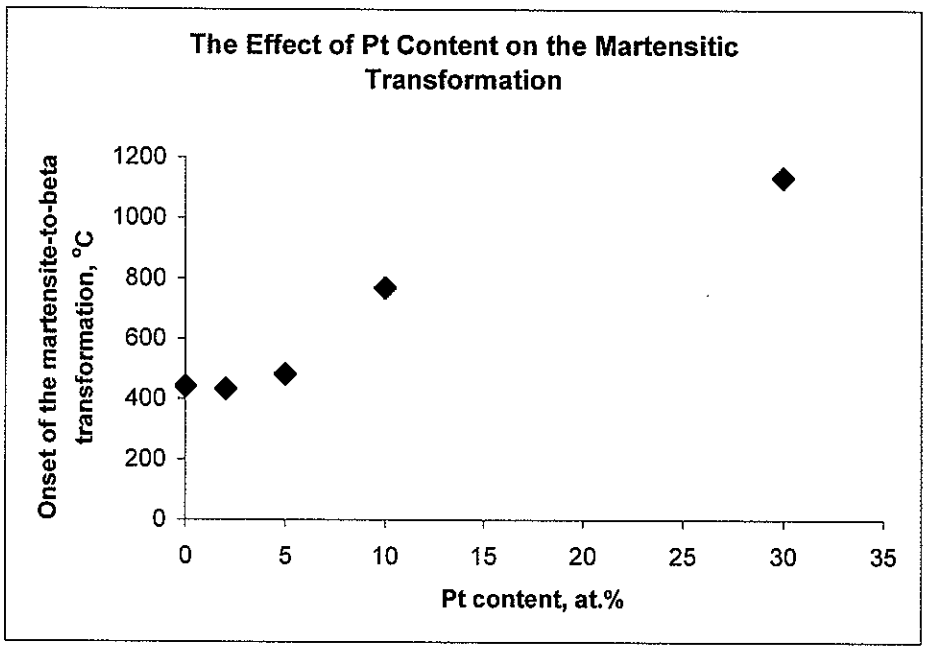

Figure 41. The onset temperature of the beta to martensite transformation for Ni-37-xPt alloys

In addition to the Ni-37Al series of alloys, Ni-40Al-15Pt (S20) was also subjected to DSC experimentation. From the cyclic oxidation experiments presented in section 8.3, it was known that very slow cooling rates or isothermal holds longer than 15 minutes at 760°C were necessary to form significant volume fractions of martensite. The DSC results repeatedly showed an endothermic peak with an onset around 800°C but never any corresponding exothermic peak upon cooling. Figure 42 shows the results from a 40°C/min experiment showing the single peak upon heating. It is possible that the β-to-martensite transformation occurred over a very wide temperature range and didn't show up in the DSC plot, while the reverse transformation occurred over a much shorter temperature range, making it readily apparent in the plot. The area of the peak generally varied between 5 and 10 J/g, a value much less than the value of 55 J/g for Ni-40Al-15Pt, indicating that only a small volume fraction of martensite was formed. While providing some very interesting results, the DSC

does not provide any method of determining which phases are present at any given time. The results sometimes must be combined with other experimental methods, such as HT-XRD, in order to gain a true understanding of what is observed.

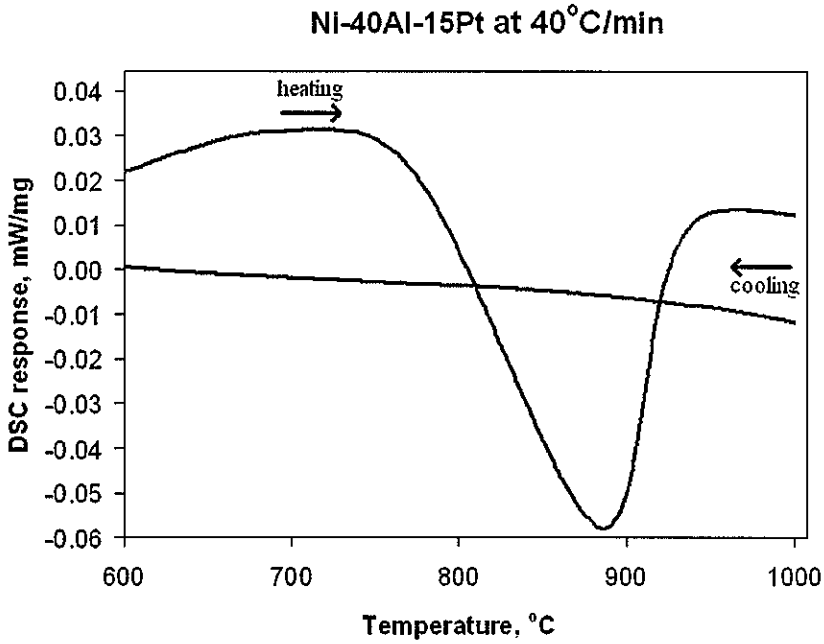

Figure 42. DSC plot for Ni-40Al-15Pt

8.3.2 HT-XRD Investigation of the Martensitic Transformation

As mentioned in section 8.3.1, the HT-XRD experiments performed at Argonne National Lab provided a very useful method for examining the martensitic transformation. HT-XRD allows the researcher to determine the constituent phases present in a sample at temperature based on the crystal structures. Initial observations provided evidence that the transformation of β into martensite was not an instantaneous transformation. The data is presented using Q-values which take into account the wavelength of the x-ray radiation (approximately .0143nm) and can be converted into two-theta values using equation 4.

$$Q = \frac{4\pi}{\lambda} * \sin\left(\frac{\theta}{2}\right) \tag{4}$$

Figure 43 shows the resulting diffraction pattern resulting from an isothermal hold of Ni-40Al-15Pt at 875°C, showing that 500 minutes elapsed before a significant volume fraction of β (B2 crystal structure) had transformed into martensite ($L1_0$ crystal structure). When the temperature was decreased to 850°C, a similar volume fraction had transformed after only 9 minutes, as shown in figure 44.

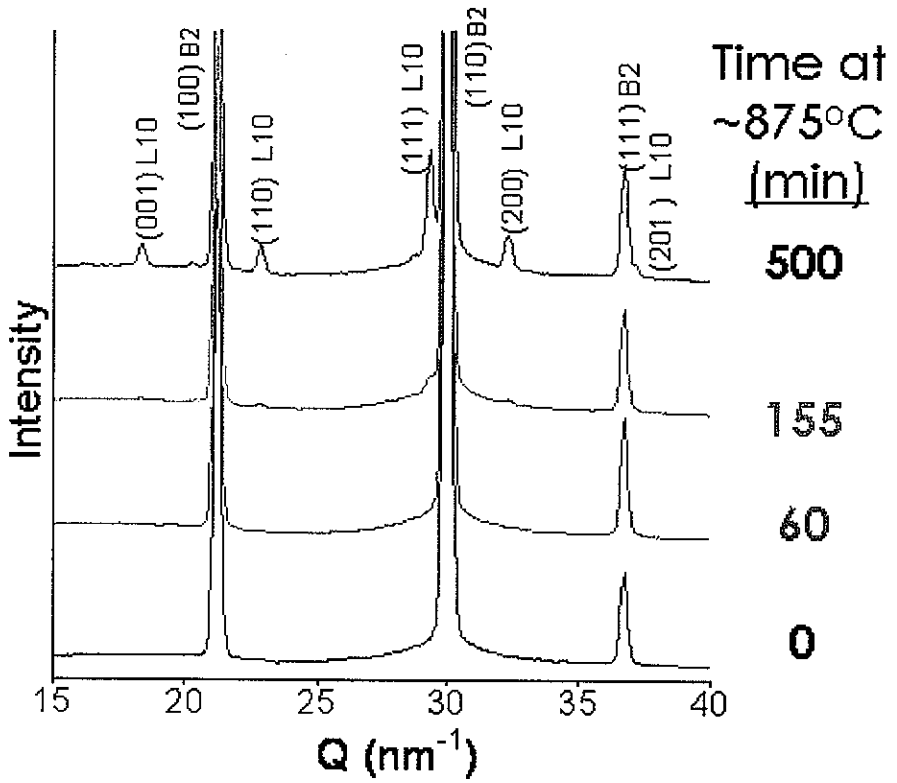

Figure 43. Diffraction pattern for Ni-40Al-15Pt held at 875°C

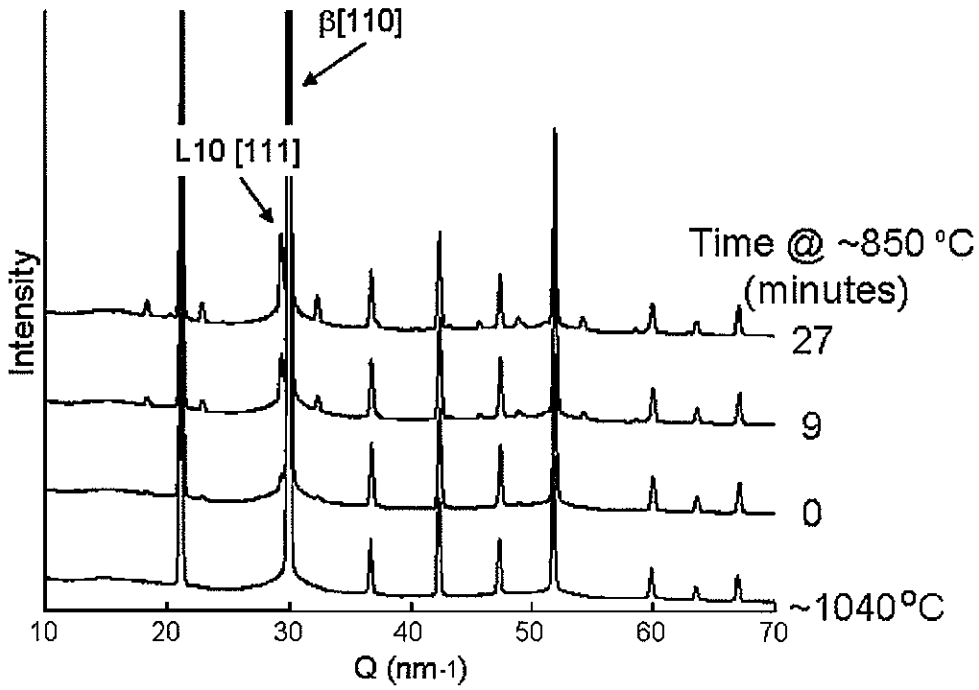

Figure 44. Diffraction pattern for Ni-40Al-15Pt held at 850°C

The isothermal transformation β into martensite over a relatively long amount of time has not been reported in literature. This observation implies that the martensitic transformation in Ni-40Al-15Pt could be avoided if the sample did not remain at the transformation temperature for a long enough time. Cyclic oxidation experiments were developed based on this implication and are presented in section 8.4.

In order to verify the interpretations of the DSC results, a HT-XRD experiment was performed that replicated one of the DSC tests performed on Ni-37Al-10Pt. A sample of the alloy was placed in the HT-XRD furnace and heated to 1150°C to ensure that it was 100% β. The resulting diffraction pattern is shown in figure 45 along with the DSC plot. An arrow on the DSC plot indicates the temperature at which the diffraction pattern was taken. It is clear from the pattern that the sample is indeed single phase β.

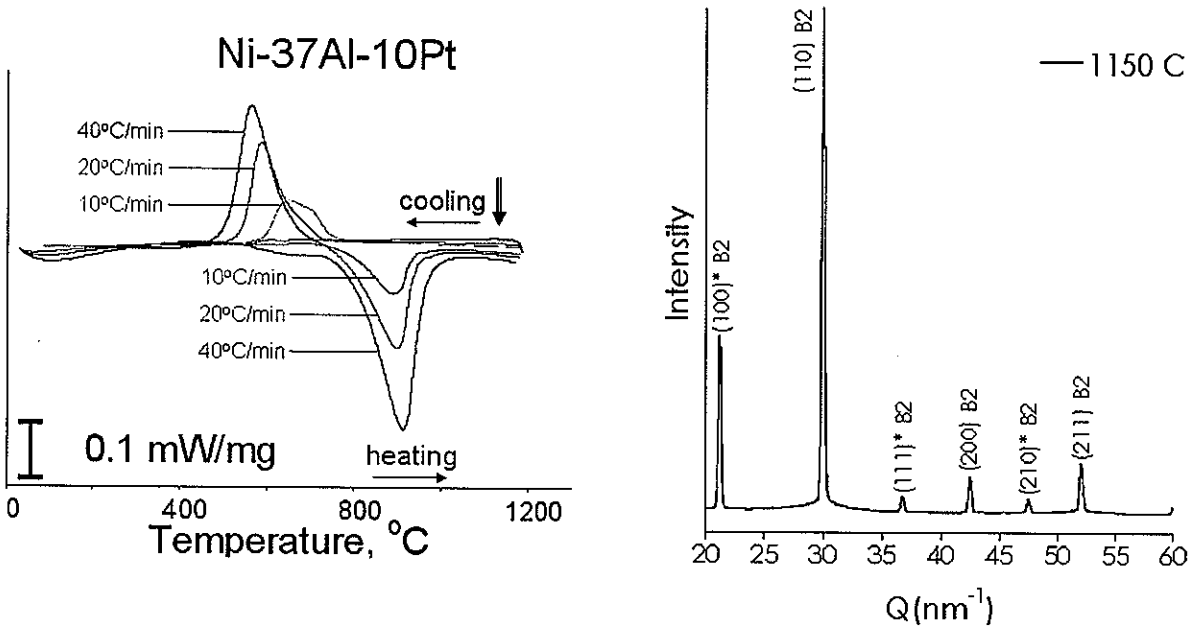

Figure 45. Diffraction pattern of Ni-37Al-10Pt at 1150°C showing single phase β

The sample was then cooled to 665°C, approximately the temperature at which martensite was first observed in the DSC experiment. Figure 46 shows the formation of a second set of peaks which correspond to the martensitic phase. Only a very small volume fraction of martensite is present, which is expected from the DSC plot. The shift in the β peak is due to the thermal contraction of the lattice. Cooling further, to 300°C, results in the diffraction pattern shown in figure 47. The martensite peak is now predominant, as expected. There is residual β present at 300°C since the cooling rate was 40°C/min. A slower cooling rate would be expected to result in less residual β as described in section 8.3.1. The results from both the DSC and HT-XRD experiments provided the information necessary to perform the cyclic oxidation experiments in section 8.4.

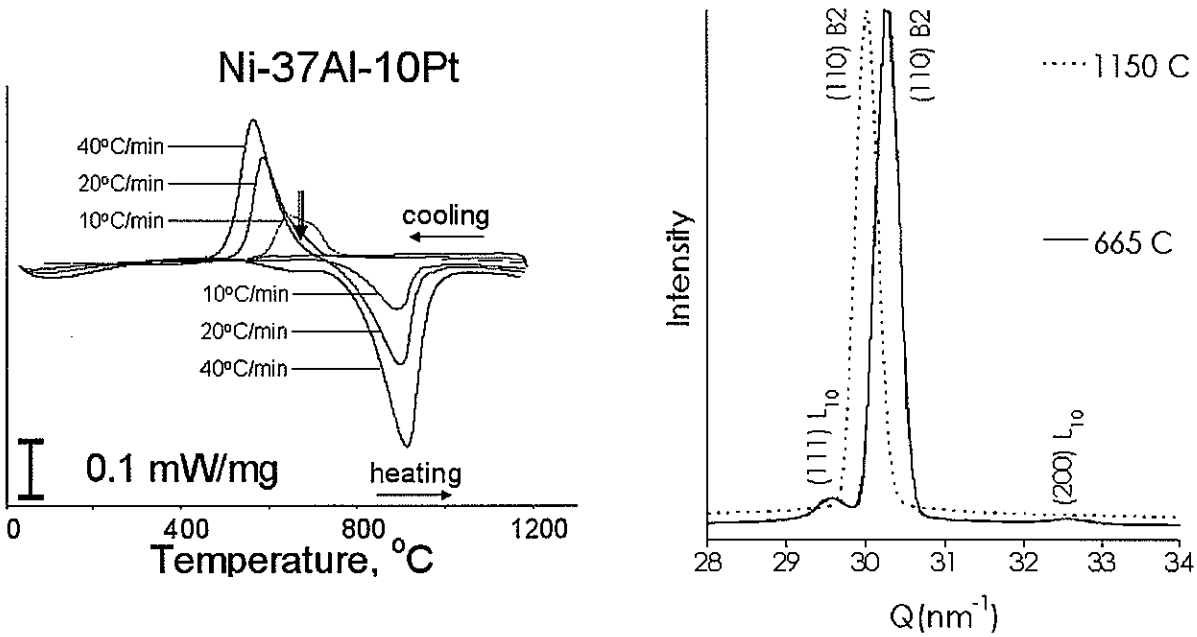

Figure 46. Diffraction pattern of Ni-37Al-10Pt at 665°C showing the formation of martensite

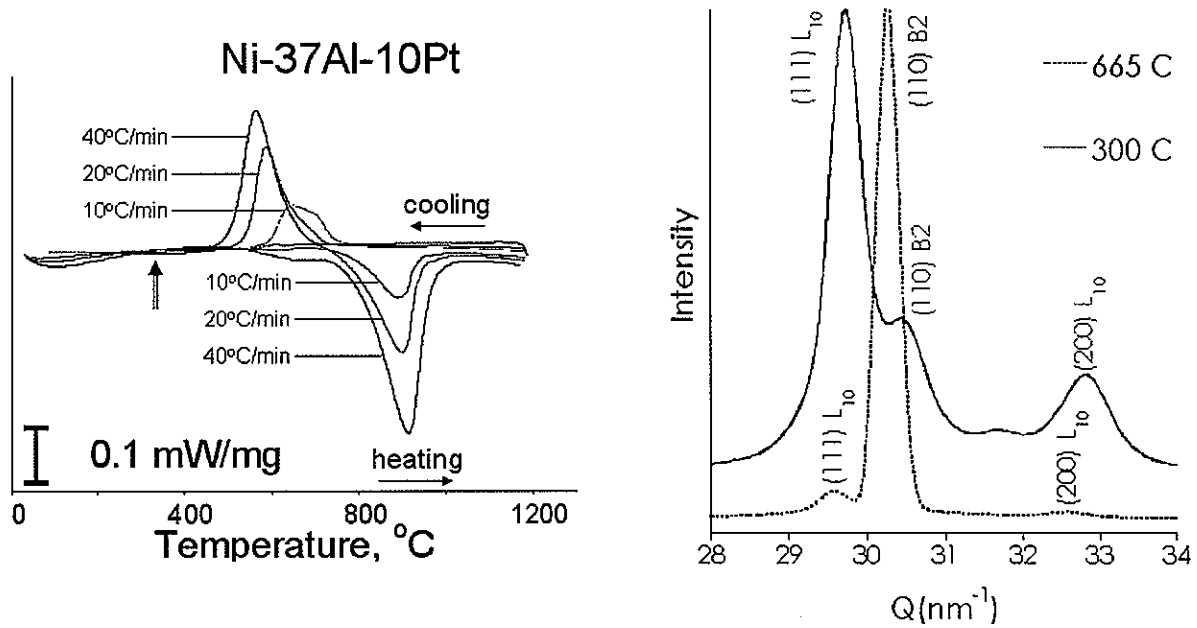

Figure 47. Diffraction pattern of Ni-37Al-10Pt at 300°C showing that martensite is the predominant phase presen

8.3.3 Potentiometric Investigation of the Martensitic Transformation

The potentiometric method used to observe the martensitic transformation in the bulk Pt-modified aluminides is very similar to the method used by researchers investigating the

transformation within binary NiAl [37-39]. The major advantage to the potentiometric method is that it can be performed very quickly and without the need for extremely specialized equipment or facilities. The results from the potentiometric measurements of Ni-37Al-10Pt are still very preliminary, but the data in figure 48 is promising. Upon cooling a relatively constant potential is measured until approximately 760°C (T3) when the potential begins to increase. It increases until approximately 660°C (T4) when it again levels off. The DSC plot in figure 61 for the 20°C/min cooling of Ni-37Al-10Pt shows the start of the martensitic transformation at approximately 730°C, and the transformation finishes at approximately 510°C. Unfortunately no DSC results were obtained for a 5°C/min cooling rate, but based on the comparison between the 20°C/min and 40°C/min cooling rates, it is reasonable to assume that the measured temperatures would shift to slightly higher values. Even with the small discrepancies in temperature, the two experimental methods seem to agree very well for the β to martensite transformation. The potentiometric method seems very promising and should prove to be a useful tool in further analysis of the martensitic transformation.

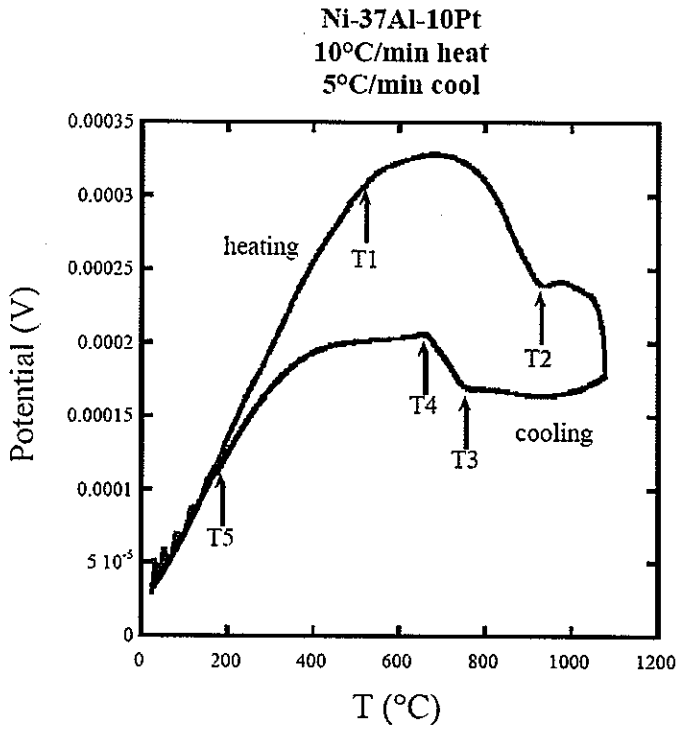

Figure 48. Potentiometric plot for Ni-37Al-10Pt

8.4 The Effect of the Martensitic Transformation on Rumpling of Bulk β alloys

Based on HT-XRD results, Ni-40Al-15Pt (S20) was chosen for cyclic oxidation testing. Alloy S20 showed evidence of a martensitic transformation at approximately 800 to 850°C. Based on this observation, an initial experiment was devised to observe the effect of the martensitic transformation on the surface morphology of the sample. Two identical samples of alloy S20 were prepared by polishing to a 600-grit finish. One sample was cycled 100 times from 750 to 1150°C and the other sample was cycled 100 times from 950 to 1150°C. Only the sample that was cycled to 750°C was expected to undergo the martensitic transformation since β had been shown by HT-XRD to be the stable phase at 950°C. Both samples had a 1-hour dwell at each temperature and a heating/cooling rate of 15°C/min. SEM surface images from this experiment are shown in figure 49. The SEM surface images that appear very similar to the resulting profilometry images in figure 50. An extracted profile of the rumpled sample is provided in figure 51. It is clear that the sample cycled to 750°C rumpled, while the other sample did not. The cross sections of the alloys are shown in figure 52 and a high-magnification image of the interior of the rumpled sample shows the presence of martensite, as shown in figure 53. The promising results from this experiment led to further experimentation on alloy S20, a summary of which is provided in Table 3.

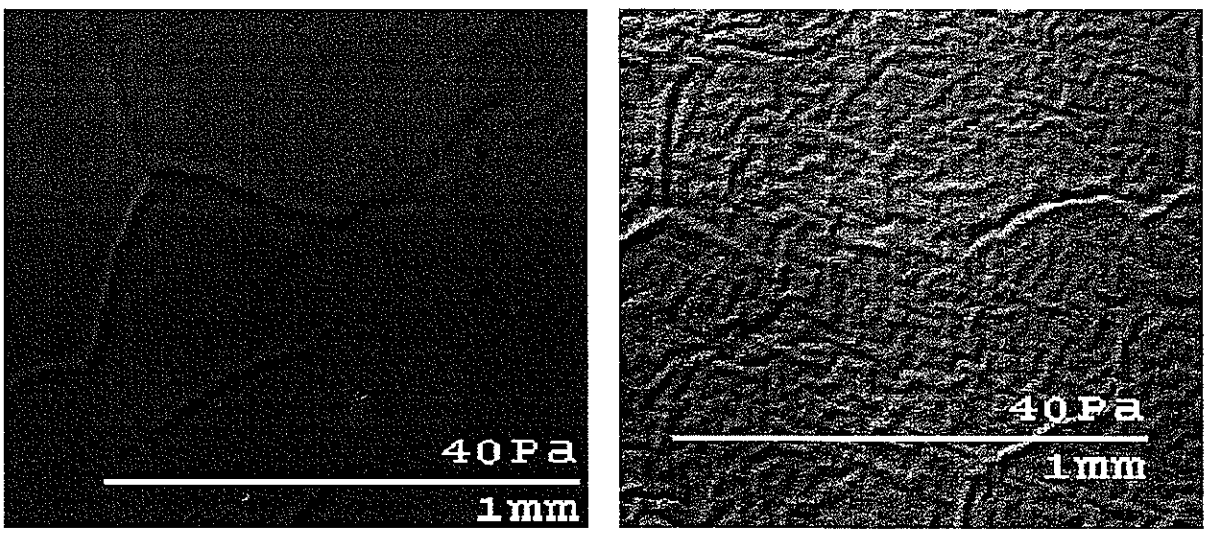

Figure 49. Surface SEM images of alloy S20 with 600-grit initial surface finish, cycled 100 times at 15°C/min from 950 to 1150°C (left) and 750 to 1150°C (right) with a 1hr hold at all temperatures

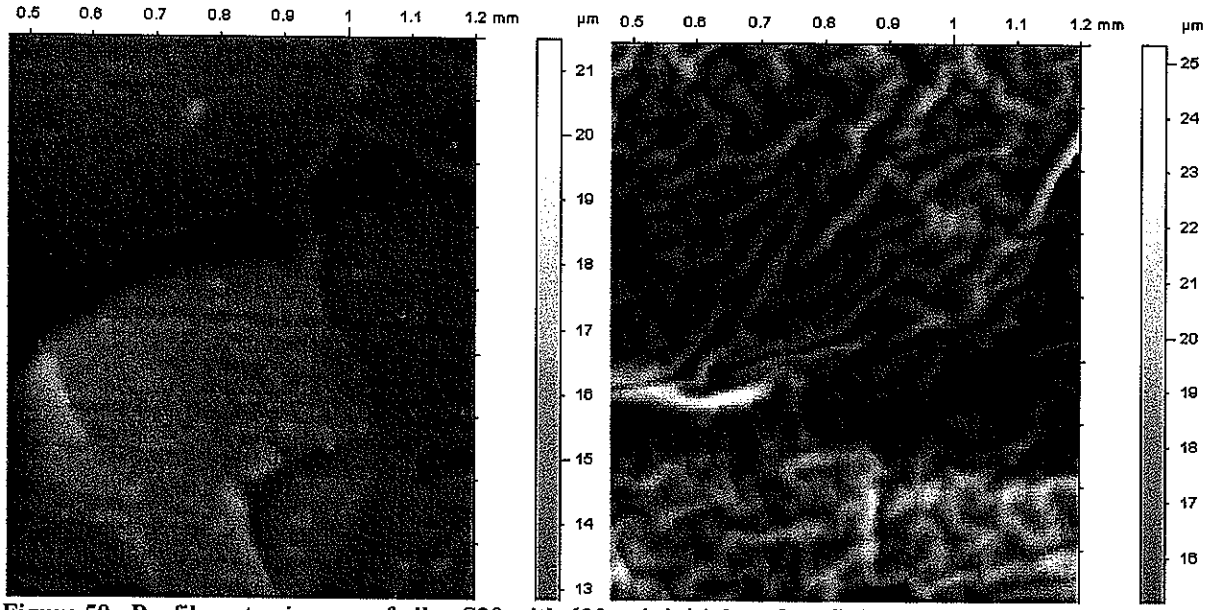

Figure 50. Profilometry images of alloy S20 with 600-grit initial surface finish, cycled 100 times at 15°C/min from 950 to 1150°C (left) and 750 to 1150°C (right) with a 1hr hold at all temperatures

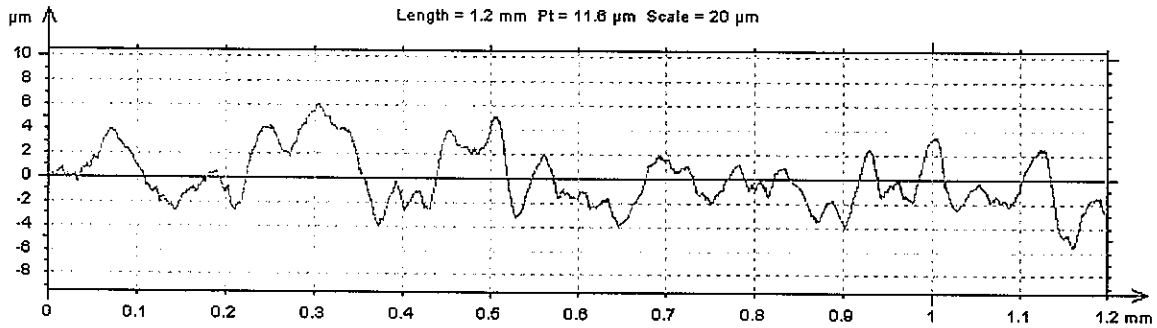

Figure 51. Extracted profile for alloy S20 with 600 grit initial surface finish, cycled 100 times at 15°C/min from 750 to 1150°C with a 1hr hold at all temperatures, $R_{z(DIN)}$ = 9.5µm and λ_a = 50.1µm

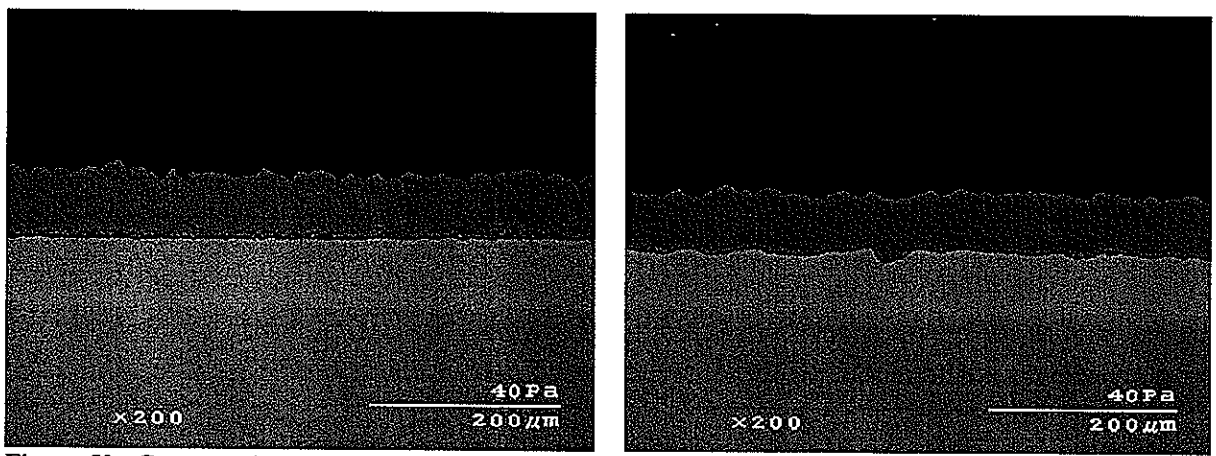

Figure 52. Cross sections of alloy S20 with 600-grit initial surface finish, cycled 100 times at 15°C/min from 950 to 1150°C (left) and 750 to 1150°C (right) with a 1hr hold at all temperatures

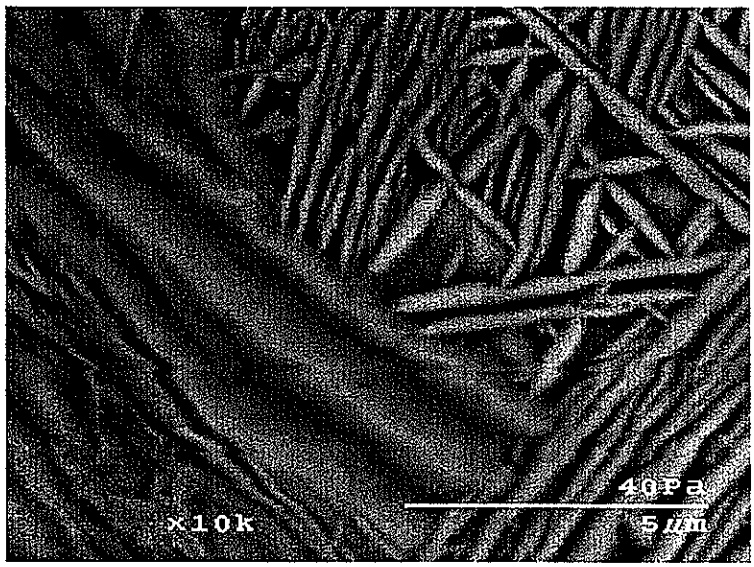

Figure 53. Image of the interior of alloy S20 with 600-grit initial surface finish, cycled 100 times at 15°C/min from 750 to 1150°C with a 1hr hold at all temperatures

Table 3. Summary of results for oxidation of alloy S20

Sample Preparation	Oxidation	Surface Observations	λ_a	R_{zDIN}
600-grit	100 cycles 950°C(1hr)-1150°C(1hr) 15°C/min	not rumpled	28	4.7
600-grit	100 cycles 750°C(1hr)-1150°C(1hr) 15°C/min	rumpled	50.1	9.5
1μm polish	100 cycles 760°C(15min)-1150°C(1hr) 500°C/min	very slight localized rumpling	19.6	3.3
cut-off wheel abrasions	100 cycles 760°C(15min)-1150°C(1hr) 500°C/min	approximately 1/2 the area is rumpled	30.3	7.6
600-grit	100 cycles 760°C(1hr)-1150°C(1hr) 500°C/min	rumpled	55.8	11.2
1μm polish	100 cycles 760°C(1hr)-1150°C(1hr) 500°C/min	rumpled	34.8	7.9
1μm polish	100 cycles Rt(1hr)-1000°C(1hr) 500°C/min	not rumpled	13.6	2
1μm polish	5 cycles 760°C(1hr)-1150°C(1hr) 500°C/min	not rumpled	9.4	1.3
1μm polish	10 cycles 760°C(1hr)-1150°C(1hr) 500°C/min	possibly very slight rumpling	11.9	1.8
1μm polish	25 cycles 760°C(1hr)-1150°C(1hr) 500°C/min	small amount of rumpling	25.2	4
1μm polish	50 cycles 760°C(1hr)-1150°C(1hr) 500°C/min	rumpled	44	7.8
1μm polish	100 cycles 760°C(1hr)-1150°C(1hr) 500°C/min	rumpled	60.7	12.8
1μm polish	100 cycles Rt(1hr)-1000°C(1hr) 15°C/min	not rumpled	16.3	2.1
1200-grit	1150°C(110hrs) isothermal, 15°C/min cooling	possibly very slight rumpling	22.4	7.1
1μm polish, oxidized 1150°C(1hr), sealed in quartz	100 cycles 760°C(1hr)-1150°C(1hr) 500°C/min	rumpled with a unique appearance	40.9	4.8

The unit cell volumes for both β and martensite were determined by HT-XRD. Figure 54 shows a volume reduction of between 0.55% and 0.85%, depending on the temperature. Room temperature measurements by Zhang et al. [33] gave a volume reduction of 2.25% for the martensitic transformation in a Pt-modified aluminide bond coat containing ~40at.%Al. The repeated volume reduction then increase upon the reverse transformation seems to be responsible for the rumpling that developed in the sample cycled to 750°C. A study of binary NiAl coatings by Lesnikova and Lesnikov [46] showed an increase in spallation of the oxide for thermally cycled coatings. The researchers determined that the spallation was caused by surface irregularities which increased in magnitude with increasing numbers of cycles, but only for the alloys which underwent martensitic transformations. While not resulting in the same type of rumpling reported in this thesis, Lesnikova and Lesnikov [46] showed that repeated martensitic transformations can increase surface roughness. A detailed analysis of the specific stresses developed during thermally cycling a martensitic sample is beyond the scope of this work and is not presented.

A different mechanism that could possibly explain the correlation between the martensitic transformation and rumpling is related to a mechanism proposed in a recent paper by Yang and Hou [47]. These researchers linked the variations in the degree of undulations in isothermally oxidized Fe-Al binary alloys to the differences in diffusivities between the two structures observed. Creep rate is related to the diffusivity by equation 5, which combines the two types of diffusion creep, Nabarro-Herring (where lattice diffusion dominates creep) and Coble creep (where grain boundary diffusion dominates creep) [48].

$$\dot{\gamma} = \left(\frac{42\,\tau\,\Omega}{kT\,\delta^2} \right) * D_{eff} \qquad (5)$$

In equation 5, $\dot{\gamma}$ is the yield rate (equal to the strain rate multiplied by $3^{1/2}$), τ is the shear stress, Ω is the atomic volume, k is the Boltzmann constant, T is the temperature, δ is the grain size, and D_{eff} is the effective diffusion coefficient which takes into account both types of diffusion.

The β phase is a more ordered structure than martensite, and because of the differences in degree of ordering it is reasonable to assume that martensite will have a much larger diffusivity than β. At high temperatures any deformation that takes place is likely due to diffusional creep, so structures such as martensitic Pt-modified NiAl with higher diffusivities would be more susceptible to creep deformation. Therefore, a sample containing martensite would be more susceptible to the compressive stresses in the oxide causing rumpling than a β sample at the same temperature and with the same stress from the oxide.

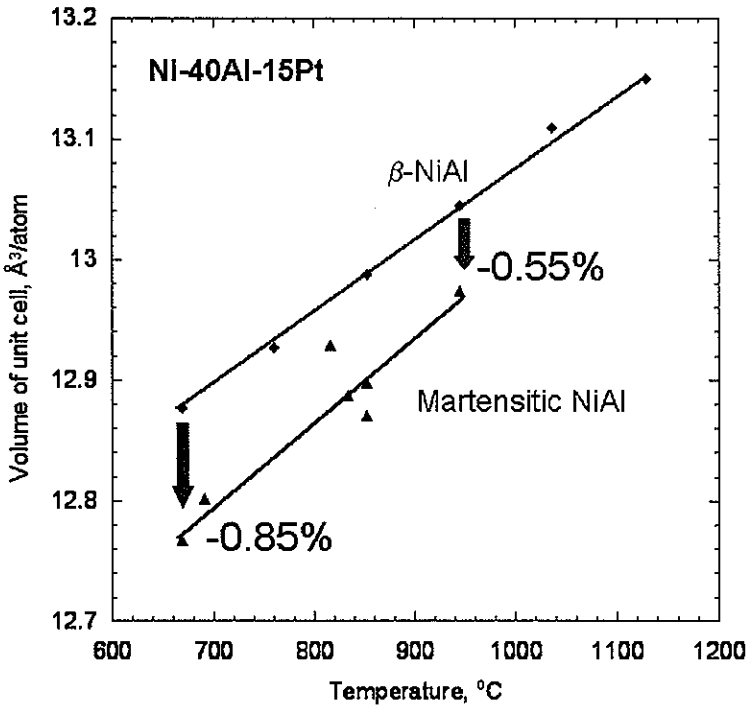

Figure 54. The volume change associated with the martensitic transformation in alloy S20

8.4.1 The Effect of Dwell Time at the Lower Hold Temperature on Rumpling

The HT-XRD data showed that, depending on the temperature, alloy S20 only gradually transformed into martensite. These results indicated that the martensitic transformation was more complicated than previously believed, and rumpling experiments were developed to provide further insight into this transformation and its effect on rumpling. An experiment in which two identical samples of alloy S20 were cycled from 760 to 1150°C 100 times was

performed. Both samples were held at 1150°C for 1 hour, then one sample was held at 760°C for fifteen minutes while the other sample was held at 760°C for 1 hour. This experiment was performed in the vertical 2-zone tube furnace and the cooling rate was approximately 500°C/min. As shown in figure 55, the sample which spent 1 hour at 760°C rumpled, while the sample that spent only 15 minutes at 760°C did not.

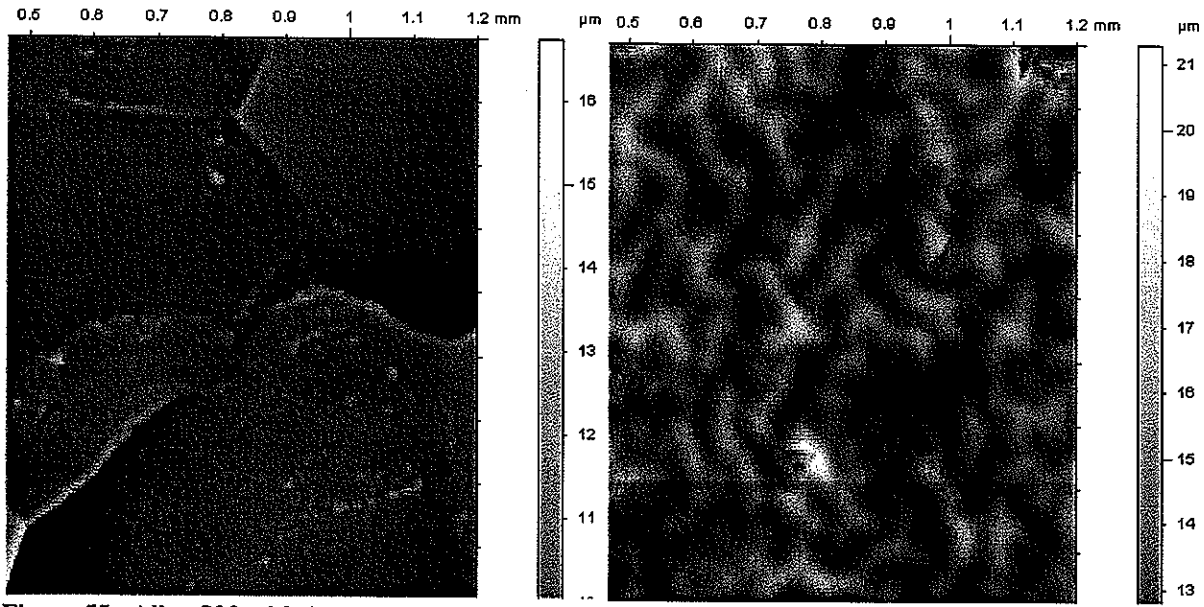

Figure 55. Alloy S20 with 1µm initial surface finish, cycled 100 times at 500°C/min from 760 to 1150°C (1hr hold), with 15 minutes (left) and 1 hour (right) at 760°C

The results presented in figures 49 through 53 seem to show that rumpling in S20 relies on the formation of martensite. Applying this conclusion to the experiment in this section, it seems that martensite did not form in the sample held for only 15 minutes at 760°C, or at least not to the same extent as it did in the sample held for 1 hour. Indeed, this speculation was validated through cross sectional analysis (figure 56) of the two samples which clearly showed martensite in the rumpled sample, but only showed the faintest indication of martensite in the non-rumpled sample. In addition to the differences in rumpling between the two samples, another rather surprising observation was made; the rumpled sample had become macroscopically deformed as shown in figure 57. While this was the first

observation of this phenomenon, it was soon found that nearly all rumpled samples of S20 exhibited macroscopic deformation to some extent.

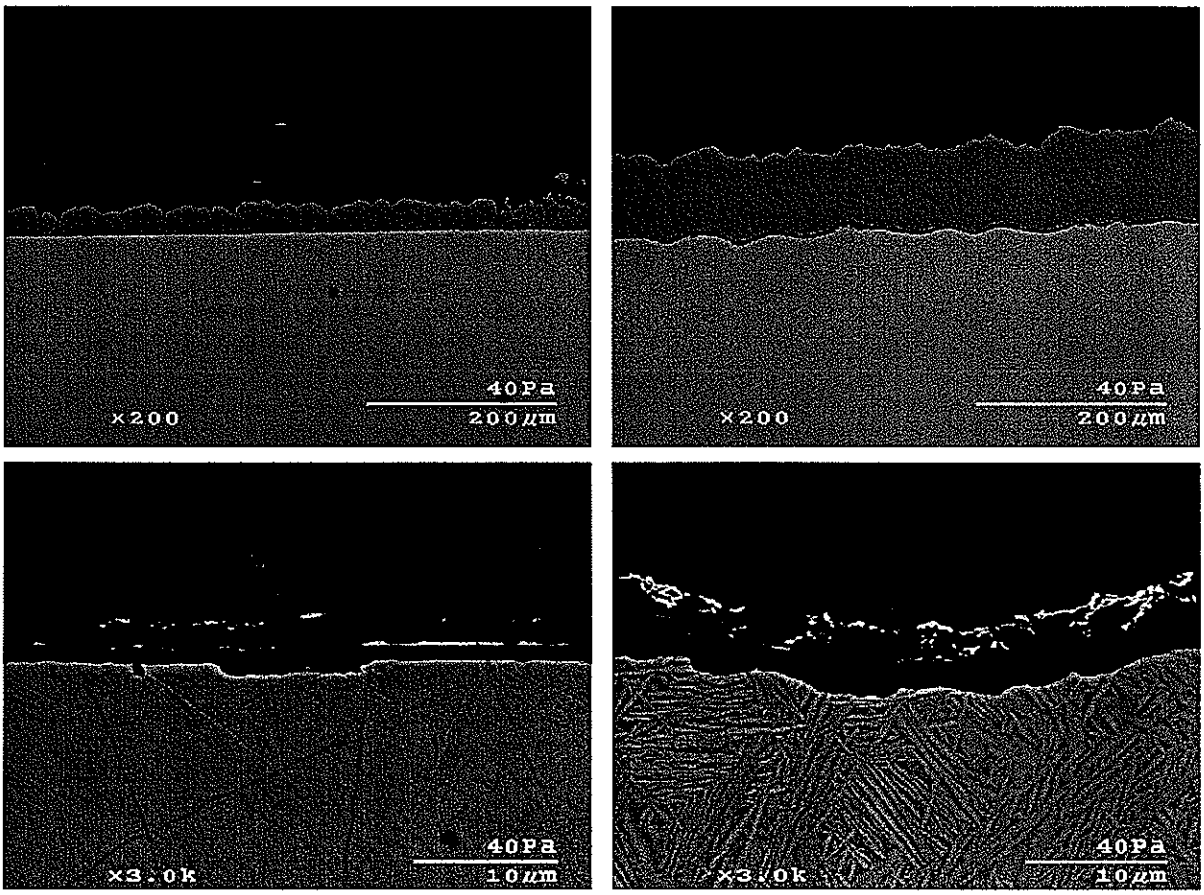

Figure 56. Cross sections of alloy S20 with 1μm initial surface finish, cycled 100 times at 500°C/min from 760 to 1150°C (1hr hold), with 15 minutes (left) and 1 hour (right) at 760°C

Figure 57. Macroscopic deformation of alloy S20 1μm initial surface finish, cycled 100 times at 500°C/min from 760 (1 hour hold) to 1150°C (1hour hold)

8.4.2 The Effect of Surface Finish on Rumpling

The two samples which were tested in section 8.3.1 were prepared using 1μm polish. The back sides of these two samples had coarser finishes. Profilometry results for the opposite side of the non rumpled surface revealed a slight amount of rumpling that was not evenly distributed across the surface, as shown in figure 58. The opposite side of the sample that did rumple had an initial 600-grit finish. Both the average wavelength and amplitude parameters are increased in comparison to the side that had a 1μm initial surface finish. Profilometry images of both samples, along with the averaged measured rumpling parameters, are shown in figure 43. There does not seem to be any anisotropy in the rumpling of the 600-grit finished sample, so it does not appear that the rumpling is superimposed on any existing flaws in the way that the rumpled 240 grit γ-γ' sample in figure 22 is.

It is not immediately clear as to why rumpling appeared only on the rougher surface of the S20 sample that was held at 760°C for 15 minutes. It is possible that the flaws in the coarser finished side provided nucleation sites which allowed the martensite to form more easily. If

the martensitic transformation is indeed a major mechanism behind rumpling, then areas of the sample which contained more martensite would be more likely to rumple.

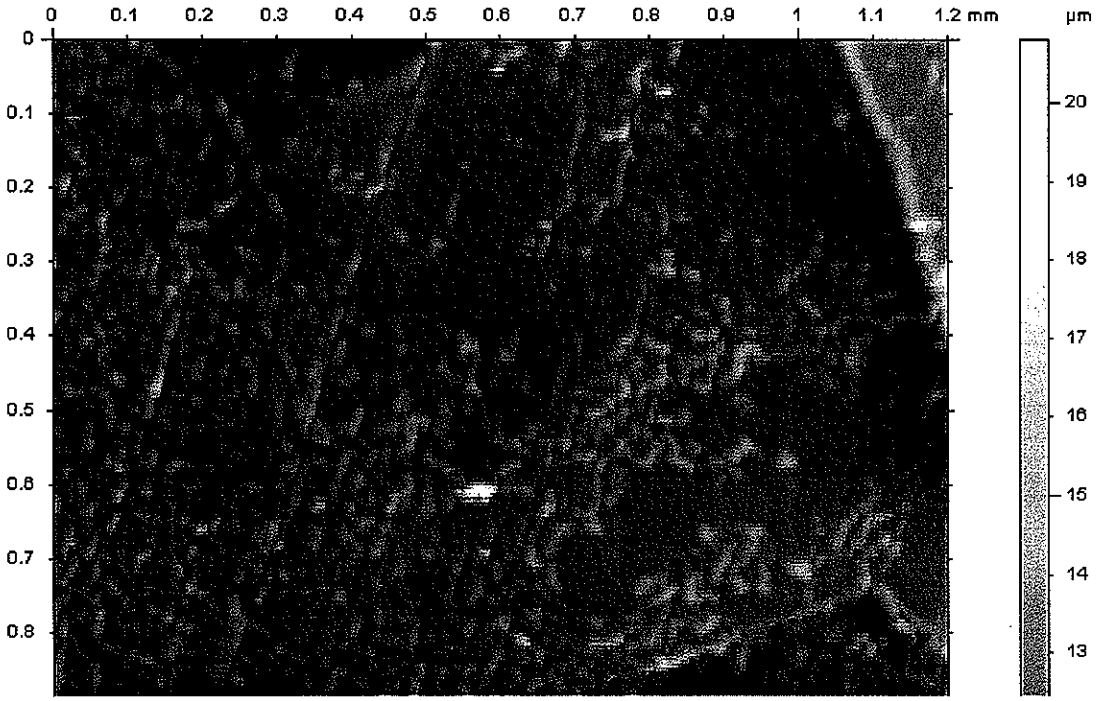

Figure 58. Alloy S20 with an abrasive saw initial surface finish, cycled 100 times at 500°C/min from 760 (15 minute hold) to 1150°C (1hr hold)

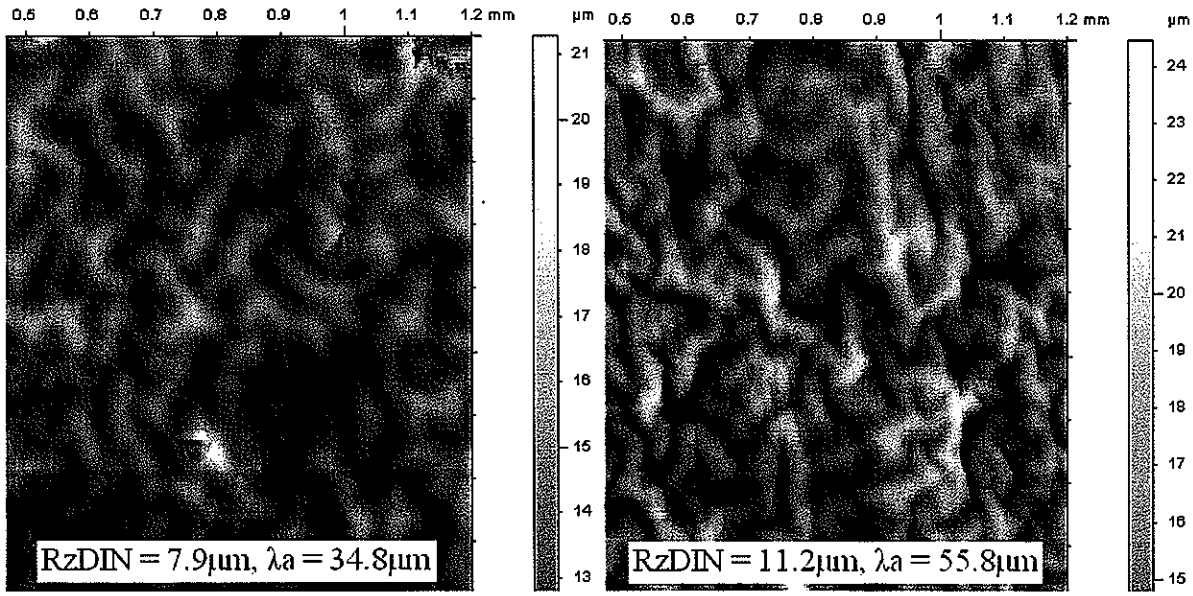

Figure 59. Alloy S20 with 1µm (left) and 600-grit (right)initial surface finishes, cycled 100 times at 500°C/min from 760 (1 hour hold) to 1150°C (1hour hold)

8.4.3 The Effect of Cooling Rate on Rumpling

Confirmation that rumpling in alloy S20 is not due to creep deformation upon heating or cooling was provided by an experiment which examined the effect of cooling rate. Two samples of alloy S20 which had 600-grit initial surface finishes and cycled under the same conditions have already been shown. Figures 50 and 55 show the profilometry images after 15°C/min and 500°C/min cooling, respectively. As shown in table 3, the $R_{z(DIN)}$ and λ_a values for the two samples differ by less than 15%. A 15% difference in either parameter falls within the expected experimental variation. The independence of rumpling on cooling rate provides evidence that rumpling primarily occurs isothermally, rather than upon heating or cooling.

8.4.4 The Effect of the Number of Cycles on Rumpling

It was reported by Tolpygo and Clarke [24] in their study of Pt-modified aluminide coatings that the amplitude of surface undulations increased with the number of thermal cycles. In order to examine the evolution of rumpling in the bulk alloy S20, 5 samples were polished to 1μm and cycled from 760 to 1150°C with 1 hour dwells at each temperature. The samples were oxidized for 5, 10, 25, 50, and 100 cycles. Profilometry images and cross sections are shown in figures 60 and 61 respectively. Figure 62 shows that martensite is present in all five samples.

The rumpling parameters are presented graphically in figure 63. The graphs clearly show that both the amplitude and wavelength of the rumpling in alloy S20 increases with increasing number of cycles. If each individual undulation simply increased in amplitude, the average wavelength would not increase. Therefore it is inferred that during the evolution of the rumpled surface, some undulations must grow at the expense of others. In other words, there would be a net decrease in the number of undulations on a given sample as the sample underwent further cyclic oxidation. From this experiment it is still not entirely clear

if the increase in the rumpling parameters is due solely to the increasing number of cycles or if the increase in cumulative time at 760°C allowed more creep to occur.

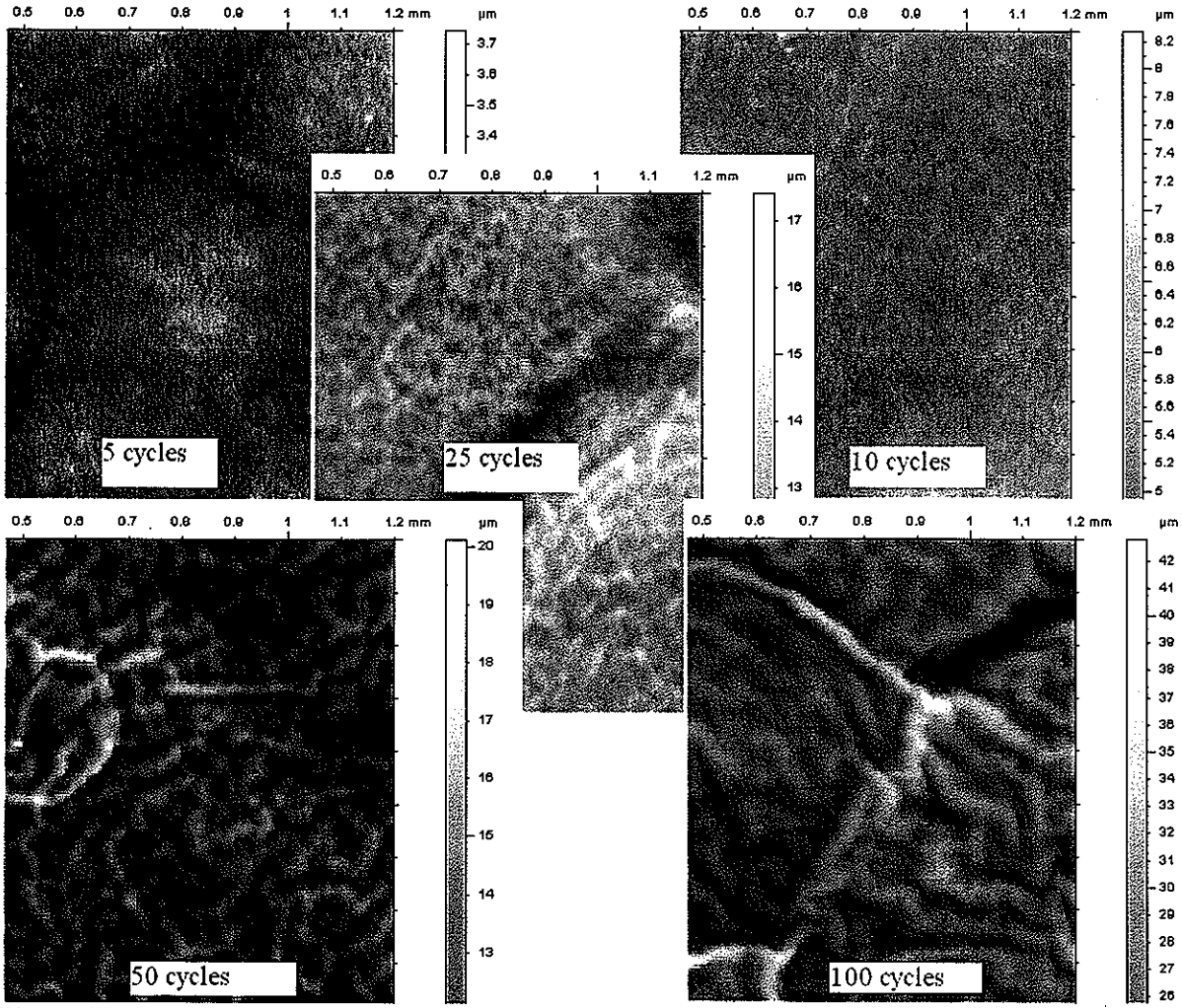

Figure 60. Alloy S20 with 1μm initial surface finish, cycled various numbers of times with a 500°C/min from 760 (1 hour hold) to 1150°C (1hour hold)

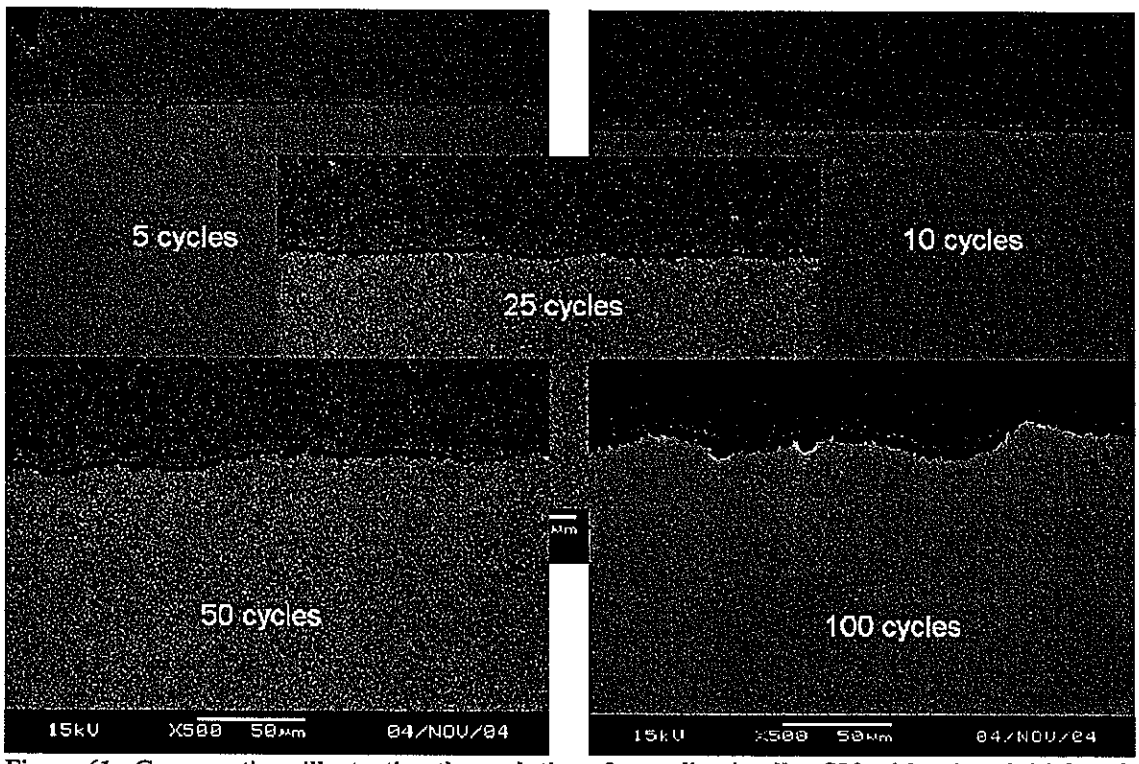

Figure 61. Cross sections illustrating the evolution of rumpling in alloy S20 with a 1µm initial surface finish, cycled various numbers of times at 500°C/min from 760 (1 hour hold) to 1150°C (1hour hold)

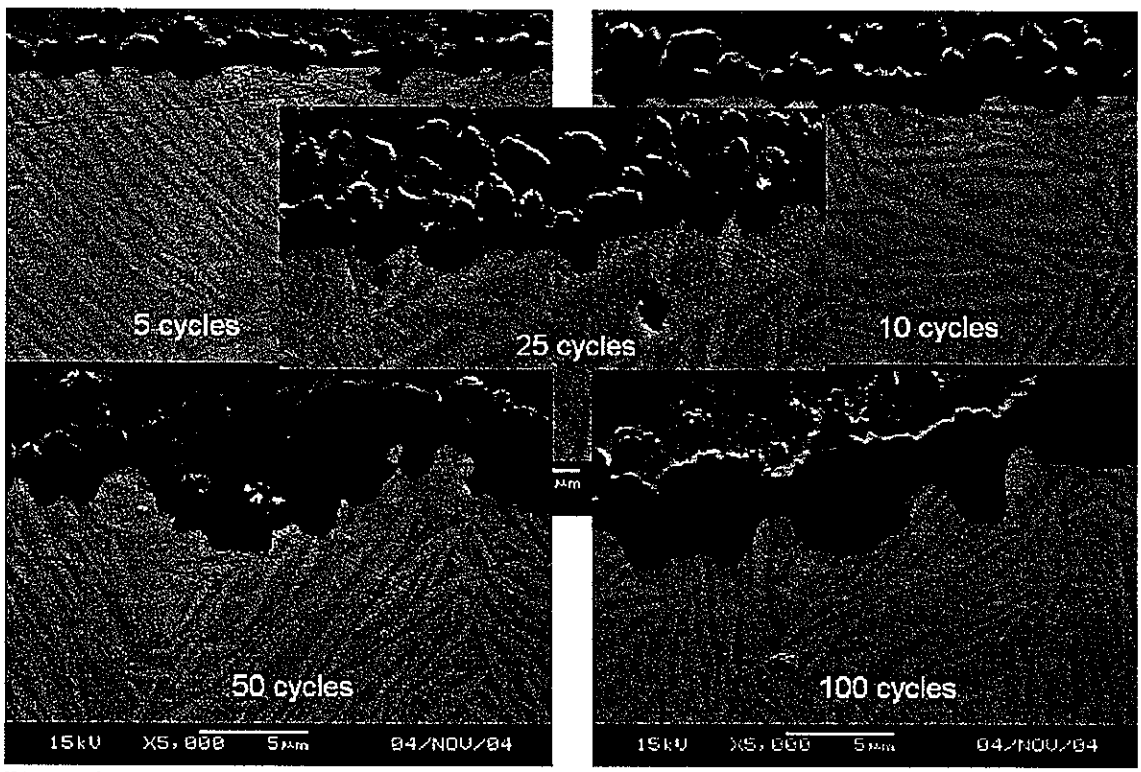

Figure 62. Cross sections showing martensite in alloy S20 with a 1µm initial surface finish, cycled various numbers of times at 500°C/min from 760 (1 hour hold) to 1150°C (1hour hold)

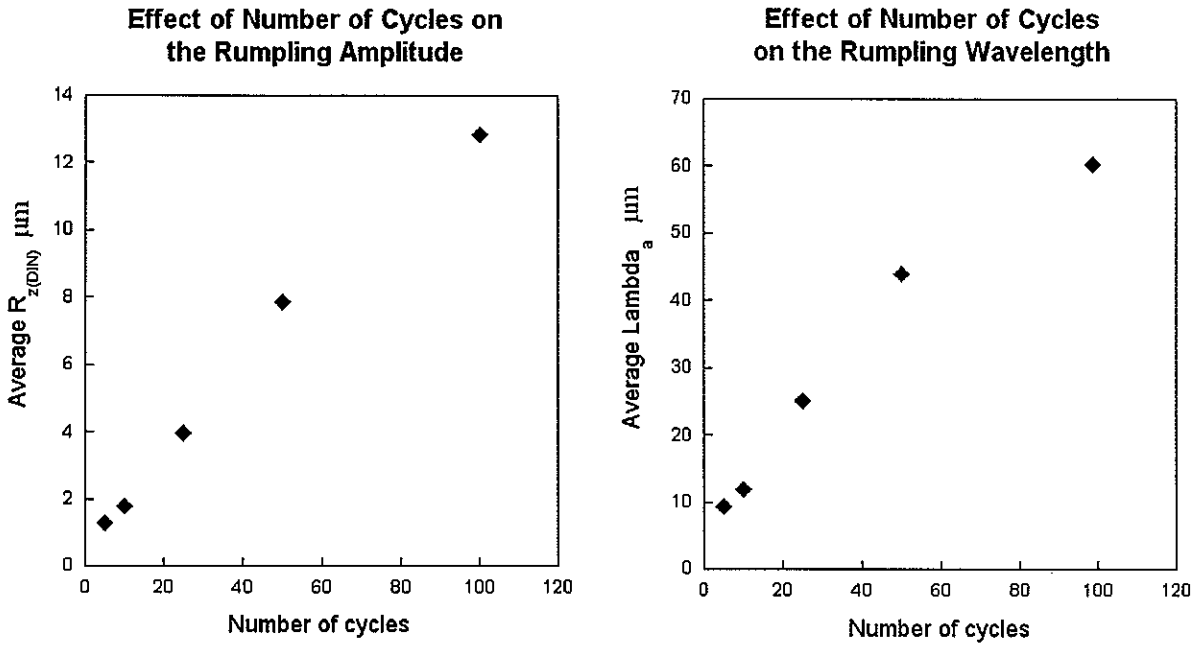

Figure 63. Rumpling parameters in alloy S20 with a 1µm initial surface finish, cycled various numbers of times at 500°C/min from 760 (1 hour hold) to 1150°C (1hour hold)

8.4.5 The Effect of Oxide Thickness on Rumpling

The use of bulk alloys in these experiments eliminated any of the possible rumpling mechanisms due to interactions between the bond coat and the substrate. In order to further eliminate other possible rumpling mechanisms besides the martensitic transformation, an S20 sample was thermally cycled in the absence of oxygen in order to avoid any interactions between the alloy and the oxide. The sample was prepared by pre-oxidizing at 1150°C in air for 1 hour then sealing in a quartz tube under 1/3atm Ar. The pre-oxidation was performed to form a very thin alumina scale to protect the sample from any reactions that might take place with the quartz tube. The sample was cycled 100 times at 500°C/min from 760 to 1150°C. The profilometry image exhibits rumpling and is shown in figure 48. An SEM image taken of the surface (figure 49) shows that the oxide has a large number of cracks. The cross sections in figure 50 show that the cracks formed at the peaks of the undulations, and they also show the presence of martensite in the sample.

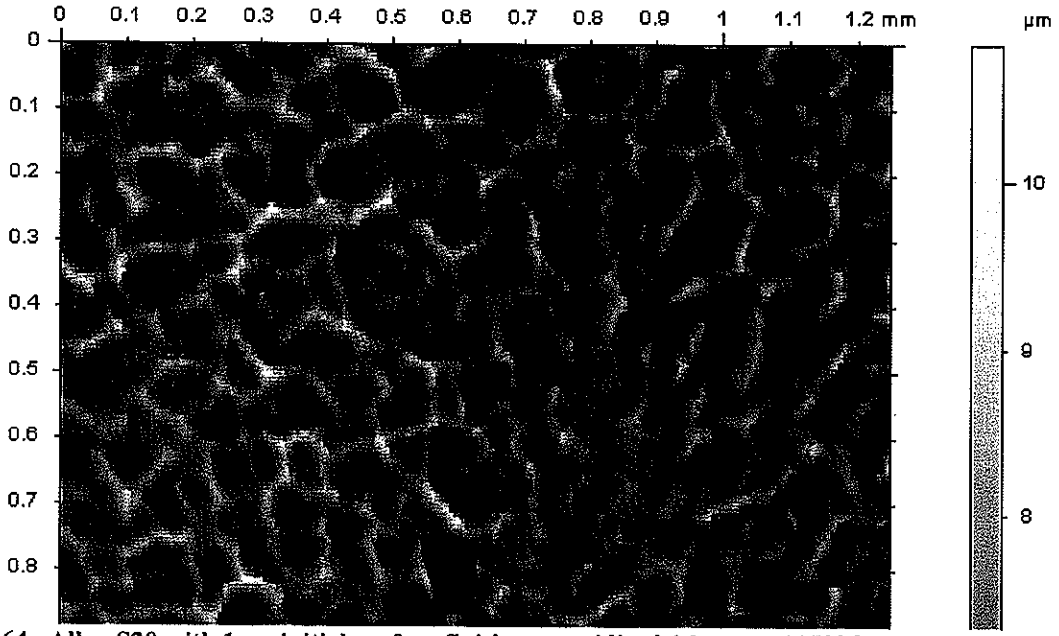

Figure 64. Alloy S20 with 1µm initial surface finish, pre-oxidized 1 hour at 1150°C, sealed in quartz, then cycled 100 times at 500°C/min from 760 (1 hour hold) to 1150°C (1hour hold)

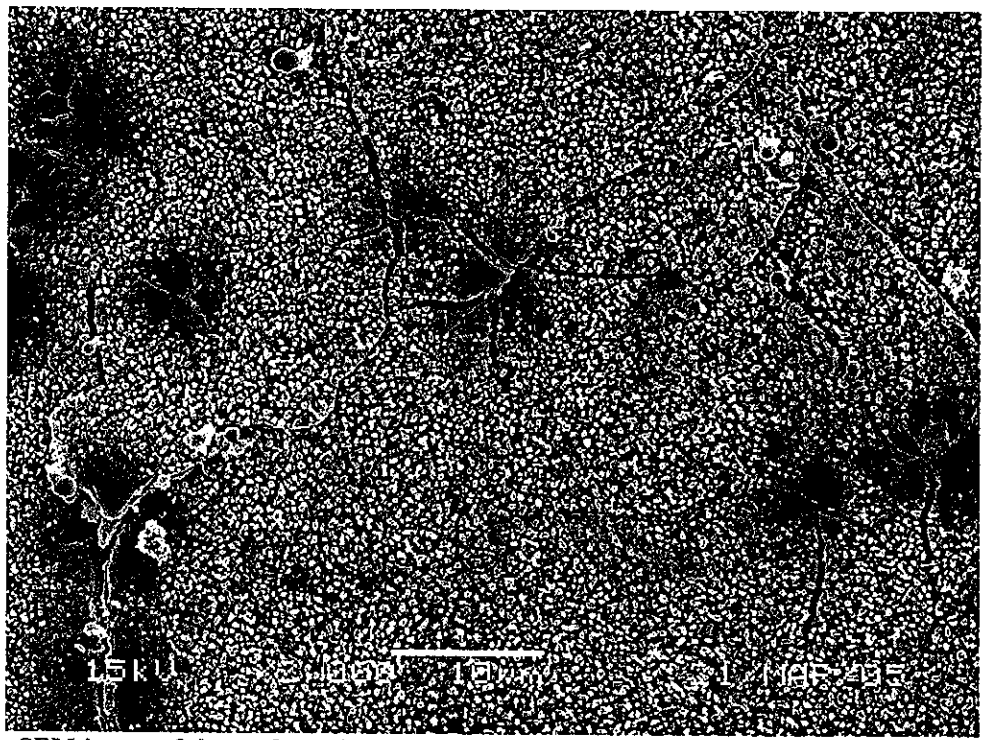

Figure 65. SEM image of the surface of alloy S20 with 1µm initial surface finish, pre-oxidized 1 hour at 1150°C, sealed in quartz, then cycled 100 times at 500°C/min from 760 (1 hour hold) to 1150°C (1hour hold)

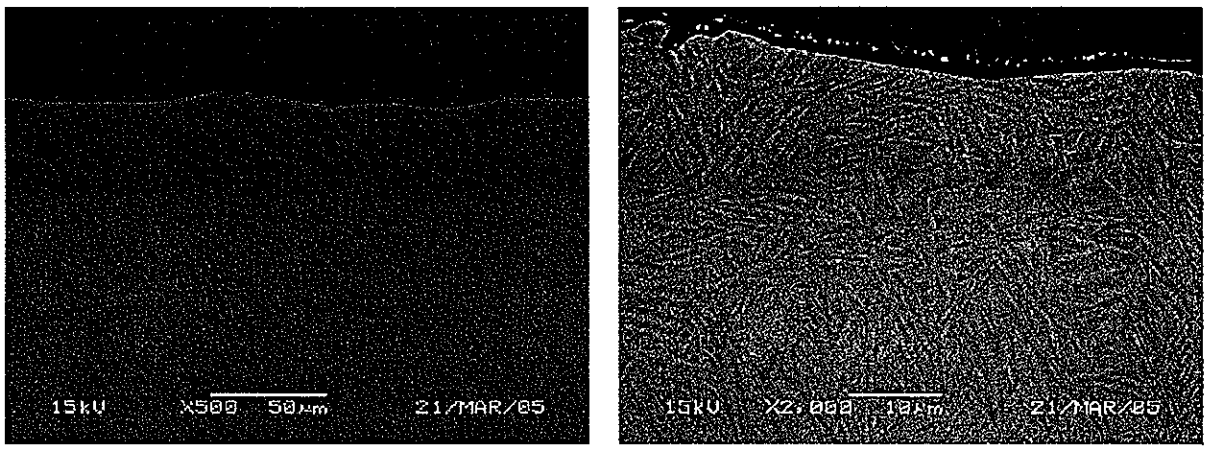

Figure 66. Alloy S20 with 1µm initial surface finish, pre-oxidized 1 hour at 1150°C, sealed in quartz then cycled 100 times at 500°C/min from 760 (1 hour hold) to 1150°C (1hour hold)

While the sample did rumple, the amplitude of the undulations was approximately 50% less than samples cycled in air. Therefore, it appears that the oxide layer has some effect on the degree of rumpling. The martensitic transformation, on the other hand, seems to be a requirement for rumpling in the Pt-modified β system. When a sample with 7at.% more aluminum than S20 is cycled 100 times at 500°C/min from 760 to 1150°C it remains completely planar as shown by the cross section in figure 67. Since the sample is higher in aluminum it is does not form martensite upon cooling. Whether the absence of the volume changes associated with the martensitic transformation or the improved creep resistance is responsible for this alloy remaining planar is not entirely clear from these two experiments.

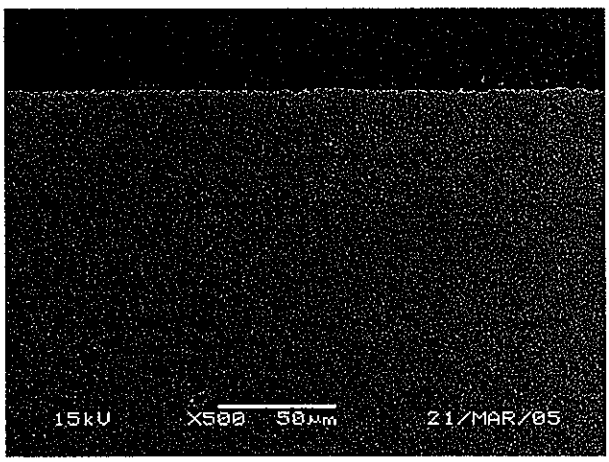

Figure 67. Ni-47Al-15Pt with 1µm initial surface finish, cycled 100 times at 500°C/min from 760 (1 hour hold) to 1150°C (1hour hold)

8.4.6 The Progression of the β-to-Martensite Transformation

It was shown in figure 56 that when S20 that was held for 15 minutes at 760°C, it did not form martensite nearly to the degree that the sample held for 60 minutes did. In order to investigate the progression of the transformation, seven specimens were held at 1150°C for 1 hour then cooled at 500°C/min to 760°C and held for 0, 0.5, 1, 6, 15, 30, and 60 minutes before cooling to room temperature at 500°C/min. The samples were then etched using a mixture of 10% chromic acid and 90% hydrochloric acid. The results showed what appear to be two separate structural variants of martensite: (i) a lath type structure that seemed to appear instantaneously (figure 68); and (ii) an acicular-like (i.e. widmanstatten-like) structure which appears to be what is visible in the SEM images in figures 53, 56, 62 and 66. The acicular-like structure seemed to nucleate at the grain boundaries and at the surface after about 15 minutes (figure 69). The extent of the acicular-like formation increased after 30 minutes (figure 70) and by 60 minutes the transformation appeared complete (figure 71).

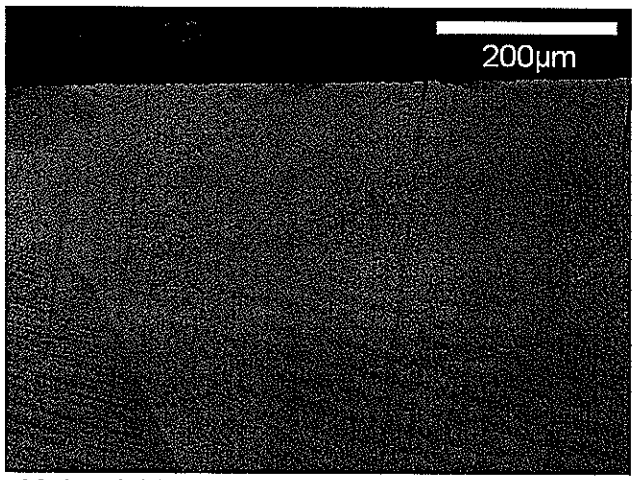

Figure 68. Ni-40Al-15Pt with 1µm initial surface finish, held at 1150°C for 1 hour then cooled at 500°C/min to room temperature

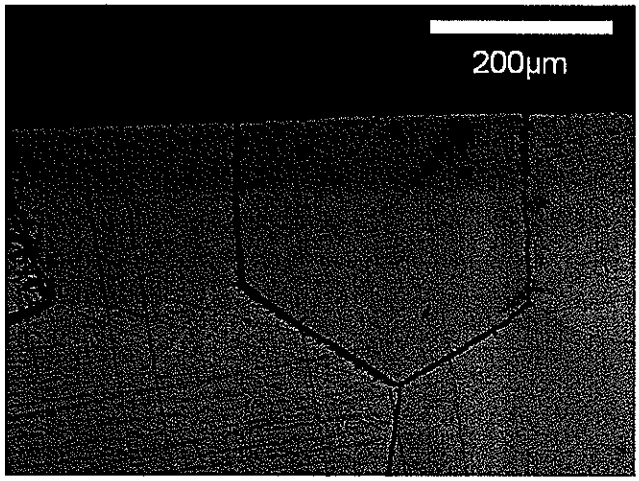

Figure 69. Ni-40Al-15Pt with 1µm initial surface finish, held at 1150°C for 1 hour then cooled at 500°C/min to 760°C and held for 15 minutes

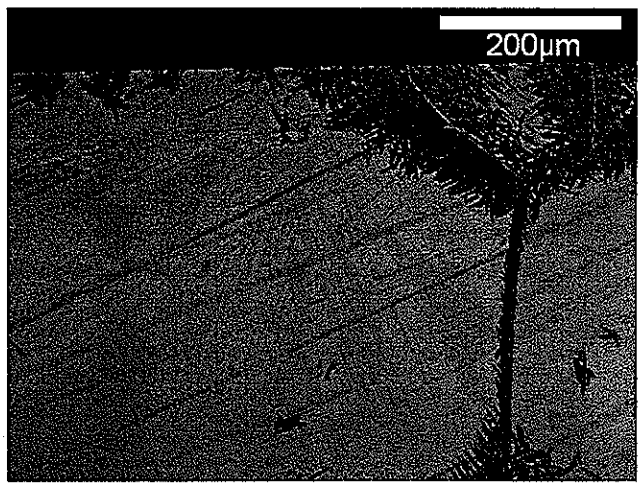

Figure 70. Ni-40Al-15Pt with 1µm initial surface finish, held at 1150°C for 1 hour then cooled at 500°C/min to room temperature

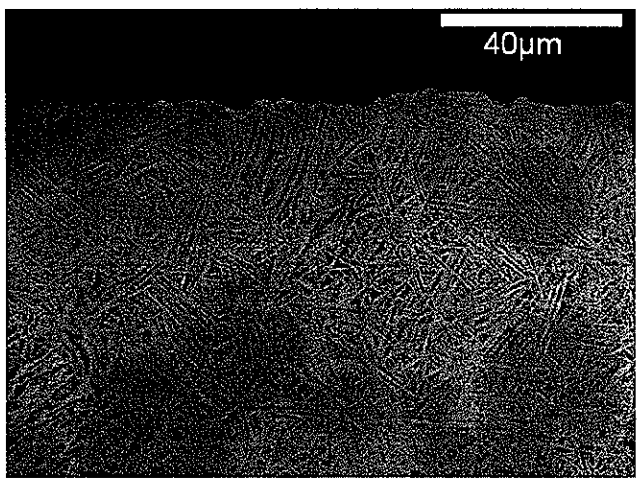

Figure 71. Ni-40Al-15Pt with 1µm initial surface finish, held at 1150°C for 1 hour then cooled at 500°C/min to 760°C and held for 15 minutes

The HT-XRD experiments on alloy S20 showed no evidence of any phases other than β and martensite. The alloy is also clearly within the β phase field, so even if a precipitate such as γ′ were to form, the volume fraction would be very small; not at all what is observed. Based on the rumpling results from the experiment where a sample that was held for 15 minutes at 760°C (which contained the lath type of martensite) did not rumple, but the sample held for 60 minutes (which contained the acicular-like variant) did, it is possible that the later-forming martensite structure may be associated with rumpling. But, if creep is responsible for rumpling, then perhaps the 15 minute sample simply did not have enough time for creep deformation to occur. Determining the differences between what appears to be two distinct structural variants of martensite may require the use of a TEM or other method, and is beyond the scope of this work.

8.4.7 Rumpling in Ni-37Al-10Pt

Another martensitic Pt-containing β alloy was cyclically oxidized from 500 to 1150°C with 1 hour dwells at each temperature. 500°C was chosen for the low temperature dwell based on the DSC results which indicated that β would readily transform into martensite at that temperature. A profilometry image and a surface SEM image of the sample are provided in figure 72. Cross sections of the sample in figure 73 show that the presence a martensitic microstructure. Ni-37Al-10Pt confirms that the rumpling phenomenon in bulk Pt-modified aluminides is not limited to alloy S20. Once again there appears to be a strong correlation between the presence of martensite and the formation of rumpling.

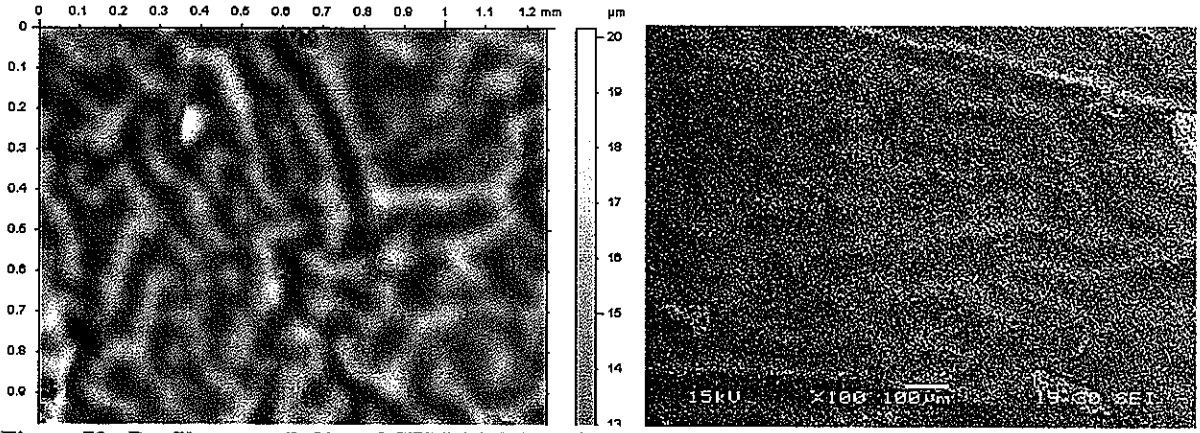

Figure 72. Profilometry (left) and SEM (right) surface images of Ni-37Al-10Pt with 1µm initial surface finish, cycled 100 times at 500°C/min from 500 (1 hour hold) to 1150°C (1hour hold)

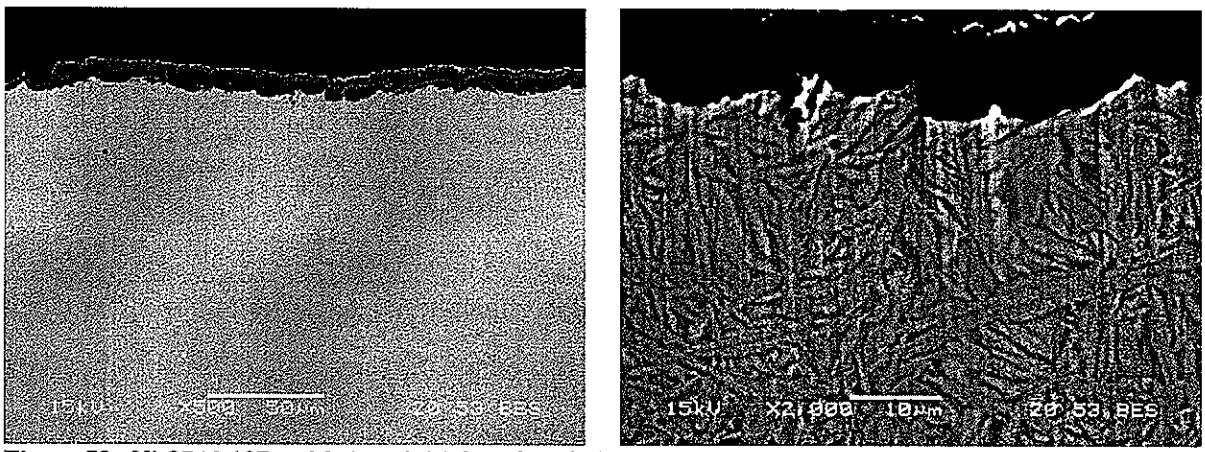

Figure 73. Ni-37Al-10Pt with 1µm initial surface finish, cycled 100 times at 500°C/min from 500 (1 hour hold) to 1150°C (1hour hold)

The profilometry results for this alloy show that the amplitude of the rumpling in Ni-37Al-10Pt is significantly less (R_{zDIN} = 5.6µm, λ_a = 47.5 µm) than for a Ni-40Al-15 sample (R_{zDIN} = 12.8, λ_a = 60.7 µm) oxidized for the same number of cycles. It is accepted that diffusion coefficients increase exponentially with temperature according to equation 6, where Q is the activation energy, R is the gas constant.

$$D = D_0 \exp\left(-\frac{Q}{RT}\right) \tag{6}$$

Since the effective diffusion coefficient would be expected to be lower for martensite at 500°C than at 760°C, the creep rate would also be expected to decrease according to equation 4. This decrease in creep rate would explain the decreased degree of rumpling in Ni-37Al-

10Pt. A final cyclic oxidation experiment was performed on Ni-37Al-10Pt after oxidizing at 900°C for one hour and then sealing in quartz under 1/3atm Ar. After 100 cycles from 500 to 1150°C with 1-hour holds at each temperature, the sample exhibited macroscopic deformation as shown in figure 74, but did not rumple as shown in the profilometry image and cross section in figure 75. The resulting oxide was only 0.25μm thick and the martensitic relief pattern is clearly visible through the oxide in the profilometry image.

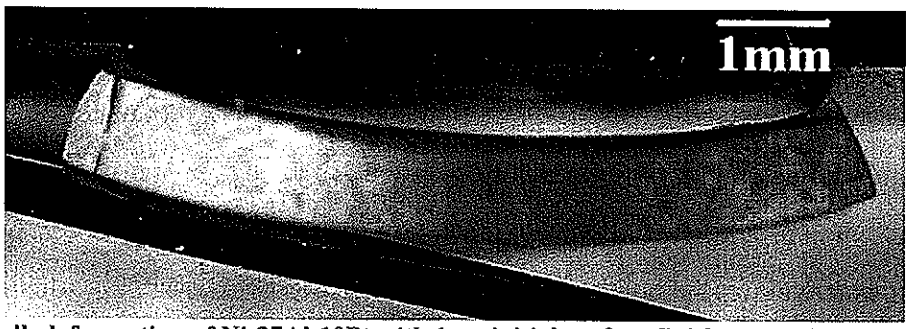

Figure 74. Bulk deformation of Ni-37Al-10Pt with 1μm initial surface finish, pre-oxidized 1 hour at 900°C, sealed in quartz then cycled 100 times at 500°C/min from 500 (1 hour hold) to 1150°C (1hour hold)

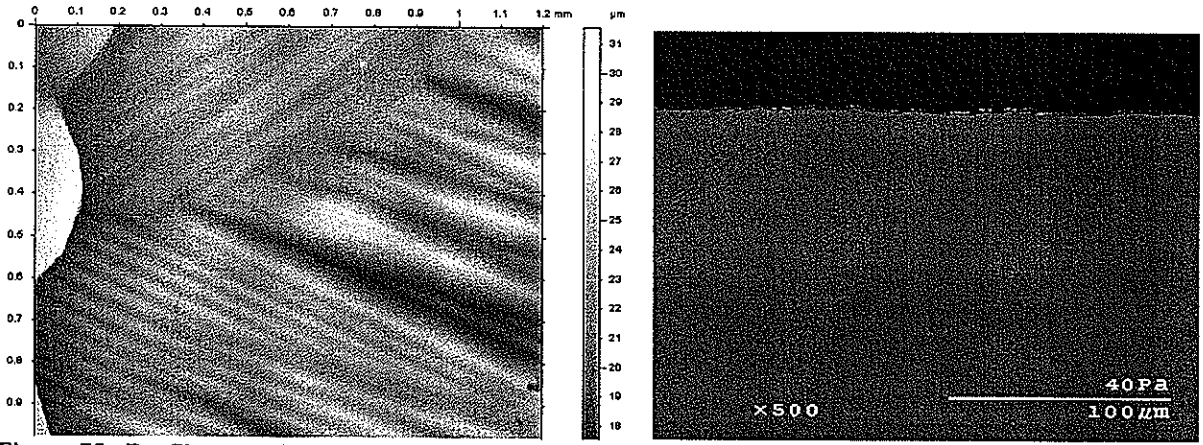

Figure 75. Profilometry image (left) and cross section (right) of Ni-37Al-10Pt with 1μm initial surface finish, pre-oxidized 1 hour at 900°C, sealed in quartz then cycled 100 times at 500°C/min from 500 (1 hour hold) to 1150°C (1hour hold)

Although small surface defects formed at the surface of the alloy, apparently because of the martensitic transformation, the very thin oxide layer did not develop enough compressive stress to cause rumpling. While the exact mechanism behind the bulk deformation of the sample is not clear, it appears to be linked to the martensitic transformation since only

martensitic alloys have exhibited this phenomenon. In the case of Pt-modified β alloys it appears that both the martensitic transformation and a relatively thick oxide scale are necessary for rumpling.

8.5 Rumpling in a Commercial Coated Alloy

A sample of a superalloy substrate with a standard Pt-modified aluminide bond coat was provided by General Electric. The initial composition of the coating was measured using EDS and was found to be Ni-41Al-10Pt. While much smaller amounts of other elements were found in the coating, they were not considered in the experiment. The sample was then cut into two halves and one half was oxidized at 1150°C for 100 hours. The purpose of the oxidation was to allow the bond coat to become depleted of Al. After oxidizing, both halves were ground using 1200 grit paper until nearly all low spots had disappeared, then polished using 1μm polish to obtain a very planar surface. The as-received coating structure is shown in figure 76, along with the structure after oxidizing and polishing. The composition of the depleted sample was Ni-33Al-8Pt.

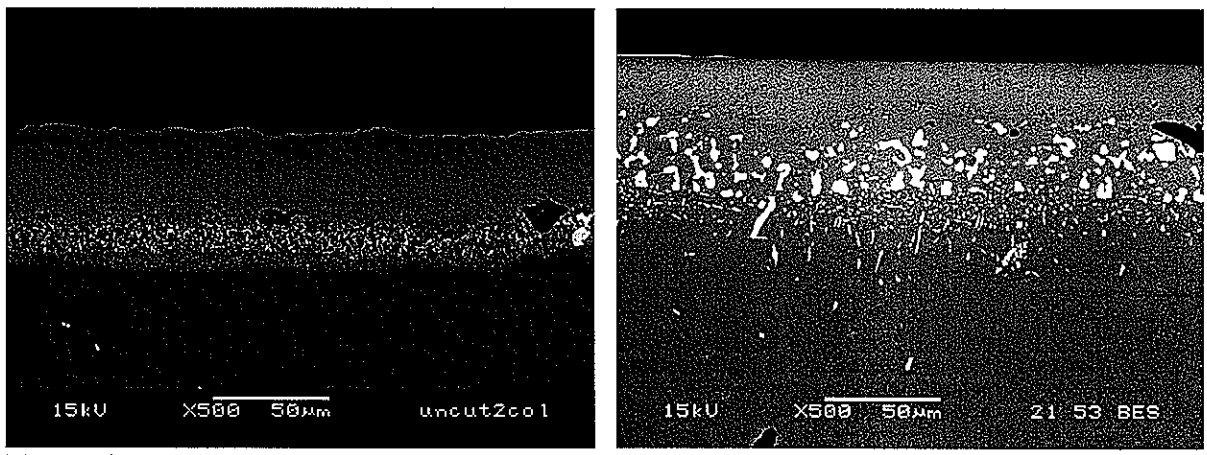

Figure 76. Commercial Pt-modified aluminide bond coat on a super alloy substrate, as-received (left) and following 100 hours at 1150°C then polished to 1μm

The two polished samples were again cut in half to create four specimens for experimentation. An as-received and a depleted sample were cyclically oxidized for 100

cycles from 30°C to 1000°C at 15°C/min and held for one hour at each temperature. The remaining two samples were also cycled 100 times to the same temperatures and held for the same amount of time, but were exposed to heating and cooling rates of 500°C/min. 1000°C was chosen as the high temperature to limit further depletion of Al and Pt in the coating so that the composition would remain relatively constant. The results of the experiments are shown in figures 77 through 79.

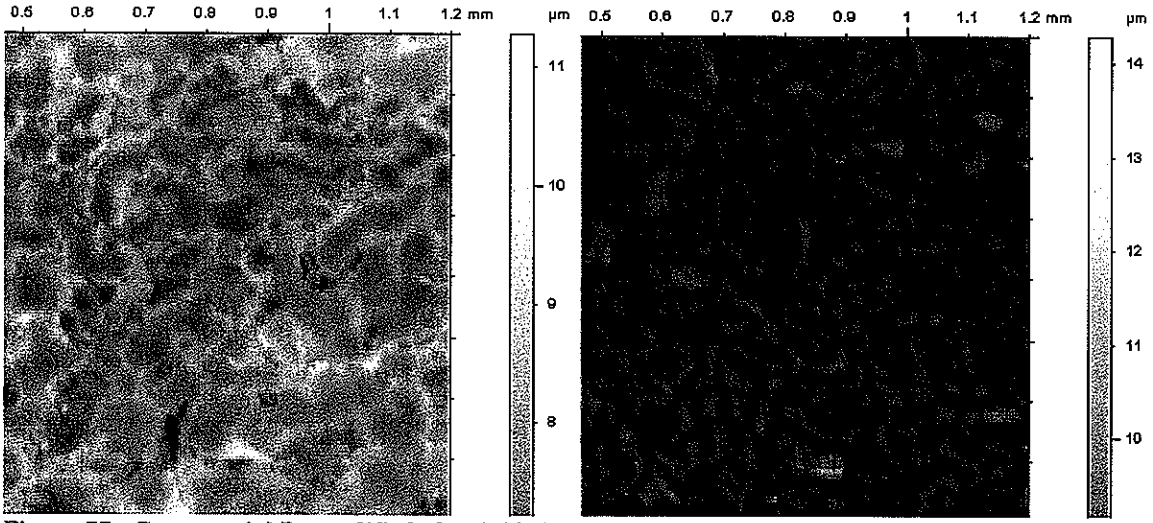

Figure 77. Commercial Pt-modified aluminide bond coat on a super alloy substrate, 1µm initial surface finish, cycled 100 times at 15°C/min from 30°C (1 hour hold) to 1000°C (1hour hold) as-received (left) and following 100 hours at 1150°C (right)

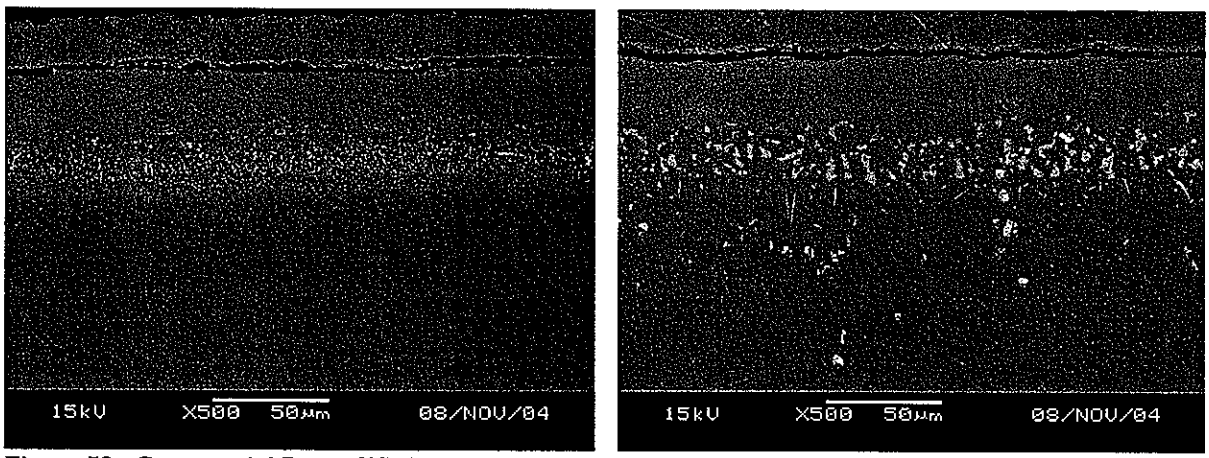

Figure 78. Commercial Pt-modified aluminide bond coat on a super alloy substrate, 1µm initial surface finish, cycled 100 times at 15°C/min from 30°C (1 hour hold) to 1000°C (1hour hold) as-received (left) and following 100 hours at 1150°C (right)

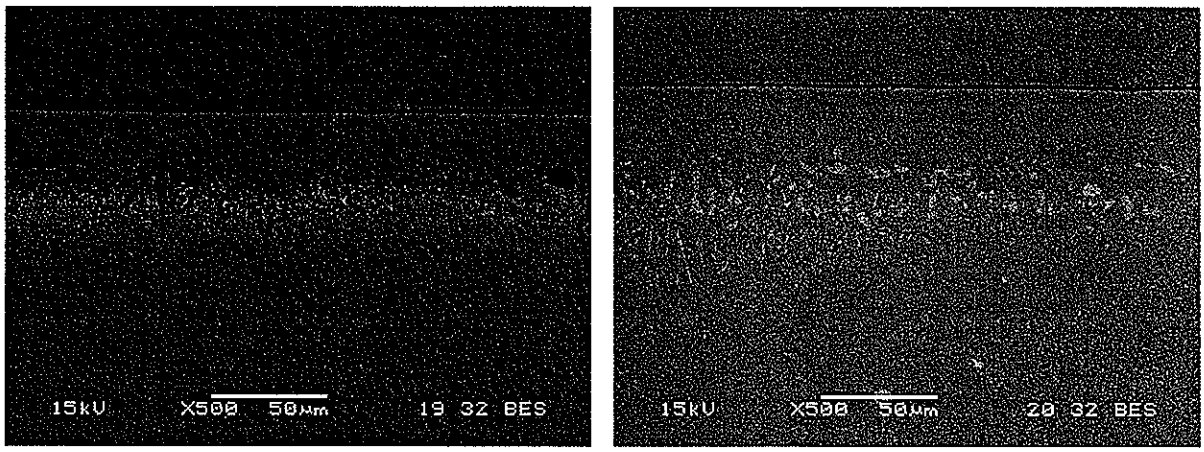

Figure 79. Commercial Pt-modified aluminide bond coat on a super alloy substrate, 1µm initial surface finish, cycled 100 times at 500°C/min from 30°C (1 hour hold) to 1000°C (1hour hold) as-received (left) and following 100 hours at 1150°C (right)

The oxide layer that formed on the samples that were cycled at 15°C/min had poor adherence to both the as-received and depleted coatings. In figure 70, the large area that appears rumpled has spalled the majority of its oxide, and is covered by a much thinner oxide that appears to have re-formed after the spallation occurred. Despite the poor oxide adherence, figure 71 shows that the metal in the as-received bond coat remained relatively planar when compared to the rumpling present in the depleted sample. Both images are in stark contrast to those that were cycled at 500°C/min. Figure 72 shows that both the as-received and depleted bond coats formed a thin and adherent oxide layer. Neither sample exhibited any rumpling. It seems that the faster rates precluded the rumpling causing mechanism. The depleted sample containing 33at.% Al has a composition which would be expected to be martensitic, while 41at.% Al would not. Since the exact temperatures for the martensitic transformation in an alloy with 33at.% Al and 8at.% Pt was not known, a slow cooling rate of 15°C/min was used instead of an isothermal hold. The hypothesis was that the sample would remain in the temperature range in which martensite can form from β for a long enough time period. The faster rate of 500°C/min was chosen so that the transformation would have less time to occur. Bulk alloy samples of Ni-40Al-15Pt and Ni-37Al-10Pt were cyclically oxidized along with the commercial coated samples and cross sections of these alloys seemed to confirm the hypothesis; martensite was evident in both alloys after 15°C/min testing but

not after 500°C/min. While the profilometry results show that something did indeed cause rumpling of the depleted commercial coated sample tested at 15°C/min, martensite was not clearly visible in the cross section. Detecting martensite in Pt-modified aluminides using back-scattered SEM is difficult since there is no compositional variation; in figure 39 no martensite is readily apparent in the sample of S20 that was held for 15 minutes, but XRD showed that martensite was indeed present. Unfortunately, the very limited supply of the commercial coated sample precluded any XRD measurements of the rumpled specimen.

Chapter 9. Summary

The rumpling phenomenon that occurs in Pt-modified nickel aluminide bond coats is known to be very detrimental to the lifetimes of TBCs. Many possible mechanisms behind the formation of rumpling have been proposed, including the β-to-martensite transformation which can occur during thermal cycling. While the martensitic transformation in binary NiAl has been relatively thoroughly studied, very limited information is available for the transformation in Pt-modified NiAl. The present study has utilized various experimental methods including DSC, HT-XRD, and potentiometric measurements to conduct a detailed investigation of the transformation in the ternary system. Based on the results of this investigation, cyclic oxidation experiments were performed to observe the effect of the martensitic transformation on the rumpling of Pt-modified nickel aluminide bulk alloys. Very recently, rumpling has also been observed in a bulk γ-γ′ Ni-Al-Pt alloy. Isothermal oxidation experiments were performed in order to determine the cause of the rumpling in this system.

It was found that the γ-γ′ alloy Ni-22Al-30Pt rumpled upon isothermal oxidation at 1150°C, while alloys with slightly lower Pt contents remained planar. The degree of rumpling was quantified using a profilometer. It was found that both the amplitude and wavelength of the rumpling were independent of the rates at which the samples were cooled from 1150°C, indicating that the rumpling occurred at temperature rather than upon cooling. Cross-sectional analysis revealed a subsurface layer containing the γ and α phases. The back-diffusion of Pt from the surface of the alloy caused the local composition of the subsurface layer to enter into the two-phase γ+α region of the phase diagram. The α phase was not observed for the non-rumpling alloy Ni-22Al-25Pt. While HT-XRD results showed that there was a greater than 2% increase in volume for the unit cell of α compared to γ and γ′, a volume expansion in the sub-surface layer would cause an increase in tension on the γ layer below the oxide. Tension in this layer would reduce rumpling. Instead, it is believed that the

reduced high-temperature strength of the $\gamma+\alpha$ layer allows creep deformation of the γ layer by the compressive growth stress within the oxide.

Because rumpling in the γ-γ' system was found to be limited to a single alloy with a very high Pt content, a larger part of this thesis focused on the martensitic transformation in Ni-rich β-NiAl and the effects of the transformation on rumpling of bulk alloy samples. HT-XRD and DSC experiments showed that the β-to-martensite transformation has a significant time-dependence. It was also found that the volume fraction of martensite would increase while being held at elevated temperatures. The martensitic transformation temperature was observed to increase with increasing Pt content. HT-XRD measurements also showed a volume decrease in the unit cell upon transformation from β into martensite transformation.

Cyclic oxidation experiments based on the results of the HT-XRD experiments were performed on a Pt-modified nickel aluminide bulk alloy. When the alloy was thermally cycled from 1150°C to a lower temperature which was above the martensitic transformation temperature, the sample did not rumple. When it was cycled to a temperature at which the martensitic transformation had been shown to occur, the sample showed significant rumpling. The cooling rate during cycling did not affect the amount of rumpling, but the length of the low temperature dwell during cycling had a very significant effect on rumpling. Thus, rumpling was shown to occur during the hold at the lower temperature and required the nearly complete transformation of β into martensite. Both the amplitude and wavelength of rumpling were shown to increase with an increasing number of cycles. A sample which was cycled in the absence of oxidation was also shown to rumple, but had a lower amplitude. A non-martensitic β alloy with an identical Pt content, but with a slightly higher Al content (47 instead of 40at.%) was exposed to identical thermal cycling without rumpling. It was determined that rumpling in Pt-modified nickel aluminide *bulk* alloys is influenced by both the presence of an oxide and the formation of martensite. Rumpling appears very likely to be caused by creep deformation at the surface due to the compressive stress of the oxide and the

increased high-temperature creep rate of martensite compared to β, rather than any volume reductions associated with the formation of martensite. While rumpling in the γ-γ′ alloy Ni-22Al-30Pt occurred during isothermal oxidation, rumpling in the β system required cyclic oxidation. Oxidation at 1150°C was necessary to form a sufficiently thick oxide, but the formation of less creep resistant martensitic phase required cooling to a lower temperature.

Although rumpling in Pt-modified nickel aluminide bond coats may be avoided if the composition of the bond coat is high enough in aluminum to avoid the martensitic transformation, the depletion of aluminum during exposure would eventually lead to the bond coat becoming martensitic. Rumpling has been shown to be reduced through the use of thicker coatings [22], but thicker or higher Al-content bond coats would still eventually deplete in aluminum and become martensitic. These bond coats would have other drawbacks such as reduced fatigue resistance for the thicker coatings [22] and difficulties in obtaining much higher Al-contents using current techniques. Completely avoiding the rumpling associated with the martensitic transformation may require the development of bond coats not based on Pt-modified β-NiAl.

It is very likely that rumpling in both the γ-γ′ and in the β system, while occurring after different oxidation conditions and being associated with completely different phase transformations, may be caused by a very similar mechanism. At elevated temperatures, an adherent oxide scale under a compressive stress seems to cause rumpling if the subsurface metal has a low resistance to creep deformation.

Chapter 10. Suggestions for Future Work

While the development of an in-depth model to explain rumpling in the γ-γ' system would prove very useful in understanding the phenomenon, the effort may not be warranted since the rumpling is limited to a single alloy with a high platinum content. Bond coats based on the γ-γ' system will have much lower amounts of platinum.

While it has been clearly shown that rumpling in bulk Pt-modified nickel aluminide alloys requires the formation of martensite, it is has not been conclusively shown whether the volume reduction associated with the transformation is the cause or if rumpling is due to the decreased high-temperature creep resistance of martensite. Elevated temperature creep measurements are currently being performed by researchers at Iowa State University.

The two apparent structural variants of martensite have not been reported in literature and will require further analysis to understand their structures. While it is unclear whether the second structural variant influences rumpling, it should at least be confirmed that it is indeed martensite.

Further experimentation on Pt-modified nickel aluminide coated substrates could further verify the link between martensite formation and rumpling. Now that HT-XRD data is available, cyclic oxidation experiments could be tailored to the composition of the specific bond coat to place emphasis on the martensitic transformation. A bond coat with a composition very close to the alloy studied in this thesis would provide an ideal method for confirming if the assumptions based on the results from bulk alloys hold true for coated systems.

References

1. M. Peters, C. Leyens, U. Schulz, W.A. Kaysser, EB-PVD Thermal Barrier Coatings for Aeroengines and Gas Turbines, *Adv. Eng. Matls.* **3 (4)** 193-204 (2001).

2. P. Seserko, J. Hotz, J. Lemke, P. R. Smith, M. Mede, EB PVD Thermal Barrier Coatings in Production, *ALD Vacuum Technologies AG* (2002).

3. G.F. Harrison, Proc. European Propulsion Forum, *Royal Aeronautical Society*, 3.1-3.16 (1993).

4. H.E. Evans and M. P. Taylor, Delamination Processes in Thermal Barrier Coating Systems, *Journ. of Corr. Sci. and Eng.* **6 (Paper H011)** (2003).

5. D.R. Clarke and C.G. Levi, Materials Design for the Next Generation Thermal Barrier Coatings, *Annu. Rev. Mater. Res.* 383-419 (2003).

6. A.G. Evans, M.Y. He, J.W. Hutchinson, Mechanics-Based Scaling Laws for the Durability of Thermal Barrier Coatings, *Prog. in Mat. Sci.* **46** 249-271 (2001).

7. D.J. Young and B. Gleeson, Alloy Phase Transformations Driven by High Temperature Corrosion Processes, *Corr. Sci.* **44** 345-357 (2002).

8. B. Gleeson, W. Wang, S. Hayashi, D. Sordelet, Effects of Platinum on the Interdiffusion and Oxidation Behavior of Ni-Al-based Alloys, *Mat. Sci. Forum* **461-464** 213-222 (2004).

9. C. Leyens, B.A. Pint, I.G. Wright, Effect of Composition on the Oxidation and Hot Corrosion Resistance of NiAl Doped with Precious Metals, *Surf. and Coat. Tech.* **133-134** 15-22 (2000).

10. J. Schramm, Increasing the Hot-Corrosion Resistance of Thermal Barrier Coating Systems by the Addition of Oxides of Cr and Mg, M.S. Thesis, *Iowa State University* (2003).

11. A.G. Evans, D.R. Mumm, J.W. Hutchinson, G.H. Meier, F.S. Pettit, Mechanisms Controlling the Durability of Thermal Barrier Coatings, *Prog. In Mat. Sci.* **46** 505-553 (2001).

12. B.A. Pint, The Role of Chemical Composition on the Oxidation Performance of aluminide coatings, *Surf. and Coat. Tech.* **188-189** 71-78 (2004).

13. Z.D. Xiang and P.K. Datta, Conditions for Pack Codepostion of Al and Hf on Nickel-base Superalloys, *Surf. and Coat. Tech.* **179** 95-102 (2004).

14. P. Deb, D.H. Boone, T.F. Manley, Surface Instability of Platinum Modified Aluminide Coatings during 1100°C Cyclic Testing, *J. Vac. Sci. Tech.* **5 (6)** 3366-3372 (1987).

15. R.C. Pennefather and D.H. Boone, Mechanical Degradation of Coating Systems in High-Temperature Cyclic Oxidation, *Surf. and Coat. Tech.* **76-77** 47-52 (1995).

16. V. K. Tolpygo and D. R. Clarke, Surface Rumpling of a (Ni, Pt)Al Bond Coat Induced by Cyclic Oxidation, *Acta Mat.* **48** 3283-3293 (2000).

17. A.M. Karlsson, J.W. Hutchinson, A.G. Evans, A Fundamental Model of Cyclic Instabilities in Thermal Barrier Systems, *J. Mech. Phys. Sol.* **50** 1565-1589 (2002).

18. M.Y. He, J.W. Hutchinson, A.G. Evans, Simulations of Stresses and Delamination in a Plasma-Sprayed Thermal Barrier System upon Thermal Cycling, *Mat. Sci. and Eng.* **A345** 172-178 (2003).

19. V.K. Tolpygo and D.R. Clarke, Morphological Evolution of Thermal Barrier Coatings Induced by Cyclic Oxidation, *Surf. and Coat. Tech.* **163** 81-86 (2003).

20. R. Panat, S. Zhang, K. J. Hsia, Bond Coat Surface Rumpling in Thermal Barrier Coatings, *Acta Mat.* **51** 239-249 (2003).

21. D.S. Balint and J.W. Hutchinson, Undulation Instability of a Compressed Elastic Film on a Nonlinear Creeping Substrate, *Acta Mat.* **51** 3965-3983 (2003).

22. V. K. Tolpygo and D. R. Clarke, Rumpling Induced by Thermal Cycling of an Overlay Coating: the Effect of Coating Thickness, *Acta Mat.* **52** 615-621 (2004).

23. V. K. Tolpygo and D. R. Clarke, On the Rumpling Mechanism in Nickel-Aluminide Coatings Part I: an Experimental Assessment, *Acta Mat.* **52** 5115-5127 (2004).

24. V. K. Tolpygo and D. R. Clarke, On the Rumpling Mechanism in Nickel-Aluminide Coatings Part II: Characterization of Surface Undulations and Bond Coat Swelling, *Acta Mat.* **52** 5129-5141 (2004).

25. B. Gleeson, High-Temperature Corrosion of Metallic Alloys and Coatings, M. Schutze (ed.), *Corrosion and Environmental Degradation, Vol. II: Vol. 19 of the Materials Science and Technology Series*, Weinheim, Wiley-VCH, 173-228 (2000).

26. C. Wagner, Theoretical Analysis of the Diffusion Processes Determining the Oxidation Rate of Alloys, *J. Electrochem. Soc.* **99** 369-380 (1952).

27. H.E Evans, Stress Effects in High Temperature Oxidation of Metals, *Int. Mat. Rev.* **40** 1-40 (1995).

28. Z. Suo, D.V. Kubair, A.G. Evans, D.R. Clarke, V.K. Tolpygo, Stresses Induced in Alloys by Selective Oxidation, *Acta Mat.* **51** 959-974 (2003).

29. J.A. Haynes, B.A. Pint, W.D. Porter and I.G. Wright, Comparison of Thermal Expansion and Oxidation of Various High-Temperature Coating Materials and Superalloys, *Mat. at High Temp.* **21** 87-94 (2004).

30. M.R. Jackson and J.R. Rairden, Aluminization of Platinum and Platinum-Coated IN-738, *Metall. Trans. A* **8** 1697 (1977).

31. J. Schaeffer, G.M. Kim, G.H. Meier, F.S. Pettit, E. Lang (ed.), The Role of Active Elements in the Oxidation Behavior of High Temperature Metals and Alloys, Elsevier, Amsterdam, 231-267 (1989).

32. T.B. Massalski, J.L. Murray, L.H. Bennett, H. Baker (Eds.), *Binary Alloy Phase Diagrams*, 1st ed., ASM International, Metals Park, OH, 1986.

33. Y. Zhang, J. A. Haynes, B. A. Pint, I. G. Wright, W. Y. Lee, Martensitic Transformation in CVD NiAl and (Ni,Pt)Al Bond Coatings, *Surf. and Coat. Tech.* **163-164** 19-24 (2003).

34. M.W. Chen, R. T. Ott, T. C. Hufnagel, P. K. Wright, K. J. Hemker, Microstructural evolution of platinum modified nickel aluminide bond coat during thermal cycling, *Surf. and Coat. Tech.* **163-164** 25-30 (2003).

35. W.A. Maxwell and E.M. Grala, Investigation of Nickel-Aluminum Alloys Containing From 14 to 34 Percent Aluminum, *National Advisory Committee for Aeronautics*, **TN 3259** 1-42 (1954).

36. J. Angenete, K. Stiller, E. Bakchinova, Microstructural and Microchemical Development of Simple and Pt-Modified Aluminide Diffusion Coatings during long term Oxidation at 1050°C, *Surf. and Coat. Tech.* **176** 272-283 (2004).

37. J.L. Smialek and R.F. Hehemann, Transformation Temperatures of Martensite in β-Phase Nickel Aluminide, *Metall. Trans.* **4** 1571 (1973).

38. J. Lašek, T. Chráska, P. Křeček, P. Bartuška, Phase Transformations in Nickel Rich NiAl Using Electrical Resistivity Measurements, *Scripta Mat.* **37** 897-902 (1997).

39. T. Chráska, J. Lašek, P. Chráska, Resistometric Investigation of Phase Transformations in NiAl Alloys, *Mat. Sci. and Eng.* **A244** 263-272 (1998).

40. U. D. Hangen and G. Sauthoff, The Effect of Martensite Formation on the Mechanical Behavior of NiAl, *Intermetallics* **7** 501-510 (1999).

41. D. Pan, M.W. Chen, P.K. Wright, K.J. Hemker, Evolution of a Diffusion Aluminide Bond Coat for Thermal Barrier Coatings During Thermal Cycling, *Acta Mat.* **51** 2205-2217 (2003).

42. M.W. Chen, M.L. Glynn, R.T. Ott, T.C. Hufnagel, K.J. Hemker, Characterization and Modeling of a Martensitic Transformation in a Platinum Modified Diffusion Aluminide Bond Coat for Thermal Barrier Coatings, *Acta Mat.* **51** 4279-4294 (2003).

43. M. Y. He, A.G. Evans, J.W. Hutchinson, The Ratcheting of Compressed Thermally Grown Thin Films on Ductile Substrates, *Acta Mat.* **48** 2593-2601 (2000).

44. D.R. Mumm, A.G. Evans, I.T. Spitsberg, Characterization of a Cyclic Displacement Instability for a Thermally Grown Oxide in a Thermal Barrier System, *Acta Mat.* **49** 2329-2340 (2000).

45. D.S. Balint and J.W. Hutchinson, An Analytical Model of Rumpling in Thermal Barrier Coatings, *J. of the Mech. and Phys. of Solids* **53** 949-973 (2005).

46. E.G. Lesnikova and V.P. Lesnikov, Influence of Instability of the β-Phase of the Aluminide Coating on the Condition and Scale Resistance of the Surface Layer, *Met. Sci. Heat Treat.* **28** 372-376 (1986).

47. Z.G. Yang and P.Y. Hou, Wrinkling Behavior of Alumina Scales Formed During Isothermal Oxidation of Fe-Al Binary Alloys, *Mat. Sci. and Eng.* **A391** 1-9 (2005).

48. M. Schutze and D.R. Holmes (ed.), Protective Oxide Scales and Their Breakdown, Wiley, West Sussex, 48-49 (1997).